Ministry of Higher Education
and Scientific Research
Babylon University
College of Engineering

Modeling and Predication of stator of Axial-Flow Compressor

A Thesis
Submitted to the College of Engineering
Of the University of Babylon in Partial
Fulfillment of the Requirements
For the degree of the Master
Of Science in Mechanical
Engineering

By

NASEER ABUDI MEDLOL

B.Sc.٢٠٠١

Abstract

A developed procedure is presented for the aerodynamic design ,modeling and predication of a stator of axial flow compressor. The mathematical model considered depends upon operating conditions of the compressor, property specifications of working fluid and geometric constraints as a required input data. The compressor efficiency, compressor pressure ratio, and the design parameters of the compressor are predicated. The inlet conditions used are $P_o = 101.3kpa, T_o = 288K$. It is found that the compressor efficiency at D=٠.٥,$\sigma = 1$ equal to ٨٩.٥٪. The study of the distribution of Mach number, pressure, velocity, and density along the blade by using Euler equations by mapping the physical domain to a computational domain is performed by using time-marching technique. The MacCormack method is used to solve unsteady, inviscid and two-dimensional flow using finite difference method. The fourth order artificial viscosity terms have been used to achieve the stability and accuracy of flow computational techniques.

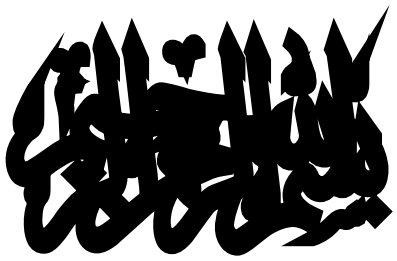

[وقل ربي زدني علماً]

صدق الله العلي العظيم

(سورة طه آية ١١٤)

الإهداء

إلى
الحق الجديد والعالم الذي علمه لا يبيد
إلى
مهدي الأمم وجامع الكلم
إلى
حجة المعبود وكلمة المحمود
إلى
القائم المنتظر والعدل المشتهر
إلى
شمس الظلام وبدر التمام
إلى
المولى صاحب الزمان الإمام المهدي

(عجل الله فرجه)

الخلاصة

يتناول هذا البحث تقديم طريقة لاجراء التصميم الديناميكي الهوائي ونمذجة للتنبؤ بعمل صف الريش الثابت ذات تدفق محوري.ويعتمد النموذج الرياضي على شروط التشغيل للضاغطة و خواص المائع المستخدم كمتطلبات ادخال. تم حساب كفاءة الضاغطة ، نسبة النظغاط و متغيرات التصميم الاخرى للضاغط .و كانت ظروف الدخول هي(T_O=٢٨٨.٢K, P_O =١٠١.٣Kpa). ووجد ان كفاءة الضاغط عند($D=٠.٥, \sigma = 1$) تساوي ٨٩.٥% . كما تمت دراسة توزيع عدد ماخ و الضغط و السرعة و الكثافة على طول ريشة الضاغطة باستخدام معادلة اويلر بعد تحويلها من المجال الفيزياوي ال المجال الحسابي باستخدام طريقة (Time Marching) .طريقة (MacCormack) تستخدم لحل الجريان غير اللزج و ثنائي الابعاد، باستخدام طريقة (Finite difference) . و استخدمت الزوجة الصناعية من الدرجة الرابعة لتأمين الاستقرارية و الدقة للجريان

LIST OF CONTENTS

ACKNOWLEDGMENTS

(In The Name of Allah, The Gracious and Merciful)

*Praise be to **"ALLAH"** and his prophet **"MOHAMMED"***

*I would like to express my deep thanks and gratitude to my supervisors, **Dr.Arkan K.Al-Taie** and **Dr.Abdul Kareem A.Wahab** for their support, guidance, and assistance throughout the various stages of the present work.*

I am also indebted to the staff of Mechanical Engineering Department for their assistance during my work.

I record my sincere gratitude to my dear family for their patience and moral support they provided me.

I am also grateful to all those who have helped in one way or other me in carrying out this research.

NASEER ABUDI MEDLOL

Appendix A

EULER EQUATIONS IN GENERALIZED COORDINATES

Transformation of Euler equation (٣.٧٢)into curvilinear coordinates (ξ,η) as independent variables may be performed as follows:

Using the chain rule of partial differentiation denoted by equations (٣.٤٤), equation (٣.٧٢) may be written as:

$$\frac{\partial Q}{\partial t}+\frac{\partial E}{\partial \xi}\xi_x+\frac{\partial E}{\partial \eta}\eta_x+\frac{\partial F}{\partial \xi}\xi_y+\frac{\partial F}{\partial \eta}\eta_y=0 \quad \ldots$$

(A.١)

Multiplying equation (A.١) by $\frac{1}{J}$ yields

$$\frac{1}{J}\frac{\partial Q}{\partial t}+\frac{1}{J}\frac{\partial E}{\partial \xi}\xi_x+\frac{1}{J}\frac{\partial E}{\partial \eta}\eta_x+\frac{1}{J}\frac{\partial F}{\partial \xi}\xi_y+\frac{1}{J}\frac{\partial F}{\partial \eta}\eta_y=0 \quad \ldots$$

(A.٢)

Consider the simple derivative expansion of the second term $\left[\frac{1}{J}\frac{\partial E}{\partial \xi}\xi_x\right]$, that is

$$\frac{\partial}{\partial \xi}\left(\frac{E}{J}\xi_x\right)=\frac{1}{J}\left(\frac{\partial E}{\partial \xi}\right)\xi_x+E\frac{\partial}{\partial \xi}\left(\frac{1}{J}\xi_x\right) \quad \ldots$$

(A.٣)

Rearranging equation (A.٣)

$$\frac{1}{J}\left(\frac{\partial E}{\partial \xi}\right)\xi_x = \frac{\partial}{\partial \xi}\left(\frac{E}{J}\xi_x\right) - E\frac{\partial}{\partial \xi}\left(\frac{1}{J}\xi_x\right) \quad \ldots$$

(A.٤)

And for other term

$$\frac{1}{J}\left(\frac{\partial E}{\partial \eta}\right)\eta_x = \frac{\partial}{\partial \eta}\left(\frac{E}{J}\eta_x\right) - E\frac{\partial}{\partial \eta}\left(\frac{1}{J}\eta_x\right) \quad \ldots$$

(A.٥)

Summation the right and left hand sides of equations (A.٤) and (A.٥)

$$\frac{1}{J}\left[\frac{\partial E}{\partial \xi}\xi_x+\frac{\partial E}{\partial \eta}\eta_x\right]=\frac{\partial}{\partial \xi}\left(\frac{E\xi_x}{J}\right)+\frac{\partial}{\partial \eta}\left(\frac{E\eta_x}{J}\right)-E\left[\frac{\partial}{\partial \xi}\left(\frac{\xi_x}{J}\right)+\frac{\partial}{\partial \eta}\left(\frac{\eta_x}{J}\right)\right]$$

…

(A.٦)

Substituting the matrices ξ_x and η_x of equations (٣.٦٣) in the last term of equation (A.٦)

$$-E\left[\frac{\partial}{\partial \xi}\left(\frac{\xi_x}{J}\right)+\frac{\partial}{\partial \eta}\left(\frac{\eta_x}{J}\right)\right]=-E\left[\frac{\partial}{\partial \xi}y_\eta-\frac{\partial}{\partial \eta}y_\xi\right]$$

$$=-E\left[\frac{\partial^2 y}{\partial \xi \partial \eta}-\frac{\partial^2 y}{\partial \eta \partial \xi}\right]=0$$

Thus, equation (A.٦) becomes

$$\frac{1}{J}\left[\frac{\partial E}{\partial \xi}\xi_x+\frac{\partial E}{\partial \eta}\eta_x\right]=\frac{\partial}{\partial \xi}\left(\frac{E\xi_x}{j}\right)+\frac{\partial}{\partial \eta}\left(\frac{E\eta_x}{J}\right)$$ …

(A.٧)

Applying the same manner for the term F

$$\frac{1}{J}\left(\frac{\partial F}{\partial \xi}\right)\xi_y=\frac{\partial}{\partial \xi}\left(\frac{F}{J}\xi_y\right)-F\frac{\partial}{\partial \xi}\left(\frac{1}{J}\xi_y\right)$$ …

(A.٨)

$$\frac{1}{J}\left(\frac{\partial F}{\partial \eta}\right)\eta_y=\frac{\partial}{\partial \eta}\left(\frac{F}{J}\eta_y\right)-F\frac{\partial}{\partial \eta}\left(\frac{1}{J}\eta_y\right)$$ …

(A.٩)

Summation the right and left hand sides of equations (A.٨) and (A.٩)

$$\frac{1}{J}\left[\frac{\partial F}{\partial \xi}\xi_y+\frac{\partial F}{\partial \eta}\eta_y\right]=\frac{\partial}{\partial \xi}\left(\frac{F\xi_y}{J}\right)+\frac{\partial}{\partial \eta}\left(\frac{F\eta_y}{J}\right)-F\left[\frac{\partial}{\partial \xi}\left(\frac{\xi_y}{J}\right)+\frac{\partial}{\partial \eta}\left(\frac{\eta_y}{J}\right)\right]$$

…

(A.١٠)

Substituting the matrices ξ_y and η_y of equations (٣.٦٣) in the last term of equation (A.١٠)

$$-F\left[\frac{\partial}{\partial\xi}\left(\frac{\xi_y}{J}\right)+\frac{\partial}{\partial\eta}\left(\frac{\eta_y}{J}\right)\right]=-F\left[\frac{\partial}{\partial\xi}\left(-x_\eta\right)+\frac{\partial}{\partial\eta}x_\xi\right]$$

$$=-F\left[-\frac{\partial^2 x}{\partial\xi\partial\eta}+\frac{\partial^2 x}{\partial\eta\partial\xi}\right]=0$$

The equation (A.١٠) becomes

$$\frac{1}{J}\left[\frac{\partial F}{\partial\xi}\xi_y+\frac{\partial F}{\partial\eta}\eta_y\right]=\frac{\partial}{\partial\xi}\left(\frac{F\xi_y}{J}\right)+\frac{\partial}{\partial\eta}\left(\frac{F\eta_y}{J}\right) \quad \ldots$$

(A.١١)

Substituting equations (A.٧) and (A.١١) in equation (A.٢) yields:

$$\frac{1}{J}\frac{\partial Q}{\partial t}+\frac{\partial}{\partial\xi}\left[\frac{E\xi_x}{J}\right]+\frac{\partial}{\partial\eta}\left[\frac{E\eta_x}{J}\right]+\frac{\partial}{\partial\xi}\left[\frac{F\xi_y}{J}\right]+\frac{\partial}{\partial\eta}\left[\frac{F\eta_y}{J}\right]=0$$

$$\frac{\partial}{\partial t}\left[\frac{Q}{J}\right]+\frac{\partial}{\partial\xi}\left[\frac{E\xi_x+F\xi_y}{J}\right]+\frac{\partial}{\partial\eta}\left[\frac{E\eta_x+F\eta_y}{J}\right]=0 \quad \ldots$$

(A.١٢)

Let

$$\overline{Q}=\frac{Q}{J}$$

$$\overline{E}=\frac{1}{J}\left(E\xi_x+F\xi_y\right)$$

$$\overline{F}=\frac{1}{J}\left(E\eta_x+F\eta_y\right)$$

And substituting them into equation (A.١٢) yields:

$$\frac{\partial\overline{Q}}{\partial t}+\frac{\partial\overline{E}}{\partial\xi}+\frac{\partial\overline{F}}{\partial\eta}=0 \quad \ldots$$

(A.١٣)

Which also represents the Euler equation (٣.٧٢) in conservation law form but in curvilinear coordinates (ξ,η) where $\overline{Q},\overline{E}$ and $\overline{F}$ are vectors given by:

$$\overline{Q}=\frac{1}{J}\begin{bmatrix}\rho\\ \rho u\\ \rho v\\ e_{\circ}\end{bmatrix}$$

$$\overline{E}=\frac{1}{J}\begin{bmatrix}\rho U\\ \rho uU+\xi_x p\\ \rho vU+\xi_y p\\ (e_{\circ}+p)U\end{bmatrix}$$

$$\overline{F}=\frac{1}{J}\begin{bmatrix}\rho V\\ \rho uV+\eta_x p\\ \rho vV+\eta_y p\\ (e_{\circ}+p)V\end{bmatrix}$$

And U, V are called contravarient velocity components defined by:

$$U=\xi_x u+\xi_y v$$

$$V=\eta_x u+\eta_y v$$

EXAMINING COMMITTEES CERTIFICATE

We certify that we have read this thesis entitled **"TRANSIENT BEHAVIOR OF HEAT TRANSFER IN FIN ARRAYS"** and as an examining committee, examined the student, **"Rehab Noor Mohammed"**, in its contents and that in our opinion it meets standard of a thesis for the degree of Master of Science in Mechanical Engineering.

Signature:
Name: Asst.Prof.
Dr. Arkan k. Al-Taie
(Supervisor)
Date: / / ٢٠٠٤

Signature:
Name: Asst.Prof.
Dr. Haroun A.K.Shahad
(Supervisor)
Date: / / ٢٠٠٤

Signature:
Name:Asst.Prof.
Adil A.Al-Mousoy
(Supervisor)
Date: / /٢٠٠٤

Signature:
Name: Asst.Prof.
Dr. Majid H. Magieed
(Member)
Date: / / ٢٠٠٤

Signature:
Name: Asst.Prof.
Dr. Tahseen A.Al-Hatab
(Member)
Date: / / ٢٠٠٤

Signature:
Name:Asst. Prof.
Dr. Jalal M. Jaleel
(Chairman)
Date: / / ٢٠٠٤

Approval of the Mechanical Engineering Department.
Head of the Mechanical Engineering Department.

Signature:
Name: Asst.Prof.
Dr. Emad S.Ali
Date: / / ٢٠٠٢

Approval of the College of Engineering.
Dean of the College of Engineering.

Signature:
Name: Asst.Prof.
Haroun A.K. Al-Shahad
Date: / /٢٠٠٤

Chapter One

INTRODUCTION

١.١ General

Turbomachines are devices in which energy is transferred either to or from a continuously flowing fluid by the dynamic action of one or more moving blade rows.

The above definition of turbomachinery embraces both open and closed types. Open turbomachinery (such as propellers, windmills, and unshrouded fans) influence an indeterminate quantity of fluid. While in closed turbomachinery (such as centrifugal, axial flow compressors, etc.) a finite quantity of fluid passes through a casing in unit time, in this work focus on the closed turbomachinery namely (axial-flow compressor) used in gas turbine engines .

In the gas turbine engine, compression of the air before expansion through the turbine is effected by one of two basic types of the compressor, one giving a centrifugal flow and the other an axial flow. Both types are driven by the engine turbine and are usually coupled directly to the turbine shaft. The centrifugal flow compressor is a single or two-stage unit employing an impeller to accelerate the air and a diffuser to produce the required pressure rise. The axial flow compressor is a multi-stage unit employing alternate rows of rotating (rotor) blades and stationary (stator) blades, to accelerate and diffuse the air until the required pressure rise is obtained.

١.٢ Axial –flow compressor

An axial flow compressor is built up of stages, with each stage consisting of a row of rotating blades (rotor blades) and a row of fixed blades (stators). The rotating blades are attached to a number of disks mounted on a central shaft forming the rotor. The stators are fastened to the inside of the compressor casing as shown in Fig.(١.١). Usually, the number and size of the rotor and stator blades gradually decrease from the compressor inlet to outlet with a subsequent reduction in the cross-sectional flow area.

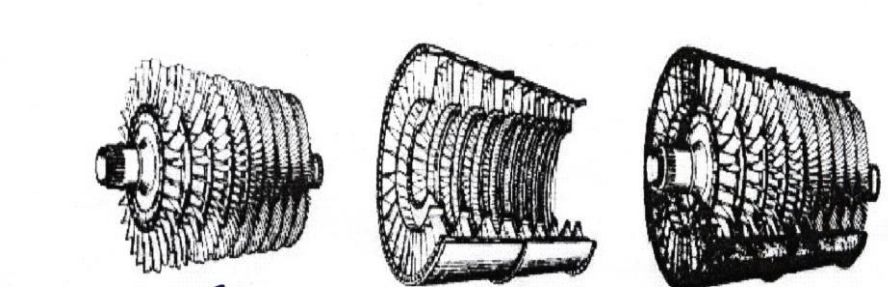

c b a

a: Axial-flow compressor assembly sectional view.

b: Axial-flow compressor rotor.

c: Axial-flow compressor stator.

Fig. (١.١) The axial-flow compressor

The function of the compressor is to raise the pressure of the air prior to entering the combustor. Within each stage, the airflow is first accelerated and then decelerated with a resulting increase in pressure and temperature, and a decrease in air volume. One of the key factors which affect the compressor and engine efficiency is the compressor pressure ratio, which is a measure of the compressor's outlet pressure to its inlet pressure. To improve engine efficiency, the trend has been toward ever increasing pressure ratios, sometimes in excess of ٢٥:١.

The aerodynamic study of an axial flow compressor is necessary to help the designer select any parameter required in the design process.

It can be seen from literature that the simple implicit techniques are difficult to apply nonlinear problems and require large computer time. Even the explicit techniques suffer from similar problems when dealing with nonlinear, two-and three-dimensional problem. The MacCormack method is an explicit finite difference technique, which is second-order-accurate in both space and time.

The algebraic expression technique is used to transform the body shape in the physical domain into rectangular shape in the computational domain. In the algebraic grid generation scheme, known functions are used to map the curvilinear coordinate system in the physical space to a convenient (usually rectangular) system in the computational domain. The technique is based on the use of interpolation functions [٢].

The compressor considered in the present work is a multistage of axial flow type and the an explicit method will be used to calculate the fluid properties in the passage between blades and the Euler equations governing the motion of an inviscid, non heat- conducting fluid flow require will be solved.

١.٣ Work Objective

The aim of the present work is:

١. Modeling and predication of a stator of axial-flow compressor for the predication of optimum design.

٢. Study of the flow conditions in compressor blade passages using the time marching method.

٣. Construction of a computer program to implement the computational steps in design procedure with capability of studying

the effects of design variables (inlet absolute flow angle, blade speed ratio, inlet and outlet angles of blades) on compressor design.

١.٤ Thesis layout

The thesis falls into five chapters. Chapter one presents the introduction. Chapter two is concerned with a brief literature review. Chapter three is divided into four sections; section one presents the aerodynamic design, section two presents the grid generation, section three presents the numerical solution and section four presents the computer program. Chapter four presents the results and their discussion while chapter five presents the conclusions drawn from this work with suggestions for further work.

Chapter Two

Literature Review

Ron H., ١٩٨٢, [٣], present a fast explicit numerical scheme for solving the unsteady Euler flow equations to obtain steady solutions. The scheme is constructed by combining the multiple-grid technique with a new second-order accurate finite volume integration method. Special formulas, consistent with local wave propagation are utilized to determine corrections of flow properties at each grid point. These formulas are found to provide useful insights into the solution procedure. Calculated results for both internal and external flow problems are given to demonstrate the accuracy and the computational efficiency of this scheme.

Denton, ١٩٨٣, [٤], presents the solutions of the Euler equations by using time -marching technique which are very widely used for calculation of the flow through turbomachinery blade rows. All methods suffer from the disadvantages of shock smearing, lack of entropy conservation and comparatively long run times A new method is described, which reduces all these problems. The method is based on the author opposed difference scheme but this is applied to a new grid consisting of quadrilateral elements which do not overlap and have nodes only at their corners. The use of a non-overlapping grid reduces finite differing errors and gives a complete freedom to vary the size of the

elements. Both these factors help to improve entropy conservation. Considerables saving in run time (by a factor of about ٣) are obtained by using a simple multigrid method where by the solution is advanced simultaneously on a course and on a fine grid. The resulting method is simpler, faster, and more accurate.

Moon, ١٩٨٦, [٥], presents a new efficient procedure for the numerical solution of the Navier-Stokes equations, using line Gauss-Seidel and Newton iterative methods which are recently presented by Mac-Cormack. The numerical procedure was applied to the compressible viscous flow of a two-dimensional flow within a transonic converging-diverging nozzle. Although the present method showed a very high numerical efficiency, the fact that the grid size might severely affect convergence was questionable. It was suggested that the number of iterations would vary directly with the number of grid points. The effect of grid size on convergence was tested by refining the grid size by factors of two and four for the same transonic problem presented by Mac-Cormack.

Lavante, ١٩٨٧, [٦], presents the development of a numerical method for solving the two-dimensional Euler equations for steady-state solutions by using flux vector splitting. The equations are expressed in curvilinear coordinates and the finite volume approach is used. The energy equation is omitted since only steady-state solutions are required. A simplified implicit operator is employed to reduce the computational effort of the present method. Convergence characteristics are compared with predictions obtained by other authors.

Gerolymos, ١٩٨٨, [٧], has developed an algorithm for numerically integrating the Euler equations in blade-to-blade surface formulation. The method simulates all the interblade channels of an annular cascade. The equations are discretized in a grid that moves in order to follow the vibration of the blades. The equations are integrated by using the explicit Mac-Cormack scheme in finite difference formulation. A number of numerical results show the aptitude of the method to simulate both started and unstarted supersonic flow in vibrating cascades.

An explicit, time- marching multiple grid technique was demonstrated by **Davis et al, ١٩٨٨, [٨],** for prediction of a quasi-three-dimensional turbomachinery compressor cascade performance. A numerical investigation was performed by the use of Navier-Stokes technique. The algebraic two –equation turbulence model was used for turbulence modeling.

Peraire, Jaime and Ken Morgan, ١٩٨٨, [٩], an explicit finite element solution procedure for the three-dimensional Euler equations is presented. The solution domain is automatically meshed using a tetrahedral mesh generator, which is an extension of our previous two-dimensional work. Several examples are included to illustrate the performance of the generator and the solver. An adaptive mesh regeneration procedure is used for the first time in three dimensions.

Sanz and Gehrer, ١٩٩٥, [١٠], presents a finite-difference, implicit, TVD (Total Variation Diminishing) upwind scheme based on Roe's approximate Riemann solver for calculating the flow in transonic cascades. In the present solver, the relaxation is performed with a line Gauss-Seidel technique. To obtain time-accurate solutions at each time

level, inner iterations, so-called Newton iterations, are introduced. A comparison of this modern scheme is presented with an explicit scheme and an explicit four-stage Runge-Kutta scheme with regard to obtainable accuracy, maximal Courant Friedrichs and Lewy stability criterion (CFL) number and convergence characteristics. Finally, the computed results concerning the VKI-١ blade profile are discussed and some experimental data, to be regarded as initial operation of the institutes cascade test stand, are presented for visual comparison of the respective flow field.

Mohd. Zamri, ١٩٩٧, [١١], describes a two-dimensional time-accurate time-marching Euler solver for turbomachinery applications. It uses the second-order accurate cell-vertex finite-volume spatial discretization and fourth-order accurate Runge-Kutta temporal integration. Three convergence acceleration techniques i.e. local time-stepping, enthalpy damping and implicit residual averaging are added to the basic scheme and increase the convergence rate by a factor of ٤ in steady flow computations. The solver has been extensively validated against exact solutions and experimental measurements in convergence-divergence nozzle, unsteady flow in two-dimensional channel and blade-to blade flow in a nozzle cascade. The agreements obtained have been excellent.

Demeulenaere, ١٩٩٨, [١٢], outlines an iterative procedure for three- dimensional blade design, in which the three-dimensional blade shape is modified by using a physical algorithm, based on the transpiration model. The transpiration flux is computed by means of a modified Euler solver, in which the target pressure distribution is imposed along the blade surfaces. Only a small number of modifications are needed to obtain the final geometry. A three-dimensional analysis

code was successfully transformed into a design code, by changing the boundary conditions on the blade walls, and by means of a geometry modification algorithm. The method shows a rapid convergence to the blade geometry corresponding to the target pressure distribution, for subsonic and transonic design. The solver is able to treat highly three-dimensional flows and geometries, and the effects of a blade lean are taken into account, which is considered as an advantage, when compared to two-dimensional design methods. An important advantage of the method is the possibility of using the same code for the design and analysis of a blade.

Amano, ٢٠٠٠, [١٣], presents a time-marching algorithm that have been mostly used in gas turbine cascade flow analysis. A new efficient implicit scheme based on the second-order time and spatial difference algorithm for solving steady flow by using time-marching Navier-Stokes equations, was developed for predicting turbine cascade flows. The difference scheme comprises an explicit part in the intermediate time-step and an implicit part in the local time-step. The viscous flux vectors are decomposed to simplify the flow calculation in the explicit step. The time difference terms are expressed in terms of the viscous dependent terms that appear in the diffusion terms in the form by adding eigenvalues of viscous flux matrices into the time derivation term. This method has been used to calculate the flow around cascades. The computed results were compared with experimental data as well as with other published computations. The comparisons for both surfaces pressures showed a good agreement with experiments.

Pulliam, ١٩٨٦, [١٤], analyzes various artificial models that are central difference algorithms for the Euler equations for their effect on

accuracy, stability and convergence rates. In particular, linear and nonlinear models are investigated by using an implicit approximate factorization code for transonic airfoils. It is shown that accurate, error free solutions with sharp shocks can be obtained using a central difference algorithm coupled with an appropriate nonlinear artificial dissipation model.

Arkan Altaie and Talib Farge, ١٩٩٤, [١٥], presented a simplified method for designing an axial flow compressor. They showed that increasing the diffusion factor and solidity allows a greater stage pressure ratio and hence the possibility of reducing compressor stages. The optimum range of diffusion factor is to be in range of (٠.٤ to ٠.٦), while the solidity factor is in range of (٠.٩ to ١.١). Also they concluded that at a fixed diffusion factor and solidity, the only way to increase stage compression ratio is by increasing the inlet Mach number.

Uzol, ١٩٩٥, [١٦], presents a construction of a very fast, loosely-coupled, quasi-three-dimensional design system is constructed for the preliminary prediction of the turbomachinery blade shapes. It is obtained by coupling a duct-flow solver and a blade-to-blade solver. The duct-flow solver is used for calculating the upstream and downstream radial evolutions of the flow variables. The blade-to-blade solver is a two-dimensional transonic Euler solver, which uses intrinsic streamline grid, a cell-centered finite volume scheme and Newton-Raphson linearization technique. The unknowns are reduced to two, density and grid node displacement, at each grid node and this creates the speed of the blade-to-blade solver, thus the design system. After the radial distributions of the flow variables are determined by the duct-flow solver, the blade-to-blade solver is run at each radial station. For the rotor blades, the loading which

results from this calculation is compared with the desired one and accordingly the blade shape is modified by changing the lift on the blade and running the blade-to-blade solver, now in design mode. Similar design procedure is applied for the design of stator blades and the turning angle is used as the design target instead of the loading. A sample design is accomplished for a rotor and a stator blade. The blade-to-blade solver is applied to two analytical test cases for the verification of the analysis and design capability and an experimental rotor test case for the verification of the modification of the code for the rotating frame of reference. Being an inviscid solver and the lack of possibility of the three dimensional effects due to the loose coupling of the duct-flow solver and the blade-to-blade solver are the main drawbacks of the method.

Montgomery and Verdon, ١٩٩٦, [١٧], present an analysis of three-dimensional, linearized, Euler developed to provide an efficient unsteady aerodynamic analysis that can be used to predict the aeroelastic and aeroacoustic response characteristics of axial-flow turbomachinery balding. The field equations and boundary conditions needed to describe nonlinear and linearized inviscid unsteady flows through a blade row operating within a cylindrical annular duct. In addition, a numerical model for linearized inviscid unsteady flow, which is based upon an existing nonlinear, implicit, wave-split, finite volume analysis, is described. These aerodynamic and numerical models have been implemented into an unsteady flow code, called LINFLUX. A preliminary version of the LINFLUX code is applied to select, benchmark three-dimensional, subsonic, unsteady flows, to illustrate its current capabilities and to uncover existing problems and deficiencies. The numerical results indicate that good progress has been made toward developing a reliable and useful three-dimensional prediction capability.

However, some problems, associated with the implementation of an unsteady displacement field and numerical errors near solid boundaries, still exist. Also, accurate far-field conditions must be incorporated into the LINFLUX analysis, so that this analysis can be applied to unsteady flows driven by external aerodynamic excitations.

Sabanca and Murat, ١٩٩٧, [١٨], presents a solution of two-dimensional inviscid compressible equations of fluid flow solved by using fourth order Runge-Kutta scheme for time stepping and upwind finite volume with second order accurate is applied to governing equations. The development of the scheme is presented in details including the boundary condition implementation, time step selection criterion and explicit preconditioning techniques applied to unsteady compressible flows. Test cases for two-dimensional external flow around NACAOOl٢, NLR٧٣٠١ (two elements), RAE٢٨٢٢ airfoils and Bumps are solved by the developed code for supersonic, transonic, subsonic and low subsonic cases. The major superiority of the code is its capability to solve the compressible as well as incompressible flows at very low Mach numbers without using the incompressible flow equations and its second order spatial accuracy without using flux limiters.

Zhang and Camaero, ١٩٩٨, [١٩], presented different upwind strategies based on characteristic analysis. All methods are based on approximate Riemann solver in finite volume framework. They differ from each other mainly in the choice of the upwind direction. The strength and weakness of the individual schemes are addressed from their characteristic compatibility equations and are supported by numerical results. Their performance concerning solution accuracy, grid independence and convergence behavior are investigated and are

compared through various types of problems, including subsonic, transonic and supersonic flows.

Rolf Dornberger and Peter Stall, ٢٠٠٠, [٢٠], investigate particular aspects of performing multidisciplinary optimizations in different turbomachinery design steps. The differences in the optimization approaches and used methods in preliminary and final design steps are shown. An optimization environment is developed, which supports multidisciplinary turbomachinery design. The general concept and components are explained. Some of the implemented methods and tools, which are used particularly in multidisciplinary optimization, are presented. Examples show the potential of the proposed methods. Pareto-optimization enables multi-objective optimizations, very important in preliminary design steps. Various objectives are optimized concurrently. An entire set of Pareto-optimal solutions, design variants, can be computed. Response surfaces promise to accelerate the entire design process. They are able to approximate computational expensive solvers within a fraction of their original computing time. Two different schemes, polynomial approximations and neural networks, are presented. Using different examples, both methods are compared. In final turbomachinery design steps, ٣D blade design optimizations need quickly converging optimization algorithms treating one single aerodynamic objective. The other involved disciplines lead to further constraints. Extensions for using the optimization environment in such ٣D blade optimizations are presented.

Ergun, ٢٠٠٠, [٢١], evaluated the effects of sensitivities on the performance of turbomechinery cascade design optimization. The Euler equations were used for the flow analyses. A sensitivity code was

developed to analytically obtain sensitivities for the two-dimensional Euler equations. Several inverse design optimizations were performed to evaluate the merits of analytical approach in comparison with the finite-difference approach. The ease of implementation makes the finite-difference sensitivity method popular in many aerodynamic design optimization applications. But finite-difference method generally produces inaccurate sensitivities and increases the computational cost. The accuracy of FDS was evaluated and it was observed that the accuracy of sensitivities in finite-difference approach is dependent on the perturbation magnitude of design variables and the flow-field initialization. Therefore, analytical method is introduced to improve the accuracy of sensitivities. In this analytical method, the sensitivity equations were obtained by differentiating Euler equations with respect to the design variables and subsequently solved for the response sensitivities. The material derivative concept of continuum mechanics was implemented to obtain shape sensitivities. Analytical sensitivities were evaluated and compared with the finite-difference sensitivities. The results show that the analytical approach provide accurate sensitivities. Additionally, the accuracy of analytical sensitivities does not depend on the level of convergence which is desirable in design optimization. In order to evaluate the effects of the sensitivities on the performance of the design process, several inverse designs were performed using both analytical and finite-difference sensitivities. The results show that inaccurate sensitivities slow down the convergence of the optimization process. The analytical approach provides accurate sensitivities therefore, design optimizations converge faster, and hence reduce the design cost.

Helmut Sobieczky, ٢٠٠٢, [٢٢], explains the importance of preprocessing tools for successful design and optimization in practice of turbomachinery engineering. The development of problem-oriented

computational geometry generation software is illustrated for the example of aerodynamic inverse design of transonic flow elements that define the compatible boundary conditions (surfaces) in detail. Resulting from learned sensitivity of high speed flows to small changes in airplane wing or turbomachinery blade geometry, preprocessing software is provided to create parametric shapes to be varied for optimization cycles or numerical simulation of mechanical adaptation processes. Supporting the need to design from a multidisciplinary viewpoint, parameterized geometry components for aerodynamic, as well as for thermal and structural considerations are defined. Examples for turbomachinery blade design and optimization are given.

Zaid Waassil, ٢٠٠٠, [٢٣], developed a computational and experimental investigation for the flow through a cascade of a twisted compressor blades. Since the flow between twisted blades is very complex and completely three dimensional, it was simplified by considering the flow consisting of separated two-dimensional sections. Each section was solved numerically using the two-dimensional incompressible fully viscous flow equations in general orthogonal coordinate system using the finite volume method. The general orthogonal coordinate system was generated by the finite difference numerical solution of the transformation Laplace's equations. A computer program in QuickBasic was built to solve the Laplace's equations for the generation of the orthogonal coordinate system. The numerical solution of the flow equation in general orthogonal coordinates. The experimental investigation was carried out on a cascade of four twisted blades. These blades have a span of (٠.٤٥-meter) and a

chord of (٠.٢٢٥-meter), with a profile based on the NACA ٦٥series profiles.

Ali Khadir, ٢٠٠٠, [٢٤], presents an explicit, time-marching, staggered grid for solving the unsteady, incompressible, two-dimensional, isothermal and turbulent flow through NACA (٦٥) compressor cascade was modeled by using continuity, Navier-Stokes and k-ε turbulence model equations. The discretized control volume approach was used in a numerical scheme to solve the given system the differential equations. The unsteady forces acting on the cascade was measured with employing a modified version of the strain gage system and compared with a steady cases, and then was compared with the theoretical result.

There is a large number of papers deal with the aerodynamic design and calculation of the flow between blade to blade using Euler equations or Navier-Stokes equations. There are many techniques that deal with the numerical analysis of the Euler equations by using finite volume, finite element, finite difference, and multigrid for implicit schemes.

In the present work, unsteady, compressible, two-dimensional, adiabatic flow through compressor cascade will be modeled by using Euler equations and the explicit time-dependent solution by using MacCormack predictor corrector finite difference technique to solve the given system of differential equations.

Chapter Three

Theoretical Approach

٣.١ Aerodynamic Design of Axial Flow Compressor

٣.١.١ Introduction

The basic building block of the aerodynamic design of an axial flow compressor is the cascade, an endlessly repeating array of airfoils fig. (٣.١) that results from conceptual "unwrapping" of the rotating (rotor) or stationary (stator) airfoils. Each cascade passage acts as a small diffuser, and is said to be well designed or behaved when it provides a large static pressure rise without incurring unacceptable total pressure losses and /or flow instabilities due to shock waves and /or boundary layer separation. A multistage compressor may be created by placing similar stages in series to give pressure compression ratio required to gas turbine engines, because every stage gives part of this ratio. This analysis depends on behavior of the flow at average radius (halfway between the hub radius and tip radius), after this introduction the development of design tools for compressors follows [١]

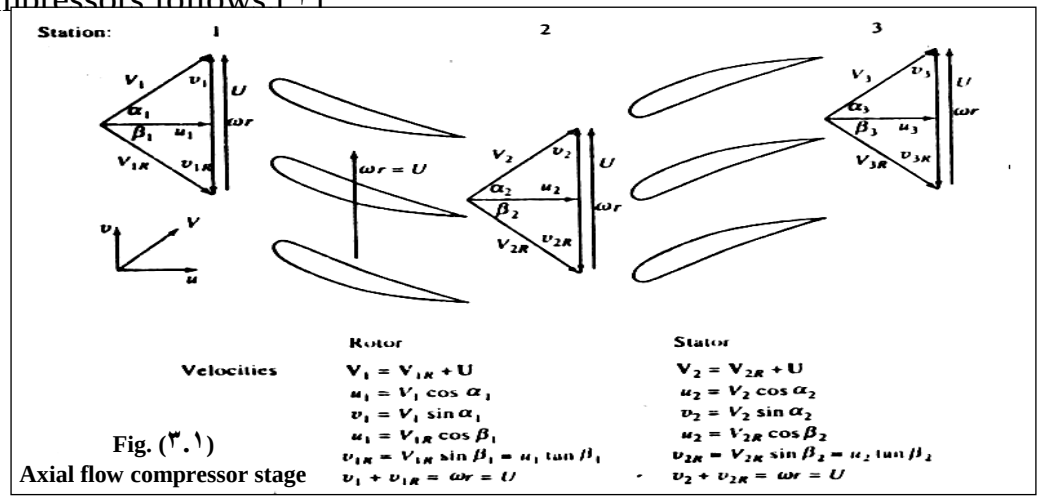

Fig. (٣.١)
Axial flow compressor stage

❖ **Assumptions**

١.Two-dimensional flow (i.e. no variation or component of velocity normal to page).

٢.Constant mean radius.

٣.Polytropic efficiency η_p is representing stage losses.

❖ **Analysis**

Given D, M١, γ, σ, η_p

❖ **Conservation of Mass**

$$\rho_1 u_1 A_1 = \rho_2 u_2 A_2 = \rho_3 u_3 A_3$$

…(٣.١)

❖ **Repeating-row constraint**

$$\beta_2 = \alpha_1$$

$$v_{2R} = v_1 = wr - v_2$$

$$v_1 + v_2 = wr$$

…(٣.٢)

Diffusion factor (D)

Since,

$$D = 1 - \frac{V_{2R}}{V_{1R}} + \frac{v_{1R} - v_{2R}}{2\sigma V_{1R}}$$

and $$D = 1 - \frac{\cos\alpha_2}{\cos\alpha_1} + \frac{\tan\alpha_2 - \tan\alpha_1}{2\sigma}\cos\alpha_2$$

…(٣.٣)

from eq.(٣.٣) after simplify we get on outlet absolute angle

$$\cos\alpha_2 = \frac{2\sigma(1-D)\Gamma + \sqrt{\Gamma^2 + 1 - 4\sigma^2(1-D)^2}}{\Gamma^2 + 1}$$

…(٣.٤)

where $\Gamma = \dfrac{2\sigma + \sin\alpha_1}{\cos\alpha_1}$

…(٣.٥)

Stage total temperature ratio τ_s.

Euler equation which relates change in energy to the change in tangential momentum.

$$C_P(T_{O3} - T_{O1}) = wr(v_2 - v_1)$$

from equation (٣.٢)

$$wr = v_1 + v_2$$

then,

$$C_P(T_{O3} - T_{O1}) = (v_2 + v_1)(v_2 - v_1)$$

$$v_2^2 - v_1^2 = V_2^2 - V_1^2$$

$$\frac{T_{O3}}{T_{O1}} = 1 + \frac{v_2^2 - v_1^2}{C_P T_{t1}}$$

or $\tau_s = \dfrac{T_{O3}}{T_{O1}} = \dfrac{(\gamma - 1)}{1 + \left[(\gamma - 1)/2\right] M_1^2}\left(\dfrac{\cos^2\alpha_1}{\cos^2\alpha_2} - 1\right) + 1$

…(٣.٦)

and $\pi_s = \dfrac{P_{O3}}{P_{O1}} = \left(\dfrac{T_{O3}}{T_{O1}}\right)^{\left(\frac{\gamma\eta_p}{\gamma - 1}\right)}$

$$\pi_s = (\tau_s)^{\left(\frac{\gamma\eta p}{\gamma - 1}\right)}$$

…(٣.٧)

Stage efficiency η_s

$$\eta_s = \frac{\left(\frac{P_{O3}}{P_{O1}}\right)^{\left(\frac{\gamma-1}{\gamma}\right)} - 1}{\left(\frac{T_{O3}}{T_{O1}}\right) - 1}$$

or

$$\eta_s = \frac{(\pi_s)^{\frac{\gamma-1}{\gamma}} - 1}{(\tau_s) - 1}$$

…(٣.٨)

for multistage axial flow compressor

Compressor pressure ratio π_c

$$\pi_c = (\pi_s)^n$$

…(٣.٩)

Compressor efficiency η_c

$$\eta_c = \frac{(\pi_c)^{\frac{\gamma-1}{\gamma}} - 1}{(\tau_s) - 1}$$

…(٣.١٠)

Inlet velocity/wheel speed ratio

$$V_1 = \frac{u_1}{\cos\alpha_1}$$

and $wr = v_1 + v_2 = u_1 + (\tan\alpha_1 - \tan\alpha_2)$

so, $$\frac{V_1}{wr} = \frac{1}{(\cos\alpha_1)(\tan\alpha_1 + \tan\alpha_2)}$$

…(٣.١١)

٣.٢ General solution

The behavior of all possible repeating –row compressor stages with given values of D, M١, $\gamma, \sigma, and \eta_p$ can now be computed. This is done by selecting any and using the following sequence of equations, expressed as functional relationships:[١]

$$\alpha_2 = f(D, \sigma, \alpha_1)$$

...(٣.٤)

$$\Delta\alpha = \alpha_2 - \alpha_1$$

$$\tau_s = f(M_1, \gamma, \alpha_1, \alpha_2)$$

...(٣.٦)

$$\pi_s = f(\tau_s, \gamma, \eta_p)$$

...(٣.٧)

$$\eta_s = f(\tau_s, \pi_s, \gamma, \eta_p)$$

...(٣.٨)

$$\pi_c = f(\pi_s, n)$$

...(٣.٩)

$$\eta_c = f(\pi_c, \tau_s, \gamma)$$

...(٣.١٠)

$$\frac{V_1}{wr} = f(\alpha_1, \alpha_2)$$

...(٣.١١)

To find the properties of air in the compressor, the flow is assumed frictionless, adiabatic, and isothermal. The following equations can be used to find these properties. The mathematical model developed is based upon the following equations as shown in fig. (٣.١),[١].

The static temperature is calculated as follows: -

$$T_1 = \frac{T_{o1}}{1+\left(\frac{\gamma\ -1}{2}\right)M_1^2}$$

…(٣.١٢)

Air absolute velocity: -

$$V_1 = M_1\sqrt{\gamma\ R\ T_1}$$

…(٣.١٣)

From velocity triangles of fig.(٣.١)

The axial velocity inlet to the rotor is: -

$$u_1 = V_1.\cos\alpha_1$$

…(٣.١٤)

The tangential velocity at inlet to the rotor: -

$$v_1 = V_1.\sin\alpha_1$$

…(٣.١٥)

The static pressure at inlet to the rotor: -

$$P_1 = \frac{P_{O1}}{\left[1+\left(\frac{\gamma-1}{2}\right)M_1^2\right]^{\frac{\gamma}{\gamma-1}}}$$

…(٣.١٦)

The inlet relative velocity angle: -

$$B_1 = \tan^{-1}\left(\frac{wr - v_1}{u_1}\right)$$

…(٣.١٧)

The inlet relative Mach number: -

$$M_{1R} = \frac{V_{1R}}{\sqrt{\gamma R T_1}}$$

…(٣.١٨)

Relative total temperature inlet to the rotor: -

$$T_{O1R} = T_1\left(1 + \frac{\gamma - 1}{2} M_{1R}^2\right)$$

…(٣.١٩)

Relative total pressure inlet to the rotor: -

$$P_{O1R} = p_1\left(\frac{T_{O1R}}{T_1}\right)^{\frac{\gamma}{\gamma-1}}$$

…(٣.٢٠)

Relative total pressure exit from the rotor: -

$$P_{O2R} = P_{O1R}\left[1 - \phi_{cr}\frac{\frac{\gamma M_{1R}^2}{2}}{\left[1 + \left(\frac{\gamma - 1}{2}\right)M_{1R}^2\right]^{\frac{\gamma}{\gamma-1}}}\right]$$

…(٣.٢١)

As the flow is assumed adiabatic, then: -

$$T_{O2R} = T_{O1R}$$

…(٣.٢٢)

Total temperature at exit from rotor: -

$$T_{O2} = T_{O1} + \Delta T_O$$

…(٣.٢٣)

The exit relative velocity angle: -

$$B_2 = \tan^{-1}\frac{u_2}{u_1}\left[\tan B_1 - \frac{Cp}{wr^{*}u_1}(T_{O3} - T_{O1})\right]$$

…(٣.٢٤)

The axial velocity at inlet to the stator: -

$$u_2 = \frac{u_2}{u_1}u_1$$

…(٣.٢٥)

The axial relative velocity at outlet from the rotor: -

$$v_{2R} = u_2 \tan B_2$$

…(٣.٢٦)

The relative velocity at outlet from the rotor: -

$$V_{2R} = \sqrt{u_2^2 + v_{2R}^2}$$

…(٣.٢٧)

The inlet absolute flow angle for stator: -

$$\alpha_2 = \tan^{-1}\frac{u_2 - v_{2R}}{u_2}$$

…(٣.٢٨)

The velocity at inlet to the stator: -

$$V_2 = \sqrt{u_2^2 + v_2^2}$$

…(٣.٢٩)

The static pressure at inlet to the stator: -

$$P_2 = P_{O2R}\left(\frac{T_2}{T_{O2R}}\right)^{\left(\frac{\gamma}{\gamma-1}\right)}$$

…(٣.٣٠)

The total pressure at inlet to the stator: -

$$P_{O2} = P_2\left(\frac{T_{O2}}{T_2}\right)^{\left(\frac{\gamma}{\gamma-1}\right)}$$

…(٣.٣١)

The total pressure at exit from the stator: -

$$P_{O3} = P_{O2}\left[1-\phi_{cs}\frac{\gamma M_2^2/2}{\gamma M_{1R}/\left[1+\left(\gamma-1/2\right)M_2^2\right]^{\frac{\gamma}{\gamma-1}}}\right]$$

…(٣.٣٢)

For isothermal flow: -

$$T_{O3} = T_{O2}$$

…(٣.٣٣)

The static temperature at exit from the stator: -

$$T_3 = \frac{T_{O3}}{1+\frac{\gamma-1}{2}M_3^2}$$

…(٣.٣٤)

The absolute velocity at exit from the stator : -

$$V_3 = M_3\sqrt{\gamma RT_3}$$

…(٣.٣٥)

The axial velocity at exit from the stator :

$$u_3 = V_3.\cos\alpha_3$$

…(٣.٣٦)

The tangential velocity at exit from the stator: -

$$v_3 = V_3.\sin\alpha_3$$

…(٣.٣٧)

The stage efficiency: -

$$\eta_s = \frac{\left(\frac{P_{O3}}{P_{O1}}\right)^{\frac{\gamma-1}{\gamma}} - 1}{\left(\frac{T_{O3}}{T_{tO}}\right) - 1}$$

...(٣.٣٨)

٣.٢.١ Flow Path Dimensions

For uniform total properties at any section i, the annulus area A_i of the flow, can be obtained from the mass flow parameter (MFP) as follows: -

$$A_i = \frac{\dot{m}\sqrt{T_{Oi}}}{P_{Oi} * \cos\alpha_i * MFP(M_i)}$$

…(٣.٣٩)

Where

α_i: Is the angle that the velocity V_i makes with the centerline of the annulus.

$$MFP(M_i) = \frac{M_i \sqrt{\gamma / R}}{\left[1 + \left((\gamma - 1)/2\right) M_i^2\right]^{\frac{\gamma+1}{2(\gamma-1)}}}$$

…(٣.٤٠)

The airfoil angles of both the rotor and stator can be calculated from the flow angles, given the incidence angle and solidity for each. To obtain the exit airfoil angle, as follows:

$$\delta_c = \frac{\gamma_i - \gamma_e}{4\sqrt{\sigma}}$$

…(٣.٤١)

Eq.(٣.٤١) is rearranged, the exit angle of blade

$$\gamma_e = \frac{4\alpha_e\sqrt{\sigma} - \gamma_i}{4\sqrt{\sigma} - 1}$$

…(٣.٤٢)

٣.٣ Grid Generation

Grid generation technique can be roughly classified into three categories [٢٥]:

١.Algebraic methods.

٢.Conformal mapping based on complex variables.

٣.Partial differential methods.

Algebraic and differential equation techniques show a promise for continued development when used in conjunction with finite difference method.

Because the governing equations in fluid dynamics contain partial differentials and are too difficult in most cases to solve analytically, these partials are generally replaced by the finite difference terms. This procedure discretizes the field into a finite number of states. These states, when plotted from a grid, or mesh of points or field points, can give the solution. The numerical method generally used in CFD can be classified as finite difference, finite volume, and finite element.

The generation of a grid, with uniform spacing is a simple exercise within a rectangular physical domain. Grid points may be specified as coincident with the boundaries of the physical domain, thus making specification of boundary conditions considerably less complex.

Unfortunately, the majority of the physical domains of interest are nonrectangular.

Therefore, imposing a rectangular computational domain on such a physical domain will require some sort of interpolation for the implementation of the boundary conditions. Since the boundary conditions have a dominant influence on the solution of the equation, such an interpolation causes inaccuracies at the place of greatest sensitivity.

To overcome these difficulties, a transformation from physical space to computational space is introduced. This transformation is accomplished by specifying a generalized coordinate system, which will map the nonrectangular grid system, the physical space to a rectangular uniform grid spacing in the computational space.

٣.٣.١ Grid Generation Techniques

The problem of grid generation is that of determining the mapping which takes the grid points from the physical domain to the computational domain. Several requirements must be placed on such mapping. Therefore a grid system with the following features is desired [٢٦]:

١. A mapping which guarantees one-to-one correspondence ensuring grid lines of the same family do not cross each other.

٢. Smoothness of the grid distribution.

٣. Orthogonality or near orthogonality of the grid lines.

٤. Options for grid clustering.

٣.٣.٢ Algebraic Mesh Generation

The simplest grid generation technique is the algebraic method. The derivatives of the boundary in the physical plane provide even more flexibility in the mapping. For instance, orthogonality at the boundary can be forced in the physical plane. In most problems, the boundaries are not analytic function but are simply prescribed as a set of data points. In this case, the boundary must be approximated by a curve fitting procedure to employ algebraic mapping [٢٦,٢٧].

٣.٣.٣ Assessment of Algebraic Grid Generator

The major advantages of algebraic methods (as compared to differential methods) are:

١. The speed, simplicity and flexibility with which a grid can be generated.

٢. Algebraic procedures have low computational cost and explicit control of grid points distribution.

٣.Matrix may be evaluated analytically, thus avoiding numerical approximation.

٤.The ability to cluster grid points in different regions can be easily implemented.

The major disadvantages of algebraic methods are:

١.The grids are less smooth than those generated by the solution of PDEs.

٢.Discontinuities at a boundary may propagate into the interior region, which could lead to errors due to sudden changes in the metrics.

٣.٣.٤ Generalized Coordinate Transformation: -

The equations of motion are transformed from the physical space (x, y) to computational space (ξ,η) [٢٧]:

$$\xi = \xi(x, y)$$

…(٣.٤٣a)

$$\eta = \eta(x, y)$$

…(٣.٤٣b)

The chain rule of partial differentiation provides the following expressions for the Cartesain derivatives:

$$\frac{\partial}{\partial x} = \frac{\partial}{\partial x}\frac{\partial \xi}{\partial x} + \frac{\partial}{\partial \eta}\frac{\partial \eta}{\partial x}$$

…(٣.٤٤a)

$$\frac{\partial}{\partial y} = \frac{\partial}{\partial \xi}\frac{\partial \xi}{\partial y} + \frac{\partial}{\partial \eta}\frac{\partial \eta}{\partial y}$$

…(٣.٤٤b)

Let, $\frac{\partial \xi}{\partial x} = \xi_x$, $\frac{\partial \xi}{\partial y} = \xi_y$

$$\frac{\partial \eta}{\partial x} = \eta_x \quad , \frac{\partial \eta}{\partial y} = \eta_y$$

Equation (٤٤) may be written in matrix forms as:

$$\begin{bmatrix} \frac{\partial}{\partial x} \\ \frac{\partial}{\partial y} \end{bmatrix} = \begin{bmatrix} \xi_x & \eta_x \\ \xi_y & \eta_y \end{bmatrix} \begin{bmatrix} \frac{\partial}{\partial \xi} \\ \frac{\partial}{\partial \eta} \end{bmatrix}$$

...(٣.٤٥)

The inverse transformation of equations (٤٦) are defined as:

$$X=X(\xi,\eta)$$

…(٣.٤٦a)

$$Y=Y(\xi,\eta)$$

…(٣.٤٦b)

$$Dx= x_{\xi}d\xi + x_{\eta}d\eta$$

…(٣.٤٧a)

$$Dy= y_{\xi}d\xi + y_{\eta}d\eta$$

…(٣.٤٧b)

Equations (٤٧a) and (٤٧b) are expressed in a matrix form as:

$$\begin{bmatrix} dx \\ dy \end{bmatrix} = \begin{bmatrix} x_{\xi} & x_{\eta} \\ y\xi & y_{\eta} \end{bmatrix} \begin{bmatrix} d\xi \\ d\eta \end{bmatrix}$$

…(٣.٤٨)

Reversing the role of the independent variables, we may write

$$d\xi = \xi_x dx + \xi_y dy$$

…(٣.٤٩a)

$$d\eta = \eta_x dx + \eta_y dy$$

…(٣.٤٩b)

$$\begin{bmatrix} d\xi \\ d\eta \end{bmatrix} = \begin{bmatrix} \xi_x & \xi_y \\ \eta_x & \eta_y \end{bmatrix} \begin{bmatrix} dx \\ dy \end{bmatrix}$$

…(٣.٥٠)

Multiplying both sides of equation (٤٨) by

$$\begin{bmatrix} x_{\xi} & x_{\eta} \\ y_{\xi} & y_{\eta} \end{bmatrix}^{-1}$$

yields

$$\begin{bmatrix} d\xi \\ d\eta \end{bmatrix} = \begin{bmatrix} x_\xi & x_\eta \\ y_\xi & y_\eta \end{bmatrix}^{-1} \begin{bmatrix} dx \\ dy \end{bmatrix}$$

…(٣.٥١)

comparing equation (٥٠) and (٥١) yields

$$\begin{bmatrix} \xi_x & \xi_y \\ \eta_x & \eta_y \end{bmatrix} = \begin{bmatrix} x_\xi & x_\eta \\ y_\xi & y_\eta \end{bmatrix}^{-1}$$

…(٣.٥٢)

Let

$$A = \begin{bmatrix} \xi_X & \xi_Y \\ \eta_X & \eta_Y \end{bmatrix}$$

…(٣.٥٣)

$$A^{-1} = \begin{bmatrix} x_\xi & x_\eta \\ y_\xi & y_\eta \end{bmatrix}$$

…(٣.٥٤)

Using Gramers rule. We can solve equation (٤٥) for the two unknowns $\frac{\partial}{\partial x} and \frac{\partial}{\partial y} for \frac{\partial}{\partial \xi}$ as follows:

$$\frac{\partial}{\partial \xi} = \frac{\begin{vmatrix} \frac{\partial}{\partial x} & \frac{\partial \eta}{\partial x} \\ \frac{\partial}{\partial y} & \frac{\partial \eta}{\partial y} \end{vmatrix}}{\begin{vmatrix} \frac{\partial \xi}{\partial x} & \frac{\partial \eta}{\partial x} \\ \frac{\partial \xi}{\partial y} & \frac{\partial \eta}{\partial y} \end{vmatrix}}$$

…(٣.٥٥)

The determinate in the denominator of equation (٥٥) is the Jacobian of transformation (J) defined by:

$$J = \frac{\partial(\xi,\eta)}{\partial(x,y)} = \begin{vmatrix} \xi_x & \eta_x \\ \xi_y & \eta_y \end{vmatrix}$$

...(٣.٥٦)

$$J = \frac{1}{J^{-1}} = \frac{1}{\frac{\partial(x,y)}{\partial(\xi,\eta)}} = \frac{1}{\begin{vmatrix} x_\xi & x_\eta \\ y_\xi & y_\eta \end{vmatrix}}$$

...(٣.٥٧)

$$\frac{\partial}{\partial\xi} = \frac{1}{J}\left[\eta_y \frac{\partial}{\partial x} - \eta_x \frac{\partial}{\partial y}\right]$$

...(٣.٥٨)

From equation (٥٤) and (٥٧) it follows:

$$J = \frac{1}{\left|A^{-1}\right|} = \frac{1}{x_\xi y_\eta - x_\eta y_\xi}$$

...(٣.٥٩)

$$A = \left|A^{-1}\right|^{-1} = \frac{Transposeo\ fcofactor A^{-1}}{\left|A^{-1}\right|}$$

...(٣.٦٠)

Transpose of cofactor

$$A^{-1}=\begin{bmatrix} y_\eta & -x_\eta \\ -y_\xi & x_\xi \end{bmatrix}$$

…(٣.٦١)

Substituting equations (٥٣), (٥٩), and (٦١) in equation (٦٠) yields

$$A=J\begin{bmatrix} y_\eta & -x_\eta \\ -y_\xi & x_\xi \end{bmatrix}$$

…(٣.٦٢)

The elements of matrix A may be obtained by:

$$\xi_x = Jy_\eta$$

…(٣.٦٣a)

$$\xi_y = -Jx_\eta$$

…(٣.٦٣b)

$$\eta_x = -Jy_\xi$$

…(٣.٦٣c)

$$\eta_y = Jx_\xi$$

…(٣.٦٣d)

Where J is defined by equation (٥٩)

To compute the matrices numerically, equations (٦٣) are used. These expressions are computed numerically by using finite difference approximations; in this case a second-order central difference approximation may be used to compute the transformation derivative for the interior grid points [٢٦].

$$X_\xi = \frac{X_{i+1,j} - X_{i-1,j}}{2\Delta\xi}$$

…(٣.٦٤a)

$$X_\eta = \frac{X_{i,j+1} - X_{i,j-1}}{2\Delta\eta}$$

…(٣.٦٤b)

$$Y_\xi = \frac{Y_{i+1,j} - Y_{i-1,j}}{2\Delta\xi}$$

…(٣.٦٤c)

$$Y_\eta = \frac{Y_{i,j+1} - Y_{i,j-1}}{2\Delta\eta}$$

…(٣.٦٤d)

The transformation derivatives at the boundaries are evaluated with forward or backward second-order approximations, for example, x_η at the j=١ boundary is computed by using the forward difference approximation

$$X_\eta = \frac{-3X_{i,1} + 4X_{i,2} - X_{i,3}}{2\Delta\eta}$$

…(٣.٦٥)

The desired number of grid points defined by IM (the maximum number of grid points in ξ) and JM (the maximum number of grid points in η) is specified. The equal grid spacing in the computational domain is produced as follows:

$$\Delta\xi = \frac{1}{IM - 1}$$

…(٣.٦٦a)

$$\Delta\eta = \frac{1}{JM - 1}$$

…(٣.٦٦b)

The interpretation of the matrices is obvious considering the following approximation:

$$\xi_x = \frac{\partial \xi}{\partial x} \cong \frac{\Delta \xi}{\Delta x}$$

…(٣.٦٧)

This expression indicates that the metrics represent the ratio of lengths in the computational space to that in the physical space:

٣.٤ Analytical solution

٣.٤.١ Introduction

Time-dependent solutions of the Euler equations are now widely used for the analysis of the flow through turbomachine blade rows. Their main attraction is the ability to compute mixed subsonic-supersonic flows with automatic capturing of shock waves. Solutions of the potential flow equation have also recently been extended to compute transonic shocked flow. Although these can be computationally much more efficient than solutions of the Euler equations, the limitation to potential flow rules them out for applications where strong shock waves can occur. Solving the Euler equations is also the most common way of computing fully three-dimensional flow in turbomachinery, even for subsonic flow.

The equations may be solved in either finite difference or finite volume form. It is usual to transform the computational domain into a uniform rectangular grid and to express the derivatives of the flow

variables in terms of values at the nodes at this grid. Specialized numerical technique such as MacCormack schemes is needed to ensure stability of the integration [٥].

٣.٤.٢ Inviscid Flow

Inviscid flow is, by definition flow where the dissipative, transport phenomena of viscosity, mass diffusion, and thermal conductivity are neglected. Therefore the resulting equations for unsteady, inviscid, non-heat conduction, compressible, two-dimensional flow called (Euler Equations) expressed in a conservation form are [٢٥]:

Continuity equation

$$\frac{\partial \rho}{\partial t} + \frac{\partial (\rho u)}{\partial x} + \frac{\partial (\rho v)}{\partial y} = 0$$

...(٣.٦٨)

Momentum equations

X component

$$\frac{\partial (\rho u)}{\partial t} + \frac{\partial (\rho u^2 + p)}{\partial x} + \frac{\partial (\rho uv)}{\partial y} = 0$$

...(٣.٦٩)

Y component

$$\frac{\partial (\rho v)}{\partial t} + \frac{\partial (\rho uv)}{\partial x} + \frac{\partial (\rho v^2 + p)}{\partial y} = 0$$

...(٣.٧٠)

The conservation of energy equation is

$$\frac{\partial(\rho e_\circ)}{\partial t}+\frac{\partial(\rho e_\circ u+pu)}{\partial x}+\frac{\partial(\rho e_\circ v+pv)}{\partial y}=0$$

…(٣.٧١)

٣.٤.٣ Vector Form of Euler Equations

The conservation form of the governing equations provides a numerical and computer-programming convenience in that the continuity, momentum, and energy equations in conservation form can all be expressed by the same generic equation. Therefore, the compressible Euler equations in Cartesian coordinates without body forces or external heat addition can be written in vector form as [٢٦]:

$$\frac{\partial Q}{\partial t}+\frac{\partial E}{\partial x}+\frac{\partial F}{\partial y}=0$$

…(٣.٧٢)

Where:

Q, E, and F are vectors given by: -

$$Q=\begin{bmatrix}\rho\\ \rho u\\ \rho v\\ \rho e_\circ\end{bmatrix}$$

…(٣.٧٣)

$$E=\begin{bmatrix}\rho u\\ \rho u^2+p\\ \rho uv\\ \rho e_\circ u+pu\end{bmatrix}$$

…(٣.٧٤)

$$F = \begin{bmatrix} \rho v \\ \rho uv \\ \rho v^2 + p \\ \rho e_\circ v + pv \end{bmatrix}$$

...(٣.٧٥)

٣.٤.٤ Body-Fitted Coordinate System

The need to satisfy the boundary conditions exactly led to the development of body-fitted coordinates. Such coordinates are difficult to generate for complex bodies. In body-fitted coordinate system, flow boundary surface such as blade profile shapes become coordinate lines in the computational space. The advantage of such systems is evident when incorporating boundary conditions in a finite difference computation.

٣.٤.٥ Euler Equations in Body-Fitted Coordinates

Sets of surface-oriented curvilinear coordinates, denoted by $\xi(x,y), \eta(x,y)$ are introduced in order to facilitate treatment of arbitrary flow regions. Therefore, Euler equations can be transformed from Cartesian Coordinates to general curvilinear coordinates.

Euler Equation can be written in curvilinear coordinates in vector form [٣٣]:

$$\frac{\partial \overline{Q}}{\partial t} + \frac{\partial \overline{E}}{\partial x} + \frac{\partial \overline{F}}{\partial y} = 0$$

...(٣.٧٦)

Where $\overline{Q}, \overline{E}, and \overline{F}$ are given by: -

$$\overline{\mathbf{Q}} = \frac{\mathbf{1}}{\mathbf{J}} \begin{bmatrix} \rho \\ \rho \mathbf{u} \\ \rho \mathbf{v} \\ \mathbf{e}_\circ \end{bmatrix}$$

...(٣.٧٧)

$$\overline{\mathbf{E}} = \frac{\mathbf{1}}{\mathbf{J}}\begin{bmatrix} \rho \mathbf{U} \\ \rho \mathbf{u} \mathbf{U} + \xi_{\mathbf{x}} \mathbf{p} \\ \rho \mathbf{v} \mathbf{U} + \xi_{\mathbf{y}} \mathbf{p} \\ (\mathbf{e}_{\circ} + \mathbf{p}) \mathbf{U} \end{bmatrix}$$

...(٣.٧٨)

$$\overline{\mathbf{F}} = \frac{\mathbf{1}}{\mathbf{J}}\begin{bmatrix} \rho \mathbf{V} \\ \rho \mathbf{u} \mathbf{V} + \eta_{\mathbf{x}} \mathbf{p} \\ \rho \mathbf{v} \mathbf{V} + \eta_{\mathbf{y}} \mathbf{p} \\ (\mathbf{e}_{\circ} + \mathbf{p}) \mathbf{V} \end{bmatrix}$$

...(٣.٧٩)

Where the contravariant velocity components U and V are defined by:

$$U = \xi_x u + \xi_y v$$

...(٣.٨٠)

$$V = \eta_x u + \eta_y v$$

...(٣.٨١)

The Jacobain transformation J is defined in: -

$$J = \frac{1}{x_\xi y_\eta - x_\eta y_\xi}$$

...(٣.٨٢)

٣.٣.٦ Explicit Time-Marching Method

Explicit time-marching procedures are generally used to solve Euler equatios. However, the computational time required by that procedure to arrive at an accurate solution is often prohibitive. In explicit schemes, the spatial derivatives are evaluated using known conditions at the old time level. The explicit schemes are used widely for the computation of turbomachinery flows and solving nonlinear PDEs [٢].

The predicted-corrector method proposed by MacCormack ١٩٦٩ is widely used for both internal and external flows. The method is second-order-accurate in both time and space. It can be used for both steady and unsteady compressible flows as well as for viscous and inviscid flows.

In the MacCormack method a two-step predictor-corrector squence is used with forward difference on the predictor and backward difference on the corrector. It is a second-order-accurate method.

By means of a Taylor series expansion, the flow-field variables are advanced at each grid point (i, j) in steps of time, as shown below [٢٥, ٢٨]:

$$\overline{Q}_{i,j}^{n+1} = \overline{Q}_{i,j}^{n} + \left\{\frac{\partial \overline{Q}}{\partial t}\right\}_{av} \Delta t$$

...(٣.٨٣)

Where, once again $\overline{Q}$ is a flow-field variable (from the governing equations) assumed known at time n, either from initial conditions or as a result from the previous iteration in time, $\left\{\frac{\partial \overline{Q}}{\partial t}\right\}_{av}$ is defined as

$$\left\{\frac{\partial \overline{Q}}{\partial t}\right\}_{av} = \frac{1}{2}\left[\left\{\frac{\partial \overline{Q}}{\partial t}\right\}_{i,j}^{n} + \left\{\frac{\partial \overline{Q}}{\partial t}\right\}_{i,j}^{n+1}\right]$$

...(٣.٨٤)

To obtain a value of $\left\{\frac{\partial \overline{Q}}{\partial t}\right\}_{av}$, the following steps are taken:

١. $\left\{\frac{\partial \overline{Q}}{\partial t}\right\}_{i,j}^{n}$ is calculated using forward spatial differences on the right-hand side of the governing equations from the known flow field at time n.

٢.From-step (١) predicted values of the flow-field variables can be obtained at time n+١ as follows:

$$\overline{Q}_{i,j}^{n+1'} = \overline{Q}_{i,j}^{n} + \left\{\frac{\partial \overline{Q}}{\partial t}\right\}_{i,j}^{n} \Delta t$$

…(٣.٨٥)

Combining steps (١) and (٢), predicted values are determined as follows:

$$\overline{Q}_{i,j}^{n+1'} = \overline{Q}_{i,j}^{n} - \frac{\Delta t}{\Delta \xi}\left[\overline{E}_{i+1,j}^{n} - \overline{E}_{i,j}^{n}\right] - \frac{\Delta t}{\Delta \eta}\left[\overline{F}_{i,j+1}^{n} - \overline{F}_{i,j}^{n}\right]$$

…(٣.٨٦)

٣.Using backward spatial differences, the predicted values (from step (٢)) are inserted into the governing equations such that a predicted time derivative $\left\{\frac{\partial \overline{Q}}{\partial t}\right\}_{i,j}^{n+1'}$ can be obtained.

$$\overline{Q}_{i,j}^{n+1'} = \overline{Q}_{i,j}^{n} - \frac{\Delta t}{\Delta \xi}\left[\overline{E}_{i,j}^{n+1'} - \overline{E}_{i-1,j}^{n+1'}\right] - \frac{\Delta t}{\Delta \eta}\left[\overline{F}_{i,j}^{n+1'} - \overline{F}_{i,j-1}^{n+1'}\right]$$

…(٣.٨٧)

٣.Finally, substitute $\left\{\frac{\partial \overline{Q}}{\partial t}\right\}_{i,j}^{n+1'}$ from step (٣) into equation (٨٤) to obtain corrected second-order-accurate values $\overline{Q}$ at time n+١. As in equation (٨٦) steps (٣) and (٤) are combined as follows:

$$\overline{Q}_{i,j}^{n+1} = \frac{1}{2}\left[\overline{Q}_{i,j}^{n} + \overline{Q}_{i,j}^{n+1'} - \frac{\Delta t}{\Delta \xi}\left(\overline{E}_{i,j}^{n+1'} - \overline{E}_{i-1,j}^{n+1'}\right) - \frac{\Delta t}{\Delta \eta}\left(\overline{F}_{I,J}^{n+1'} - \overline{F}_{i,j-1}^{n+1'}\right)\right]$$

...(٣.٨٨)

Steps (١) to (٤) are repeated until the flow-field variables approach a steady-state value this is desired steady-state solution.

٣.٣.٧ Initial and boundary conditions.

The description of a system of differential equations is not complete without the specifications of initial and boundary conditions. Once the problem has been specified, an appropriate set of governing equations and boundary conditions must be selected. It is generally accepted that the conservation of mass, momentum, and energy govern the phenomena of importance to the field of fluid dynamics. These may be steady or unsteady and compressible or incompressible boundary types, which may be encountered, and include solid walls, inflow and out flow boundaries.

Because the solution is marched from a set of initial conditions, the flow properties must be specified at each (i,j) location at time t=٠.٠.

Having the specified the initial conditions, the equation are marched in time to the steady state solution. In that process, conditions must be enforced at the boundary of the computational domain.

The inflow boundary conditions, and outflow boundary conditions are calculated based on extrapolation from the two adjacent interior points at the same j location as follow:

Mach number is subsonic

$P_i=P_{out}$

$u_i=٢u_{i-١}-u_{i-٢}$

$v_i=٢v_{i-١}-v_{i-٢}$

$T_i=٢T_{i-١}-T_{i-٢}$

$\rho_i = {}^{p_i}\!/_{R*T_i}$

While the surface boundary conditions of the blade of stator is calculated at the following subsection.

٣.٣.٧.١ Wall boundary conditions

At grid body surface, tangency must be satisfied for inviscid flow. The components of the momentum equation for the two-dimension flow may be expressed as:

$$\frac{\partial}{\partial t}(\rho u)+\frac{\partial}{\partial x}\left(\rho u^2+p\right)+\frac{\partial}{\partial y}(\rho uv)+\frac{1}{y}(\rho uv)=0.0$$

…(٣.٨٩)

$$\frac{\partial}{\partial t}(\rho v)+\frac{\partial}{\partial x}(\rho uv)+\frac{\partial}{\partial y}\left(\rho v^2+p\right)+\frac{1}{y}\left(\rho v^2\right)=0.0$$

…(٣.٩٠)

By definition

$$\dot{m}=\rho \mathbf{v}.\hat{\mathbf{n}}$$

…(٣.٩١)

And is equal to zero at the surface of blade.Since,

$$\hat{\mathbf{n}}=\frac{\nabla\eta}{|\nabla\eta|}$$

$$\bar{\mathbf{v}}=\left(u\hat{\mathbf{i}}+v\hat{\mathbf{j}}\right)$$

And

$$\nabla\eta=\eta_x\hat{\mathbf{i}}+\eta_y\hat{\mathbf{j}}=J\left(-y_\xi\hat{\mathbf{i}}+x_\xi\hat{\mathbf{j}}\right)$$

Substitution of these relations into Equation(٣.٩٢) yields:

$$\rho v x_\xi - \rho u y_\xi = 0.0$$

…(٣.٩٢)

At time derivative of Equation (٣.٩٣) provides

$$x_\xi \frac{\partial}{\partial t}(\rho v) - y_\xi \frac{\partial}{\partial t}(\rho u) = 0.0$$

…(٣.٩٣)

The grid system has been assumed to be independent of time. With some mathematical manipulation between metric transformations and momentum equation the following results:

$$x_\xi \frac{\partial}{\partial x}\left(\rho u^2 + p\right) + y_\xi \frac{\partial}{\partial y}(\rho uv) - x_\xi \frac{\partial}{\partial x}(\rho uv) - x_\xi \frac{\partial}{\partial y}\left(\rho v^2 + p\right) = 0.0$$

…(٣.٩٤)

Equation (٣.٩٥) is rearranges and transformation to body fitted coordinate and is in conservative form. Therefore, the concervative form of Equation (٣.٩٥)is expressed as:

$$\eta_x\left(\frac{\rho u U}{J}\right)_\xi + \eta_y\left(\frac{\rho u U}{J}\right)_\xi + \eta_x\left(\frac{\rho u V}{J}\right)_\eta + \eta_y\left(\frac{\rho u V}{J}\right)_\eta$$
$$+ \eta_x\left(\frac{\xi_x p}{J}\right)_\xi + \eta_x\left(\frac{\eta_x p}{J}\right)_\eta + \eta_y\left(\frac{\xi_y p}{J}\right)_\xi + \eta_y\left(\frac{\xi_y p}{J}\right)_\eta = 0.0$$

...(٣.٩٥)

Where U is the tangential velocity in computational domain.

In order to obtain a finite difference Equation (٣.٩٥) , a second order central difference approximation for the ξ derivatives and a second- order one sided difference approximation for the η derivatives are used. The unknowns are the values for pressure at the surface of the blade. The values at the interior points have already been computed with the second order approximation described in subsection (٣.٣.٦), the finite difference equation is obtained as:

$$\frac{\eta_{x_{i,j}}}{2\Delta\xi}\left[\left(\frac{\rho uU}{J}\right)_{i+1,1}-\left(\frac{\rho uU}{J}\right)_{i-1,1}\right]+\frac{\eta_{y_{i,j}}}{2\Delta\xi}\left[\left(\frac{\rho uU}{J}\right)_{i+1,1}-\left(\frac{\rho uU}{J}\right)i-1,1\right]$$
$$+\frac{\eta_{x_{i,j}}}{2\Delta\eta}\left[-3\left(\frac{\rho uV}{J}\right)_{i,1}+4\left(\frac{\rho uV}{J}\right)_{i,2}-\left(\frac{\rho uV}{J}\right)_{i,3}\right]$$
$$+\frac{\eta_{y_{i,j}}}{2\Delta\eta}\left[-3\left(\frac{\rho vV}{J}\right)_{i,j}+4\left(\frac{\rho vV}{J}\right)_{i,2}-\left(\frac{\rho vV}{J}\right)_{i,3}\right]$$
$$+\frac{\eta_{y_{i,j}}}{2\Delta\xi}\left[\left(\frac{\xi_x p}{J}\right)_{i+1,1}-\left(\frac{\xi_x p}{J}\right)_{i-1,1}\right]+\frac{\eta_{x_{i,j}}}{2\Delta\eta}\left[-3\left(\frac{\eta_x p}{J}\right)_{i,1}+4\left(\frac{\eta_x p}{J}\right)_{i,2}-\left(\frac{\eta_x p}{J}\right)_{i,3}\right]$$
$$+\frac{\eta_{y_{i,j}}}{2\Delta\xi}\left[\left(\frac{\xi_y p}{J}\right)_{i+1,1}-\left(\frac{\xi_y p}{J}\right)_{i-1,1}\right]$$
$$\frac{\eta_{y_{i,j}}}{2\Delta\eta}\left[-3\left(\frac{\eta_y p}{J}\right)_{i,1}+4\left(\frac{\eta_y p}{J}\right)_{i,2}-\left(\frac{\eta_y p}{J}\right)_{i,3}\right]=0.0$$

…(٣.٩٦)

The value of V is equal to zero at the surface of blade of stator,and therefore, those terms are dropped. This equation is regrouped so that a tridiagonal system is formed.

The rearrangement is as follows:

$$a_i p_{i-1,1}+b_i p_{i,1}+c_i p_{i+1,1}=d_i$$

…(٣.٩٧)

Where:

$$a_i = -\frac{1}{2\Delta\xi}\left[\eta_{x_{i,1}}\left(\frac{\xi_x}{J}\right)_{i-1,1} + \eta_{y_{i,1}}\left(\frac{\xi_y}{J}\right)_{i-1,1}\right]$$

$$b_i - \frac{3}{2\Delta\eta}\left(\frac{\eta_x^2+\eta_y^2}{J}\right)_{i,1}$$

$$c_i = \frac{1}{2\Delta\xi}\left[\eta_{x_{i,1}}\left(\frac{\xi_x}{J}\right)_{i+1,1} + \eta_{y_{i,1}}\left(\frac{\xi_y}{J}\right)_{i+1,1}\right]$$

$$d_i = -\frac{p_{i,3}}{2\Delta\eta}\left[\eta_{x_{i,1}}\left(\frac{\eta_x}{J}\right)_{i,3} + \eta_{y_{i,1}}\left(\frac{\eta_y}{J}\right)_{i,3}\right] - \frac{p_{i,2}}{2\Delta\eta}\left[\eta_{x_{i,1}}\left(\frac{\eta_x}{J}\right)_{i,2} + \eta_{y_{i,1}}\left(\frac{\eta_y}{J}\right)_{i,2}\right]$$
$$- \frac{2}{\Delta\eta}\left(\frac{\rho V}{J}\right)_{i,2}\left(\eta_{x_{i,1}}u_{i,2} + \eta_{y_{i,1}}v_{i,2}\right) + \frac{1}{2\Delta\eta}\left(\frac{\rho V}{J}\right)_{i,3}\left(\eta_{x_{i,1}}u_{i,3} + \eta_{y_{i,1}}v_{i,3}\right)$$
$$+ \frac{1}{2\Delta\xi}\left(\frac{\rho U}{J}\right)_{i-1,1}\left(\eta_{x_{i,1}}u_{i-1,1} + \eta_{y_{i,1}}v_{i-1,1}\right)$$
$$- \frac{1}{2\Delta\xi}\left(\frac{\rho U}{J}\right)_{i+1,1}\left(\eta_{x_{i,1}}u_{i+1,1} + \eta_{y_{i,1}}v_{i+1,1}\right)$$

When equation (٣.٩٧)is applied to all I at j=١ (the surface of the blade of stator), the following tridiagonal system of equations is obtained:

$$\begin{bmatrix} b_2 & c_2 & & & & \\ a_3 & b_3 & c_3 & & & \\ & & & & & \\ & & a_{1MM2} & b_{1MM2} & c_{1MM2} & \\ & & & a_{1MM1} & b_{1MM1} & \end{bmatrix}\begin{bmatrix} P_{2,1} \\ P_{3,1} \\ \\ P_{1MM2,1} \\ p_{1MM1,1} \end{bmatrix} = \begin{bmatrix} d_2 - a_2 p_{1,1} \\ d_3 \\ \\ d_{1MM2} \\ d_{1MM1} - c_{1MM1} p_{1M,1} \end{bmatrix}$$

Since $p_{1,1} = p_{2,1}$ and $\frac{p_{1M,1}}{J_{1M,1}} = \frac{p_{1MM1,1}}{J_{1MM1,1}}$. Therefore,

$$\begin{bmatrix} b_2 & c_2 & & & & \\ a_3 & b & c_3 & & & \\ & & & & & \\ & & a_{IMM2} & b_{IMM2} & c_{IMM2} & \\ & & & a_{IMM1} & b_{IMM1} \end{bmatrix} \begin{bmatrix} p_{2,1} \\ p_{3,1} \\ \\ p_{IMM2,1} \\ p_{IMM1,1} \end{bmatrix} = \begin{bmatrix} d_2 \\ d_3 \\ \\ d_{IMM2} \\ d_{IMM1} \end{bmatrix}$$

Where:

$$\bar{b}_2 = a_2 + b_2$$
$$IMM1 = IM - 1, and$$
$$\bar{b}_{IMM1} = b_{IMM1} + c_{IMM1} \frac{J_{IM,1}}{J_{IMM1,1}}$$

Velocity components and density are calculated by using the energy equation with the geometry parameters as follows:

Total enthalpy at the surface is assumed constant. This statement is expressed mathematically as:

$$\gamma e_\circ + \frac{1}{2}\left(u^2 + v^2\right) = \left(h_o\right)_{wall} = cons\tan t \qquad \ldots(٣.٩٨)$$

For perfect gas;

$$\gamma\left(\frac{p_{i,1}}{(\gamma-1)\rho_{i,1}}\right) + \frac{1}{2}\frac{C_i^2 + D_i^2}{\rho_{i,1}^2} = \left(h_\circ\right)_{wall} \qquad \ldots (٣.٩٩)$$

This equation is rearranged as:

$$\left(2(\gamma-1)(h_\circ)_{wall}\right)\dot{\rho}_{i,1}^2 - (2\gamma)p_{i,1}\dot{\rho}_{i,1} + (1-\gamma)\left(C_i^2 + D_i^2\right) = 0.0 \quad (٣.١٠٠)$$

Then the density at the wall is solved as follows:

$$\rho_{i,1} = \frac{2\gamma p_{i,1} + \sqrt{4\gamma^2 p_{i,1}^2 + 8(\gamma-1)^2(C+D)}}{4(\gamma-1)(h_t)_{wall}}$$

The positive sign is used exclusively to prevent negative density values. The velocity at the surface of the blade of stator may be initialized in different ways. One way extrapolate U from the interior points, or the same value for $\rho\vec{V}$ is imposed at the surface of the blade of stator with the vector rotated such that the velocity is tangent at the surface. Thus,

$$A_i = \left|\rho\vec{V}\right|_{i,2} = \left|\sqrt{(\rho u)^2 + (\rho v)^2}\right|$$

From the geometry parameters, it is useful to find the component of velocity u and v as follow:

$$\sin\theta = \frac{\eta_y}{bb}$$

$$\cos\theta = \frac{-\eta_x}{bb}$$

$$bb = \sqrt{\eta_x^2 + \eta_y^2}$$

$$C_i = (\rho u)_{i,1} = A_i \cos\theta$$

$$D_i = (\rho v)_{i,1} = A_i \sin\theta$$

٣.٣.٨ Artificial Viscosity

MacCormack and Baldwin (١٩٧٥) added an artificial viscosity or dissipation term in the Navier-Stokes equation. This provides the necessary stability to the code [٢]. Euler equations omit viscosity; however, discretization generally reintroduces viscosity or, more precisely, second-difference terms that have viscous-like effects. Second differences that arise naturally as a part of first-derivative approximation are called implicit artificial viscosity. Second differences purposely added to first-derivative approximation are called explicit artificial viscosity. Artificial viscosity forms sometimes suggest alterations and

improvements. The implicit artificial viscosity is too small, making unstable, and adding explicit second-order artificial viscosity with a positive coefficient has a smoothing and stabilizing effect. In other cases, a numerical method may have too much artificial viscosity, causing smearing or even instability. In this case adding explicit artificial viscosity with a negative coefficient partially cancels the implicit artificial viscosity, resulting in a sharper, and even more stable solution. Second-order artificial viscosity with a positive coefficient is sometimes called artificial dissipation; second-order artificial viscosity with a negative coefficient is sometimes also called artificial antidissipation [٢٨].

The fourth order smoothing term amounts to adding to the predictor and corrector steps the difference form of the following term;

Predictor step

$$\left(\overline{Q}^{n+1'}\right)_{i,j} = \left(\overline{Q}_{1s}^{n+1'}\right)i,j + \left(S\overline{Q}^{n+1'}\right)_{i,j}$$

$$\ldots(٣.١٠١)$$

Where

$$\left(\overline{Q}_{1s}^{n+1'}\right)_{i,j} = \overline{Q}_{i,j}^{n} - \frac{\Delta t}{\Delta\xi}\left[\left(\overline{E}_1^{n}\right)_{i+1,j} - \left(\overline{E}_1^{n}\right)_{i,j}\right] - \frac{\Delta t}{\Delta\eta}\left[\left(\overline{F}_1^{n}\right)_{i,j+1} - \left(\overline{F}_1^{n}\right)_{i,j}\right]$$

$$\ldots(٣.١٠٢)$$

And $\left(S\overline{Q}_1^{n+1'}\right)_{i,j}$ is a fourth order artificial viscosity term, defined by [٢٨]

$$\left(S\overline{Q}_1^{n+1'}\right)_{i,j} = \frac{C_\xi\left|P_{i+1,j}^{n} - 2P_{i,j}^{n} + P_{i-1,j}^{n}\right|}{\left(P_{i+1,j} + 2P_{i,j}^{n} + P_{i-1,j}^{n}\right)}\left[\left(\overline{Q}_1^{n}\right)_{i+1,j} - 2\left(\overline{Q}_1^{n}\right)_{i.j} + \left(\overline{Q}_1^{n}\right)_{i-1,j}\right]$$

$$+ \frac{C_\eta\left|P_{i,j+1}^{n} - 2P_{i,j}^{n} + P_{i,j-1}^{n}\right|}{\left(P_{i,j+1}^{n} + 2P_{i,j}^{n} + P_{i,j-1}^{n}\right)}\left[\left(\overline{Q}_1^{n}\right)_{i,j+1} - 2\left(\overline{Q}_1^{n}\right)_{i,j} + \left(\overline{Q}_1^{n}\ \right)_{i,j-1}\right]$$

...(٣.١٠٣)

Corrector step

$$\left(\overline{Q}^{n+1}\right)i,j=\left(\overline{Q}_{1s}^{n+1}\right)_{i,j}+\left(S\overline{Q}^{n+1}\right)_{i,j}$$

…(٣.١٠٤)

Where

$$\left(\overline{Q}_{1s}^{n+1}\right)_{i,j}=\frac{1}{2}\left[\left(Q_1^n\right)_{i,j}+\left(\overline{Q}_1^{n+1'}\right)_{i,j}-\frac{\Delta t}{\Delta\xi}\left[\left(\overline{E}_1^{n+1'}\right)_{i,j}-\left(\overline{E}_1^{n+1'}\right)_{i-1,j}\right]-\frac{\Delta t}{\Delta\eta}\left[\left(\overline{F}_1^{n+1'}\right)_{i,j}-\left(\overline{F}_1^{n+1'}\right)_{i,j-1}\right]\right]$$

…(٣.١٠٥)

And

$$\left(S\overline{Q}_1^{n+1}\right)_{i.j}=\frac{C_\xi\left|P_{i+1,j}^{n+1'}-2P_{i,j}^{n+1'}+P_{i-1,j}^{n+1'}\right|}{\left(P_{i+1,j}^{n+1'}+2P_{i,j}^{n+1'}+P_{i-1,j}^{n+1'}\right)}\left[\left(\overline{Q}_1^{n+1'}\right)_{i+1,j}-2\left(\overline{Q}_1^{n+1'}\right)_{i,j}+\left(\overline{Q}_1^{n+1'}\right)_{i-1,j}\right]$$

$$+\frac{C_\eta\left|P_{i,j+1}^{n+1'}-2P_{i,j}^{n+1'}+P_{i,j-1}^{n+1'}\right|}{\left(P_{i,j+1}^{n+1'}+2P_{i,j}^{n+1'}+P_{i,j-1}^{n+1'}\right)}\left[\left(\overline{Q}_1^{n+1'}\right)_{i,j+1}-2\left(\overline{Q}_1^{n+1'}\right)_{i,j}+\left(\overline{Q}_1^{n+1'}\right)_{i,j-1}\right]$$

…(٣.١٠٦)

The fourth order nature can be seen in the numerators, which are products of two second-order central difference expressions for second derivatives. $C_\xi and C_\eta$ are arbitrary specified parameters, with typical values range from .٠١ to .٣ [٢٨].

The convergence means that the solution to the finite-difference equation approaches the true solution to the partial differential equation having the same initial and boundary conditions as the mesh refined. The time step must be calculated from the Cournt-Fridrich-Lewy (CFL) stability criteria, it must be less than, or at best equal to the time taken by a sound wave to travel from one grid point to the next. The solution becomes unstable when CFL is greater than one.

Convergence criteria to reach steady state solution is based on the maximum change in pressure between two successive time integrated steps for each grid point, which should be less or equal to ١٠-٥

$$\frac{P^{n+1}-P^{n}}{P^{n}} \le 10^{-5}$$

...(٣.١٠٧)

٣.٤.٨Calculation Steps

The main steps of explicit two-dimension solution of MacCormack ' s technique may be summarized as follows:

١.Generating grid points in the physical domain.

٢.Initializing the value of p, u, v, T and ρ for all grid points in the computational domain.

٣. Computing the surfaces bounding the physical domain and generate the grid for computational domain (in ξ and η coordinates).

٤.Evaluating the Jacobian transformation parameters for each grid point.

٥.Evaluate the values of flux vector $\overline{Q}$, $\overline{E}$ and $\overline{F}$ for all grid points at time level n.

٦.Initializing the value of time step at predictor step.

٧.Applying finite difference equations at predictor step and compute $\overline{Q}_1^{n+1'}$, $\overline{Q}_2^{n+1'}$ and $\overline{Q}_3^{n+1'}$ for all grid points.

٨.Computing ρ, u, v, T and p using equation (٧٧).

٩.Evaluating $\overline{E}_1^{n+1'}$, $\overline{E}_2^{n+1'}$, $\overline{E}_3^{n+1'}$, $\overline{F}_1^{n+1'}$, $\overline{F}_2^{n+1'}$ and $\overline{F}_3^{n+1'}$ at predictor step.

١٠.Repeating steps (٦-٩) for corrector step.

١١.Computing flow parameters ρ, u, v, T and p at all grid points.

١٢.Checking the convergence of solution equation (٨٨), if not satisfied advance one time step and repeat steps (٦-١١).

٣.٥ The Computer Programs

٣.٥.١ Program (١)

An iterative Quick Basic program was written for the preliminary design of the axial flow compressor blade.

The input data required to run the program are as follows:

Specific heat ratio $\gamma = 1.4$, diffusion factor $D = .5$, solidity factor $\sigma = 1$, inlet Mach number M=.٧, inlet stagnation temperature $T_{o١}$=٢٨٨, inlet stagnation pressure $P_{o١}$=١٠١.٣ kpa.

The outputs from the program are as follows:

Stage efficiency, stage pressure ratio, compressor efficiency, compressor pressure ratio.

Fig (٣.٢) shows the flow chart of aerodynamic design of axial flow compressor.

٣.٥.٢ Program (٢)

The input data required to run the program are as follows:

Specific heat ratio $\gamma = 1.4$, specific heat at constant pressure C_p=١.٠٠٤ kj/kg.k, inlet pressure P_i=٧٨٨٥٠ pa, **i**nlet temperature T_i=٢٦٨ K and inlet Mach number M_i=٠.٦ ,T_w=٢٦٨, $\alpha_i = (30,0)$deg, P_{exit}=٩٤٠٠٠ pa

The outputs from the program are as follows:

The static properties (P_1, T_1, ρ_1), the total properties (Pt, Tt), uv١.

Fig (٣.٣) shows the flow chart for two dimensions explicit method.

Chapter Four

Results and Discussion

٤.١ Introduction

This chapter presents the results obtained from the present predication method to calculate the properties in the blade passage of axial flow compressor, by running the developed computer program using the input data mentioned in paragraph (٣.٥). The computational efficiency of flow simulation model is also studied to indicate the influence of artificial viscosity terms and time step size on convergence and accuracy of the numerical algorithms.

٤.٢ Results of aerodynamic analysis

Fig (٤.١) shows the variation of exit absolute flow angle $(\alpha_2)$with inlet absolute flow angle at different values of diffusion factor, Mach number of (٠.٧), and a solidity of (١). It shows that the exit absolute flow angle increases with increase inlet absolute flow angle according to eq.(٣.٤), α_2 should increase with α_1 when D and σ are held constant.

Fig (٤.٢) shows the variation of exit absolute flow angle $(\alpha_2)$with inlet absolute flow angle (α_1)at different values of solidity factor, Mach number of (٠.٧), and a diffusion factor of (٠.٥). It shows that the exit absolute flow angle increases with increase inlet absolute flow angle. This behavior as a result of eq. (٣.٤), with increase α_1, α_2 should increase at the constant D and σ.

Fig (٤.٣) shows the variation of turning angle $(\alpha_2 - \alpha_1)$with inlet absolute flow angle $(\alpha 1)$at different values of diffusion factor, Mach number of (٠.٧) and a solidity of (١). It shows that the turning angle decreases with increase inlet absolute flow angle according to eq.(٣.٤), the turning angle should decrease with increase α_1 when D and σ are held constant.

Fig (٤.٤) shows the variation of turning angle $(\alpha_2 - \alpha_1)$with inlet absolute flow angle (α_1)at different values of solidity factor, Mach number of (٠.٧), and a diffusion factor of (٠.٥). It shows that the turning angle decreases with increase inlet absolute flow angle. This behavior as a result of eq.(٣.٤), with increase α_1, the turning angle should decrease at constant D and σ.

Fig (٤.٥) shows the variation of stage pressure ratio $(\pi_s)$with inlet absolute flow angle(α_1)at different values of diffusion factor, Mach number of (٠.٧), and a solidity of (١). It shows that the stage pressure ratio increases with increase inlet absolute flow angle according to eq.(٣.٧), π_s should increase with α_1 when D and σ are held constant.

Fig (٤.٦) shows the variation of stage pressure ratio $(\pi_s)$with inlet absolute flow angle (α_1)at different values of Mach number, diffusion factor of (٠.٥), and a solidity of (١). It shows that the stage pressure ratio increases with increase inlet absolute flow angle. This behavior as a result of eq.(٣.٧), with increase α_1, π_s should increase at constant D and σ.

Fig (٤.٧) shows the variation of stage pressure ratio $(\pi_s)$with inlet absolute flow angle (α_1)at different values of solidity factor, Mach number of (٠.٧), and a diffusion factor of (٠.٥). It shows that the stage

pressure ratio increases with increase inlet absolute flow angle according to eq.(٣.٧), π_s should increase with α_1 when D and σ are held constant.

Fig (٤.٨) shows the variation of stage total temperature ratio (τ_s) with inlet absolute flow angle (α_1) at different values of diffusion factor, Mach number of (٠.٧), and a solidity of (١). It shows that the stage total temperature ratio increases with the increase of inlet absolute flow angle according to eq.(٣.٦), τ_s should increase with α_1 when D and σ are held constant.

Fig (٤.٩) shows the variation of stage total temperature ratio (τ_s) with inlet absolute flow angle (α_1) at different values of solidity factor, Mach number of (٠.٧), and a diffusion factor (٠.٥). It shows that the stage total temperature ratio increases with increase inlet absolute flow angle. This behavior as a result of eq.(٣.٦), τ_s should increase with α_1 when D and σ are held constant.

Fig (٤.١٠) shows the variation of blade speed ratio (V_1 / wr) with inlet absolute flow angle (α_1) at different values of diffusion factor, Mach number of (٠.٧), and a solidity of (١). It shows that the blade speed ratio decreases with increase inlet absolute flow angle according to eq.(٣.١١), (V_1 / wr) should decrease with α_1 when D and σ are held constant.

Fig (٤.١١) shows the variation of blade speed ratio (V_1 / wr) with inlet absolute flow angle (α_1) at different values of solidity factor, Mach number of (٠.٧), and a diffusion factor of (٠.٥). It shows that the blade speed ratio decreases with increase inlet absolute flow angle. This behavior as a result of eq.(٣.١١), at constant D and σ, with increase $\alpha_1, (V_1 / wr)$ should decrease when D and σ are held constant.

Fig (٤.١٢) shows the variation of blade metal angle $(\gamma_\circ)$with inlet absolute flow angle (α_1)at different values of diffusion factor, Mach number of (٠.٧), and a solidity of (١). It shows that the blade metal angle increases with increase inlet absolute flow angle according to eq.(٣.٤٢), $\gamma_\circ$ should increase with α_1 at constant D and σ.

Fig (٤.١٣) shows the variation of blade metal angle $(\gamma_\circ)$with inlet absolute flow angle (α_1)at different values of solidity factor,Mach number of (٠.٧), and a diffusion factor of (٠.٥). It shows that the blade metal angle increases with increase inlet absolute flow angle according to eq.(٣.٤٢), at D and σ are held constant, $\gamma_\circ$ should increase with α_1.

Fig (٤.١٤) shows the variation of stage efficiency $(\eta_s)$with inlet absolute flow angle (α_1)at different values of diffusion factor, Mach number of (٠.٧), and a solidity of (١). It shows that the stage efficiency decreases with increase inlet absolute flow angle. This behavior as a result of eq.(٣.٨), with increase in α_1, η_s should decrease at constant D and σ.

Fig (٤.١٥) shows the variation of stage efficiency $(\eta_s)$with inlet absolute flow angle (α_1)at different values of Mach number, diffusion factor of (٠.٥), and a solidity of (١). It shows that the stage efficiency decreases with increase inlet absolute flow angle according to eq.(٣.٨), η_s should decrease with increase α_1 when D and σ are held constant.

Fig (٤.١٦) shows the variation of stage efficiency $(\eta_s)$with inlet absolute flow angle (α_1)at different values of solidity factor, Mach number of (٠.٧), and a diffusion factor of (٠.٥). It shows that the stage

efficiency decreases with increase inlet absolute flow angle according to eq.(٣.٨), η_s should decrease with increase α_1 at constant D and σ.

Fig (٤.١٧) shows the variation of compressor pressure ratio (π_c) with inlet absolute flow angle (α_1) at different values of diffusion factor,Mach number of (٠.٧), and a solidity of (١). It shows that the compressor pressure ratio increases with increase inlet absolute flow angle. This behavior as a result of eq.(٣.٩), with increase α_1, π_c should increase at constant D and σ.

Fig (٤.١٨) shows the variation of compressor pressure ratio (π_c) with inlet absolute flow angle (α_1) at different values of Mach number, diffusion factor of (٠.٥), and a solidity of (١). It shows that the compressor pressure ratio increases with increase inlet absolute flow angle. This behavior as a result of eq.(٣.٩), when D and σ are held constant , π_c should increase with increase α_1.

Fig (٤.١٩) shows the variation of compressor pressure ratio (π_c) with inlet absolute flow angle (α_1) at different values of solidity factor, Mach number of (٠.٧), and a diffusion factor of (٠.٥). It shows that the compressor pressure ratio increases with increase inlet absolute flow angle according to eq.(٣.٩), at constant D and σ, with increase in α_1, π_c should increase.

Fig (٤.٢٠) shows the variation of compressor efficiency (η_c) with inlet absolute flow angle (α_1) at different values of diffusion factor, Mach number of (٠.٧), and a solidity of (١). It shows that the compressor efficiency decreases with increase inlet absolute flow angle according to eq.(٣.١٠), η_c should decrease with increase α_1 at constant D and σ.

Fig (٤.٢١) shows the variation of compressor efficiency $(\eta_c)$with inlet absolute flow angle (α_1)at different values of Mach number, diffusion factor of (٠.٥), and a solidity of (١). It shows that the compressor efficiency decreases with increase inlet absolute flow angle according to eq.(٣.١٠), when D and σ are held constant , η_c should decrease with α_1.

Fig (٤.٢٢) shows the variation of compressor efficiency $(\eta_c)$with inlet absolute flow angle (α_1)at different values of solidity factor, Mach number of (٠.٧), and a diffusion factor of (٠.٥). It shows that the compressor efficiency decreases with increase inlet absolute flow angle according to eq.(٣.١٠), with increase α_1, η_c should decrease when D and σ are held constant.

٤.٢ Numerical Results and Disscussion.

Fig.(٤.٢٣)shows the mesh generation between blade to blade for the stator of axial flow compressor.

Fig (٤.٢٤) display of a vector quantity along the blade of stator, where the vector plot is a display of a vector quantity (usually velocity) at discrete grid points, shown both magnitude and, where the base of each vector is located at the respective grid point as shown in this figure.

Fig (٤.٢٥) shows the contour plot of density, from which can be see that the increasing of the density value from this value at inlet boundary and continuous increasing through the passage of flow. This increasing in density value is due to decreasing in velocity due to change in area with conservative of mass flow rate.

A contour line is a line along which some property is constant. Generally, contours are plotted such that the difference between the qualitative value of the dependent variable from one contour line to an adjacent contour line is held constant.

Fig (٤.٢٦) shows the contour lines of temperature. This plot shows the increasing of temperature value through the passage between two blades from this value at inlet boundary to the end of passage. Decreasing in value of velocity causing this increasing in temperature value because the alternating between kinetic energy and internal energy which causing to increase temperature with decrease of velocity, this due to energy conservation.

Fig (٤.٢٨) shows the contour plot pressure along the passage of the flow. The same behavior of density and temperature can be seeing here; the flow compressed from inlet pressure point to back pressure value at the exit. This similarity in behavior is due to state equation and momentum conservation.

Fig (٤.٢٧) shows decreasing in Mach number value from the inlet Mach number to the exit Mach number.

Chapter Five

Conclusions and Recommendations

٥.١ Conclusions

The following points can be concluded: -

١. The compressor pressure ratio increases with increase of diffusion factor, solidity factor and Mach number.

٢. The compressor efficiency increases with decrease of compressor pressure ratio at different values of diffusion factor, solidity factor, and Mach number.

٣. In the stator blade, the flow is decelerated due to change in area with consertive of mass flow rate.

٤. The density increases due to decrease in velocity from inlet boundary condition until reach the end of the passage of flow.

٥. Decreasing in velocity causing the increasing in temperature value because the alternating between kinetic energy and internal energy which causing to increase temperature with decrease of velocity, this due to energy conservation.

٦. The pressure behavior is the same behavior of density and temperature. This similarity in behavior is due to state equation.

٥.٢ Recommendations for future work:

The following recommendation may be stated for the future work:

١. Use three-dimension analysis for solving Euler equations.

٢.Study a viscous flow analysis and studying the difference in flow calculation results between the inviscid and viscous flow analysis.

٣.Study the stresses and forces on the rotor blade by using the flow calculation results.

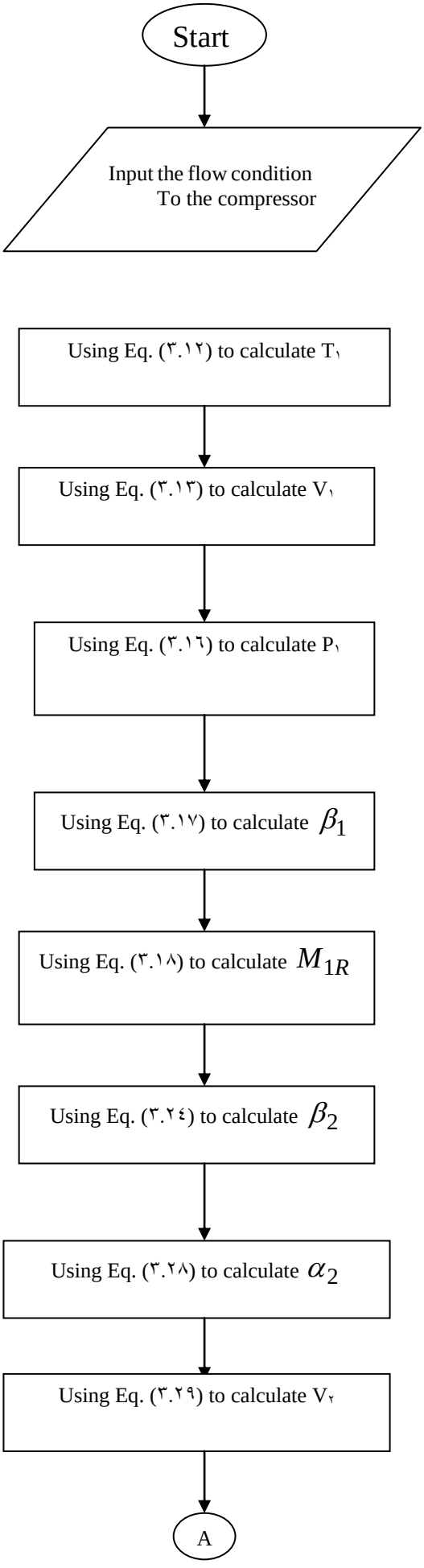
Start
Input the flow condition To the compressor
Using Eq. (٣.١٢) to calculate T١
Using Eq. (٣.١٣) to calculate V١
Using Eq. (٣.١٦) to calculate P١
Using Eq. (٣.١٧) to calculate β_1
Using Eq. (٣.١٨) to calculate M_{1R}
Using Eq. (٣.٢٤) to calculate β_2
Using Eq. (٣.٢٨) to calculate α_2
Using Eq. (٣.٢٩) to calculate V٢
A

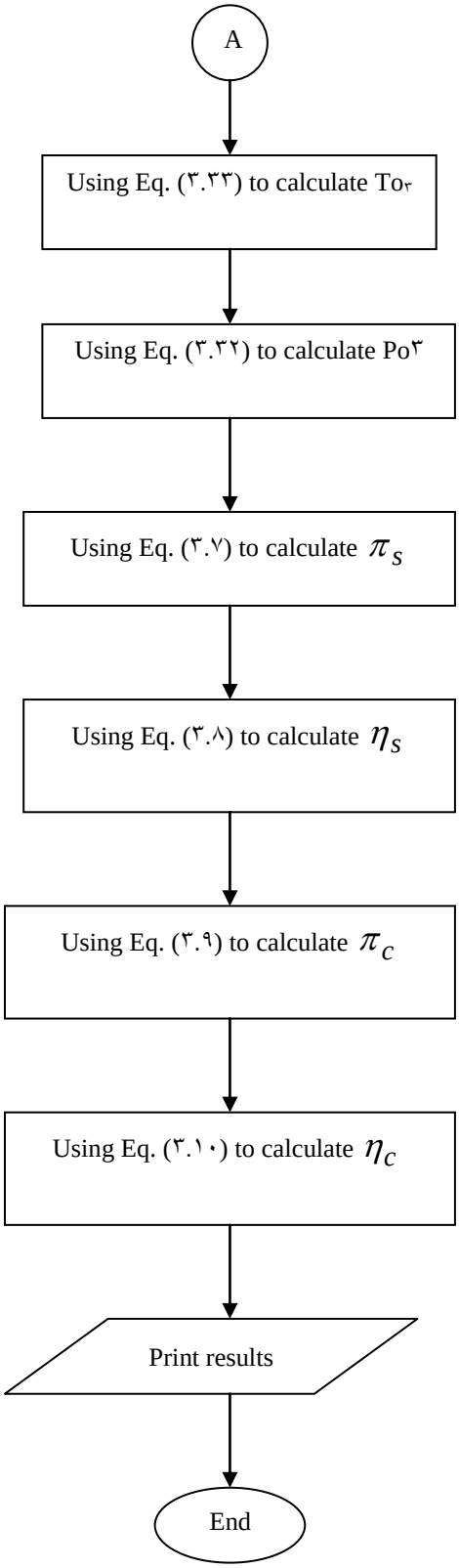

Fig (٣.٢)
Flow chart of the aerodynamic design of axial flow compressor

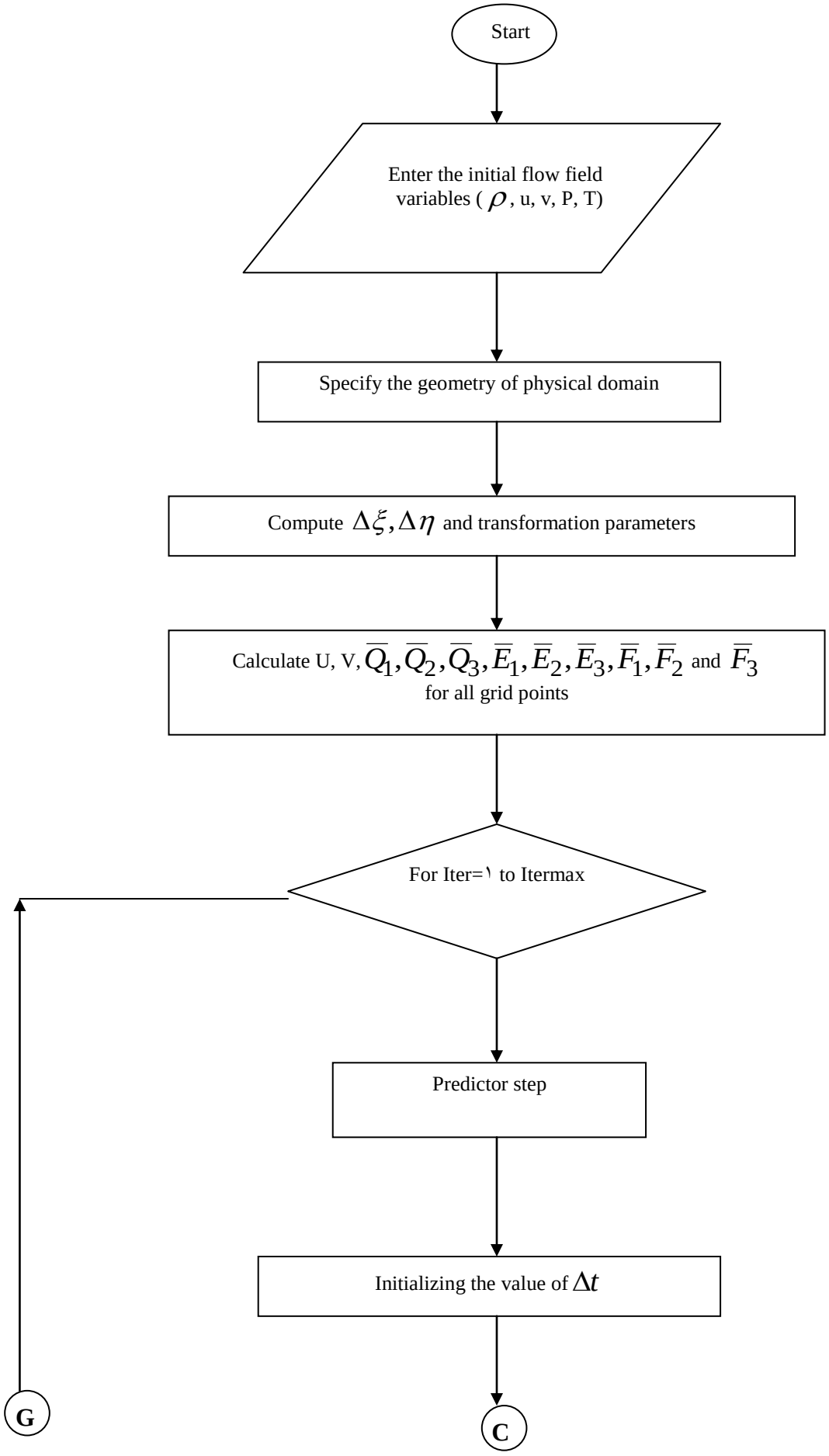
Start
Enter the initial flow field variables (ρ, u, v, P, T)
Specify the geometry of physical domain
Compute $\Delta\xi, \Delta\eta$ and transformation parameters
Calculate U, V, $\overline{Q}_1, \overline{Q}_2, \overline{Q}_3, \overline{E}_1, \overline{E}_2, \overline{E}_3, \overline{F}_1, \overline{F}_2$ and $\overline{F}_3$ for all grid points
For Iter=١ to Itermax
Predictor step
Initializing the value of Δt
G
C

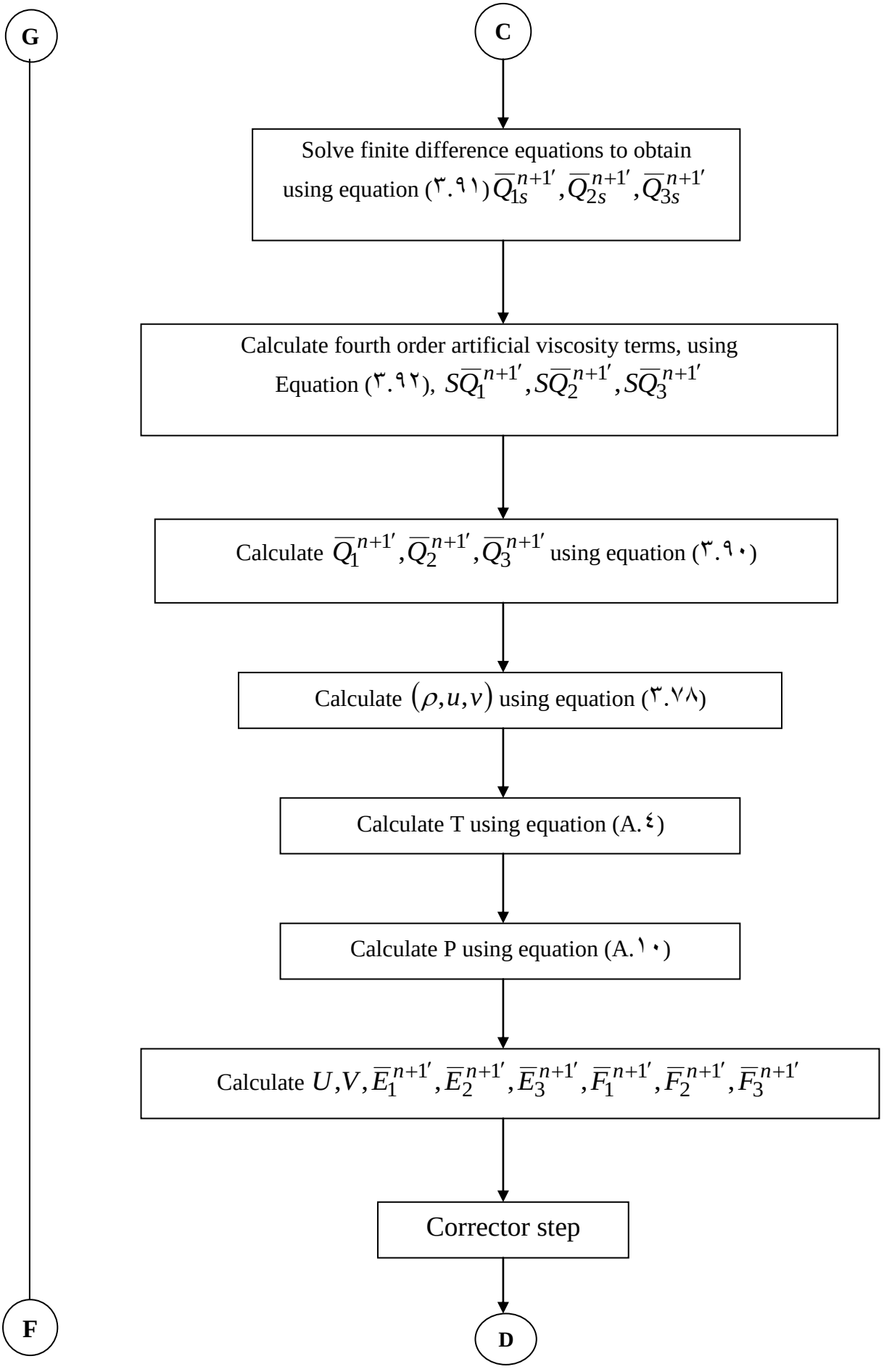
G
C
Solve finite difference equations to obtain using equation (٣.٩١) $\overline{Q}_{1s}^{n+1'}, \overline{Q}_{2s}^{n+1'}, \overline{Q}_{3s}^{n+1'}$
Calculate fourth order artificial viscosity terms, using Equation (٣.٩٢), $S\overline{Q}_1^{n+1'}, S\overline{Q}_2^{n+1'}, S\overline{Q}_3^{n+1'}$
Calculate $\overline{Q}_1^{n+1'}, \overline{Q}_2^{n+1'}, \overline{Q}_3^{n+1'}$ using equation (٣.٩٠)
Calculate (ρ, u, v) using equation (٣.٧٨)
Calculate T using equation (A.٤)
Calculate P using equation (A.١٠)
Calculate $U, V, \overline{E}_1^{n+1'}, \overline{E}_2^{n+1'}, \overline{E}_3^{n+1'}, \overline{F}_1^{n+1'}, \overline{F}_2^{n+1'}, \overline{F}_3^{n+1'}$
Corrector step
F
D

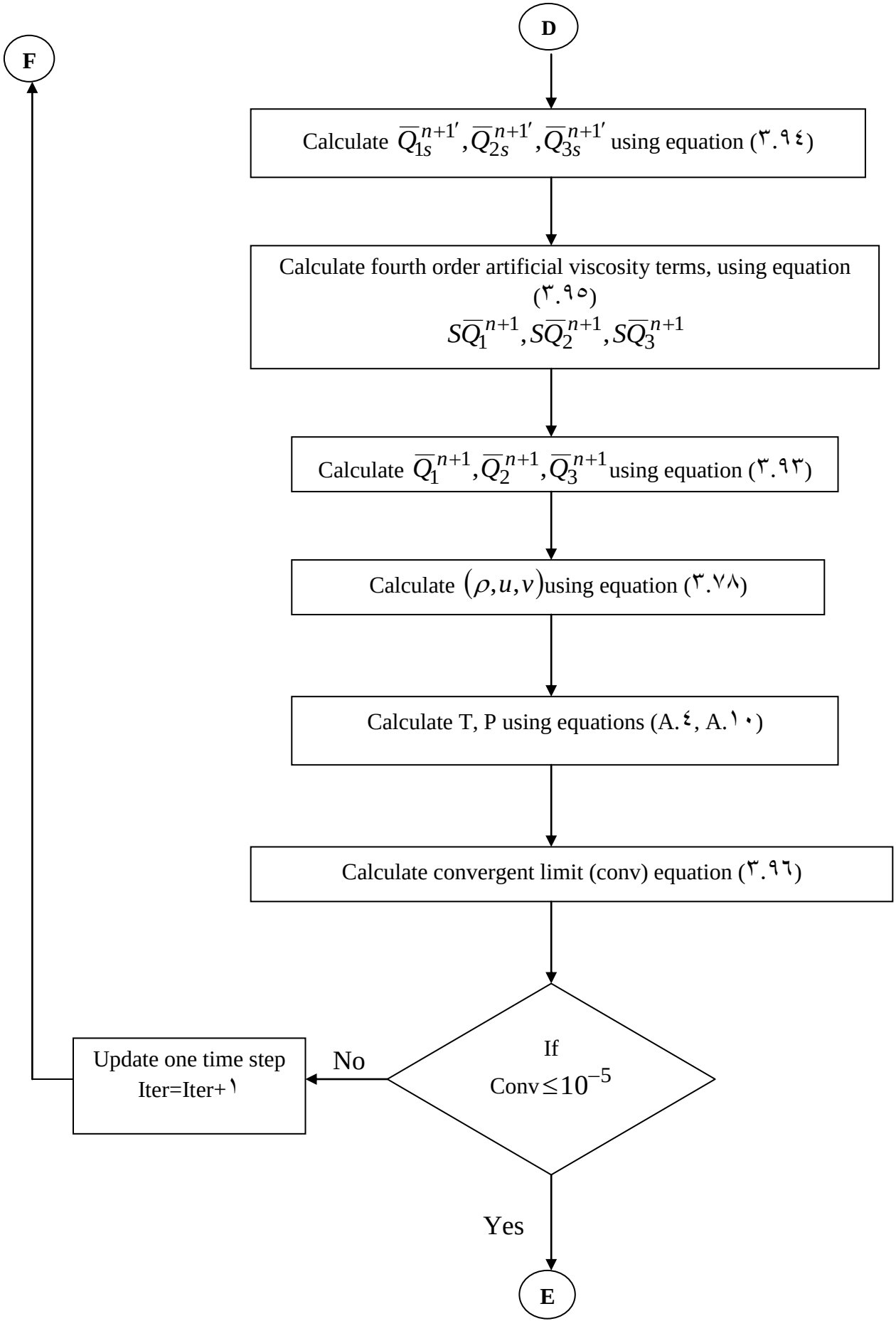
D
Calculate $\overline{Q}_{1s}^{n+1'}, \overline{Q}_{2s}^{n+1'}, \overline{Q}_{3s}^{n+1'}$ using equation (٣.٩٤)
Calculate fourth order artificial viscosity terms, using equation (٣.٩٥)
$S\overline{Q}_1^{n+1}, S\overline{Q}_2^{n+1}, S\overline{Q}_3^{n+1}$
Calculate $\overline{Q}_1^{n+1}, \overline{Q}_2^{n+1}, \overline{Q}_3^{n+1}$ using equation (٣.٩٣)
Calculate (ρ, u, v) using equation (٣.٧٨)
Calculate T, P using equations (A.٤, A.١٠)
Calculate convergent limit (conv) equation (٣.٩٦)
If
Conv $\leq 10^{-5}$
No
Update one time step
Iter=Iter+١
Yes
E
F

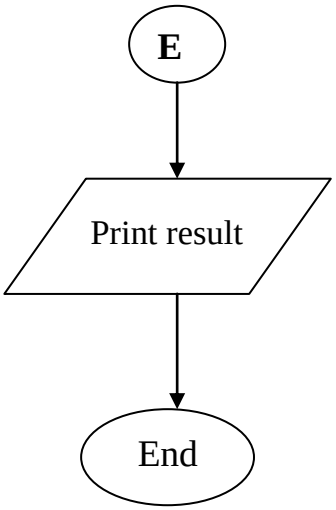

Fig (٣.٣)
The flow chart for two dimensions explicit method

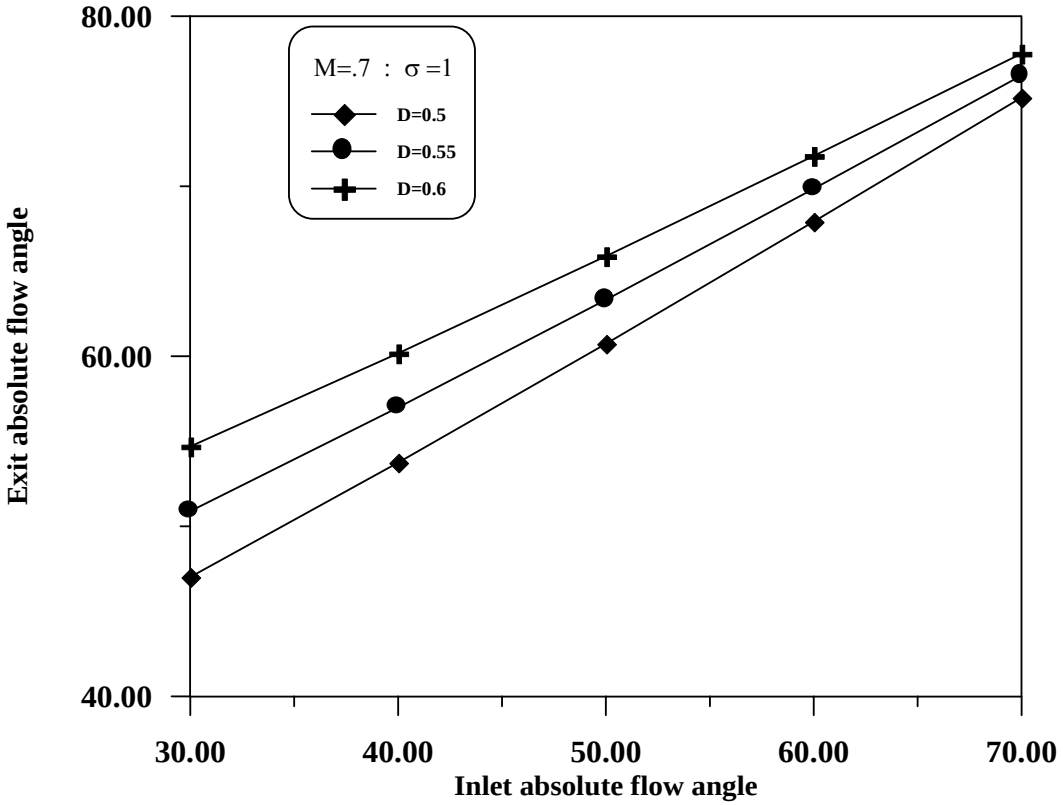

Fig.(٤.١)The variation of exit absolute flow angle with inlet absolute flow angle at different diffusion factor

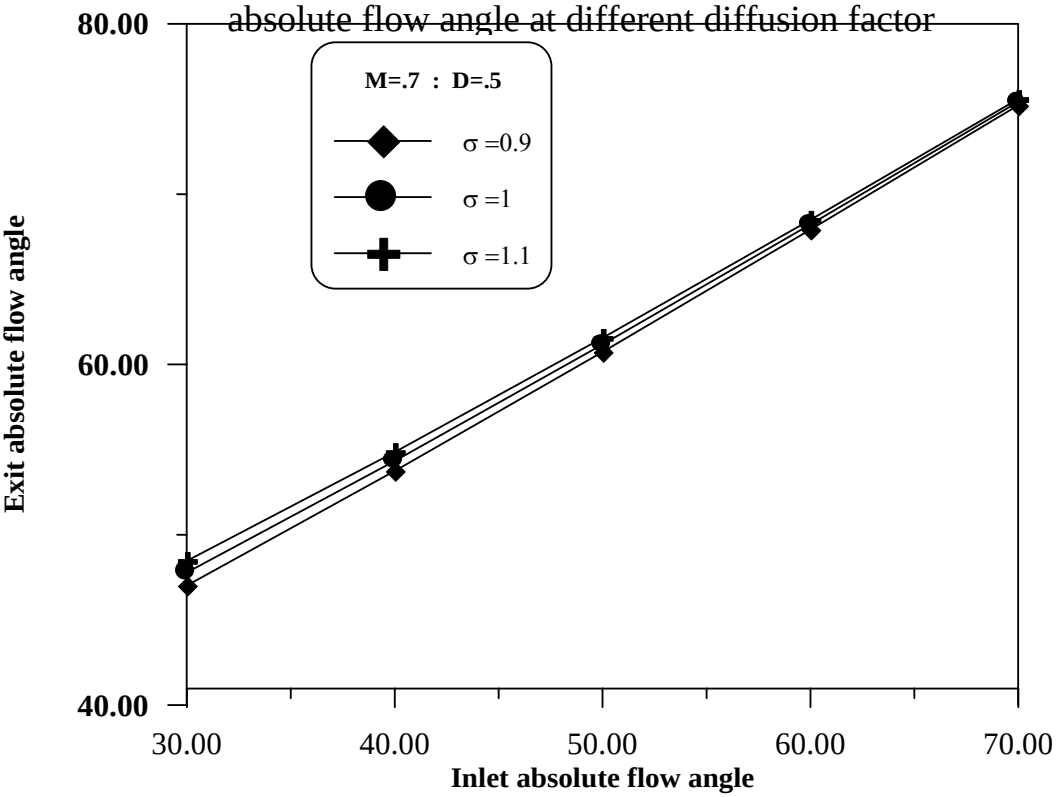

Fig.(٤.٢)The variation of exit absolute flow angle with inlet absolute flow angle at different solidity factor

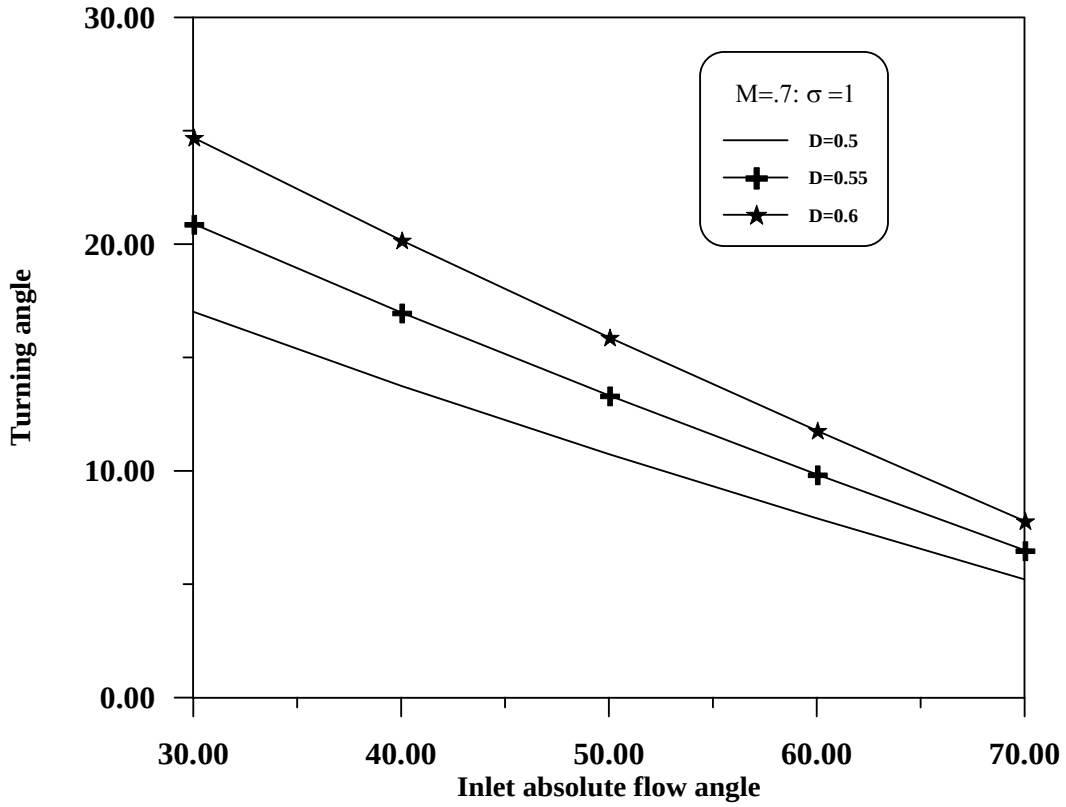

Fig.(٤.٣)The variation of turning angle with inlet absolute flow angle at different diffusion factor

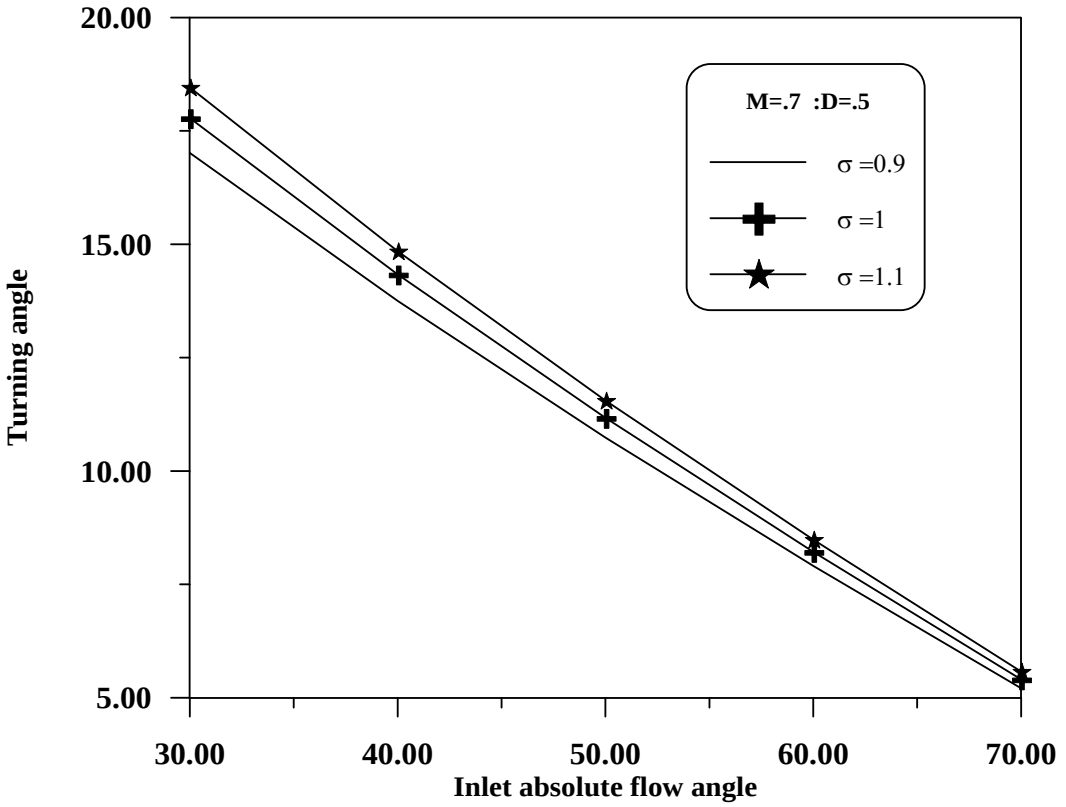

Fig.(٤.٤)The variation of turning angle with inlet absolute flow angle at different solidity factor

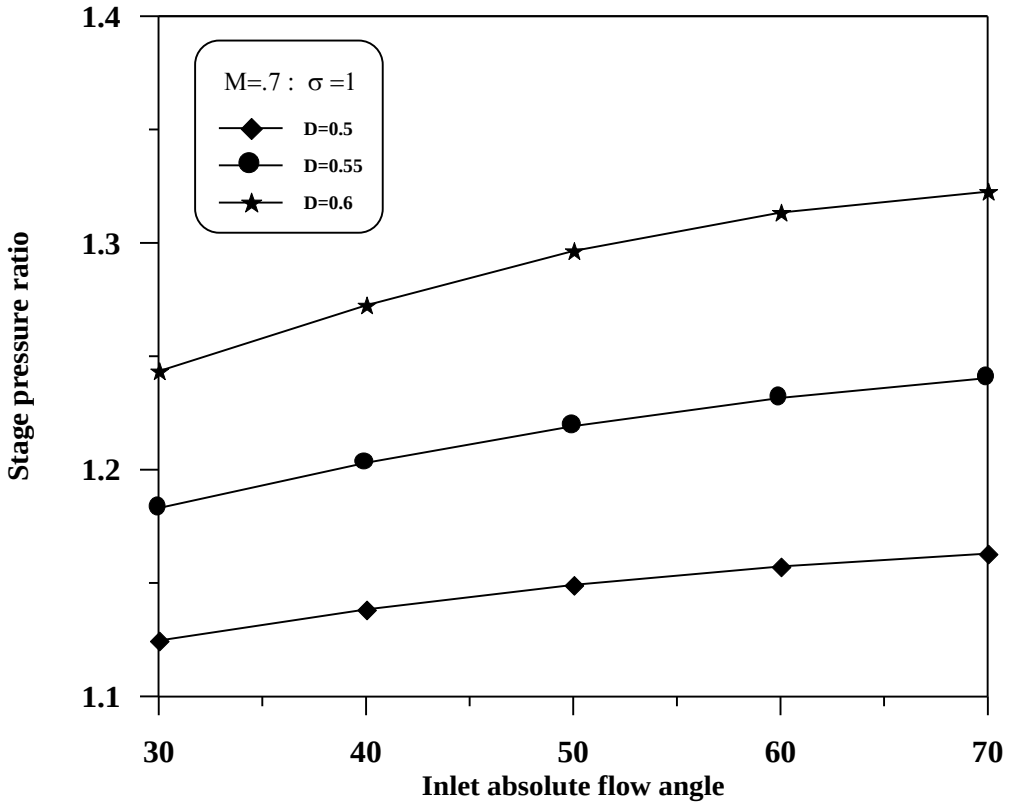

Fig. (٤.٥) The variation of stage pressure ratio with inlet absolute flow angle at different diffusion factor

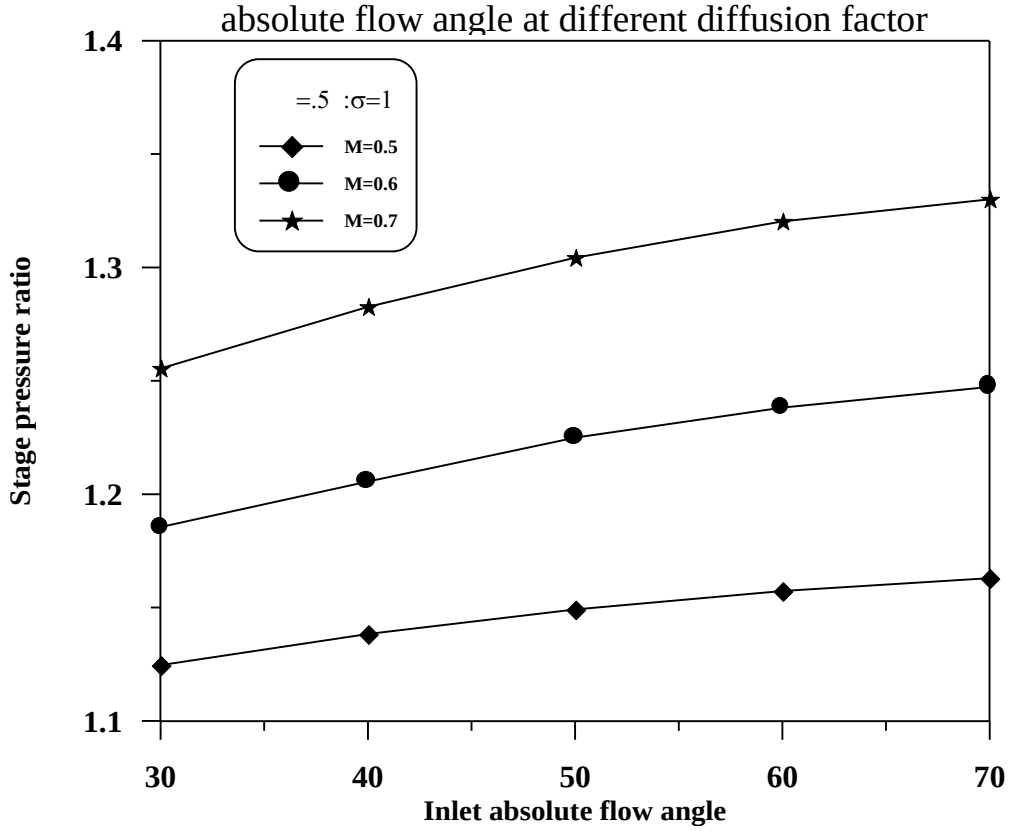

Fig. (٤.٦) The variation of stage pressure ratio with inlet absolute flow angle at different Mach number

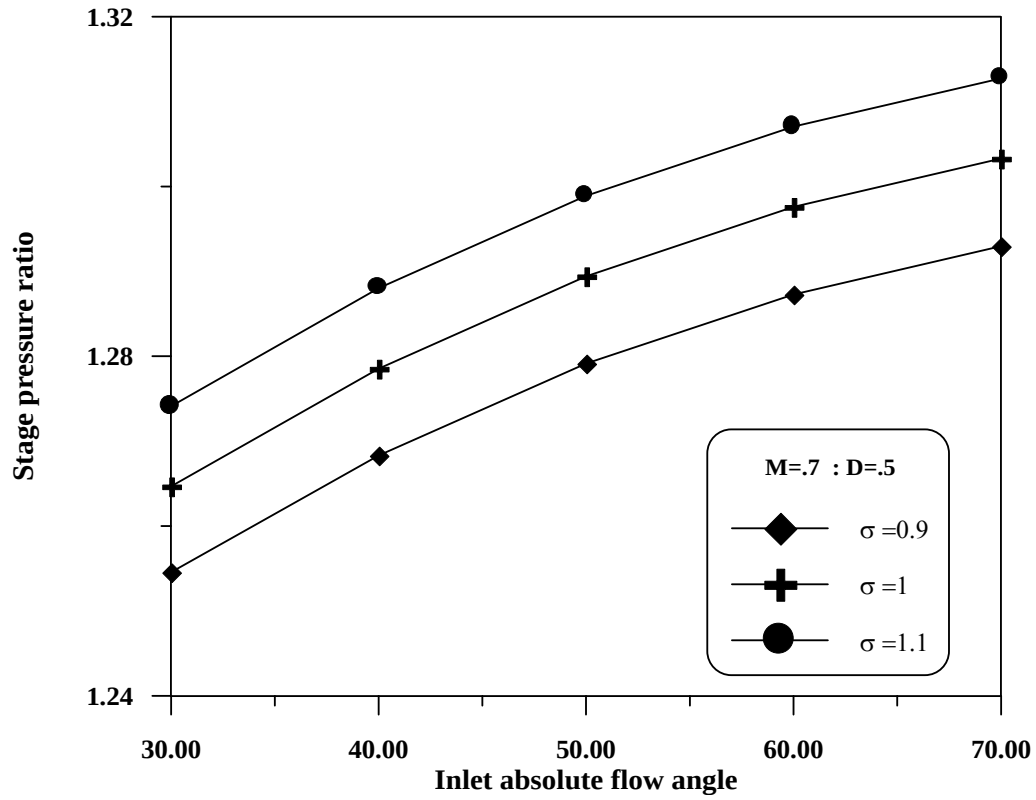

Fig. (٤.٧) The variation of stage pressure ratio with inlet absolute flow angle at different solidity factor

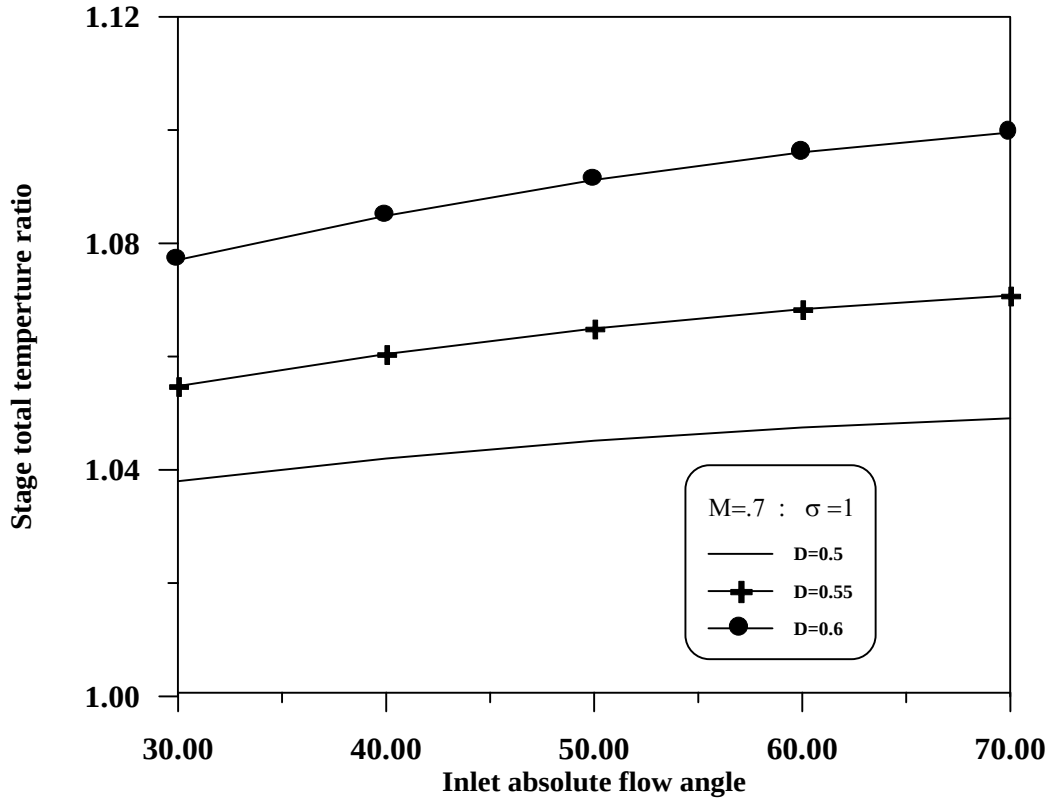

Fig. (٤.٨) The variation of stage total temperature ratio with inlet absolute flow angle at different diffusion factor

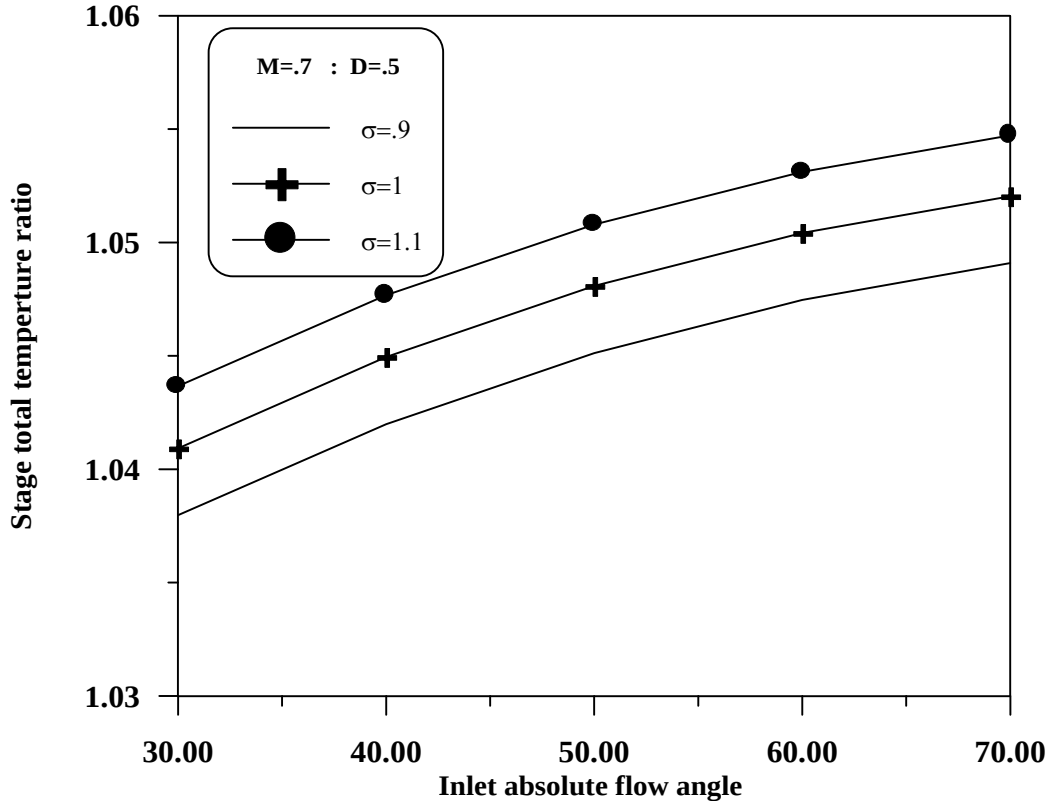

Fig. (٤.٩) The variation of stage total temperature ratio with inlet absolute flow angle at different solidity factor

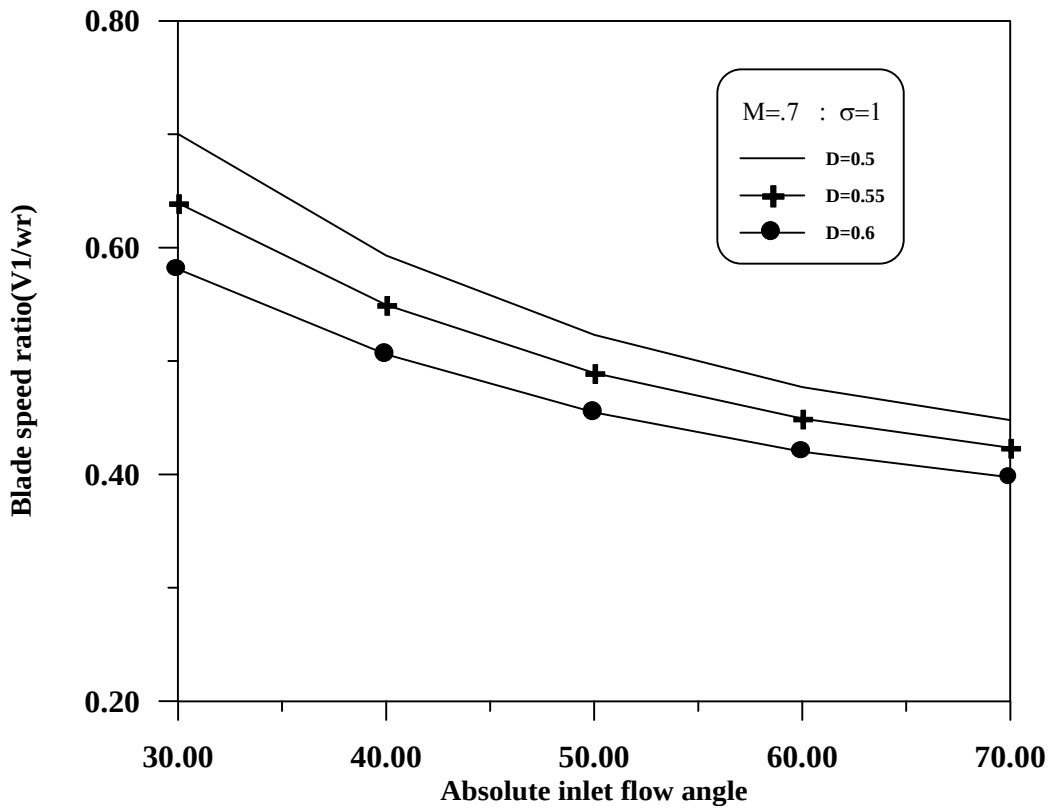

Fig.(٤.١٠) The variation of blade speed ratio with inlet absolute flow angle at different diffusion factor

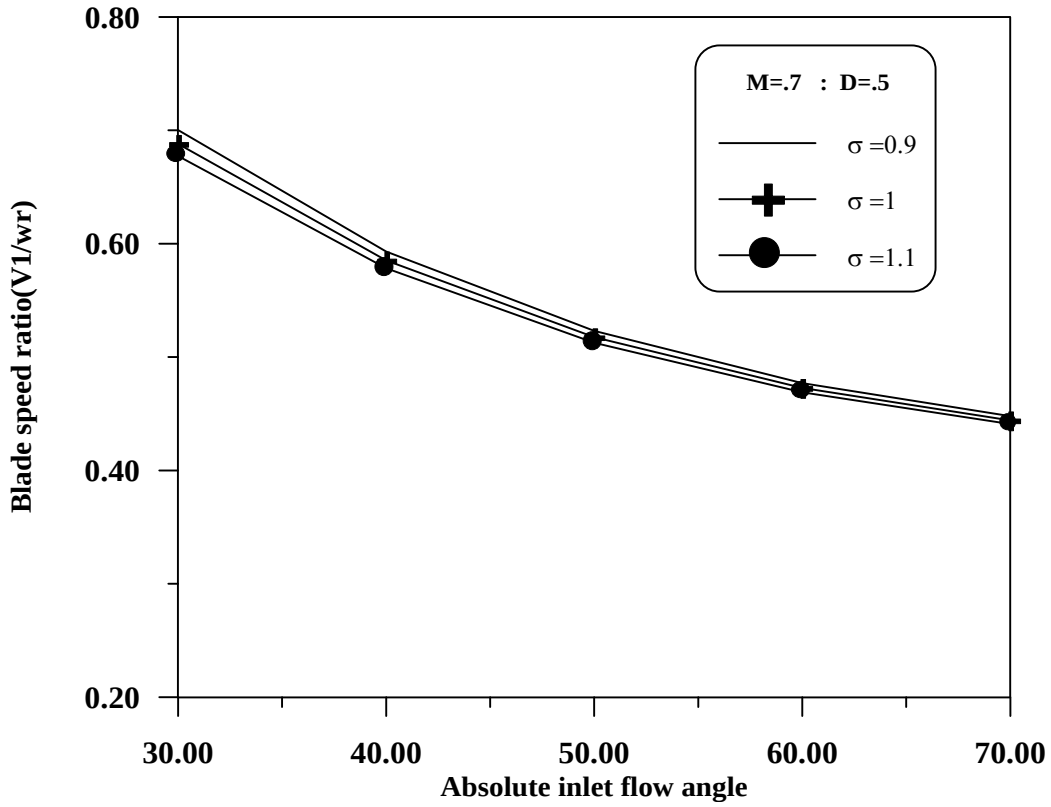

Fig.(٤.١١) The variation of blade speed ratio with inlet absolute flow angle at different solidity factor

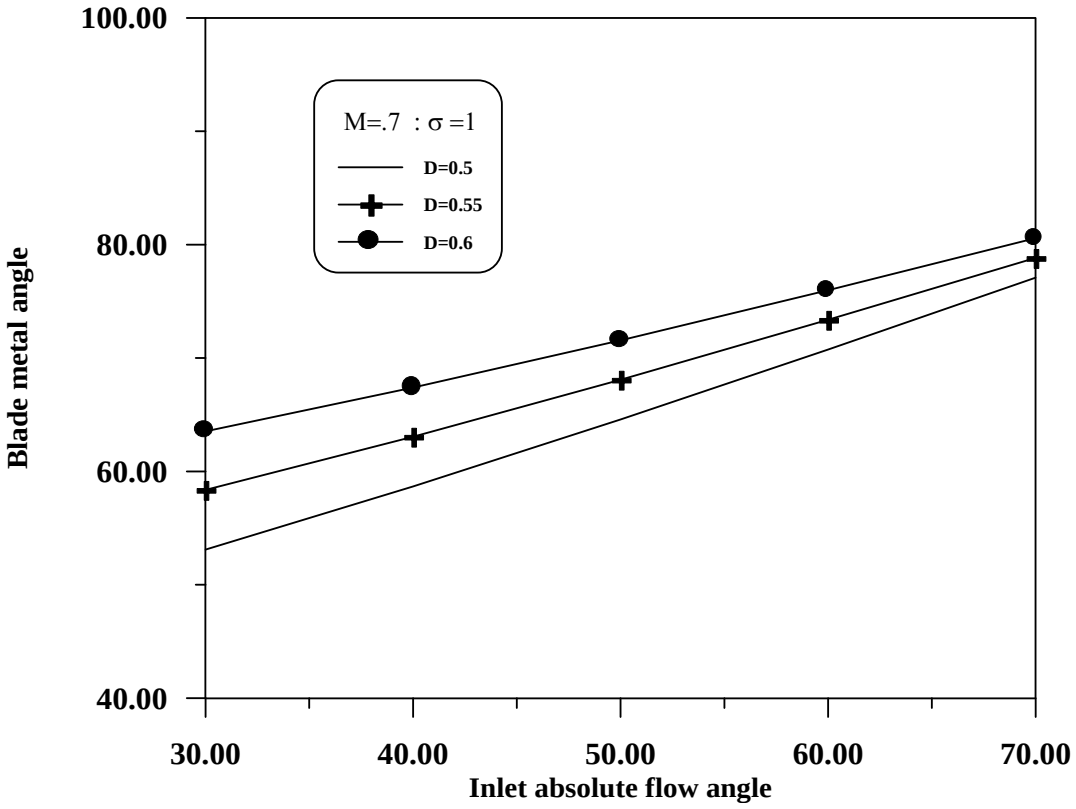

Fig.(٤.١٢) The variation of blade metal angle with inlet absolute flow angle at different diffusion factor

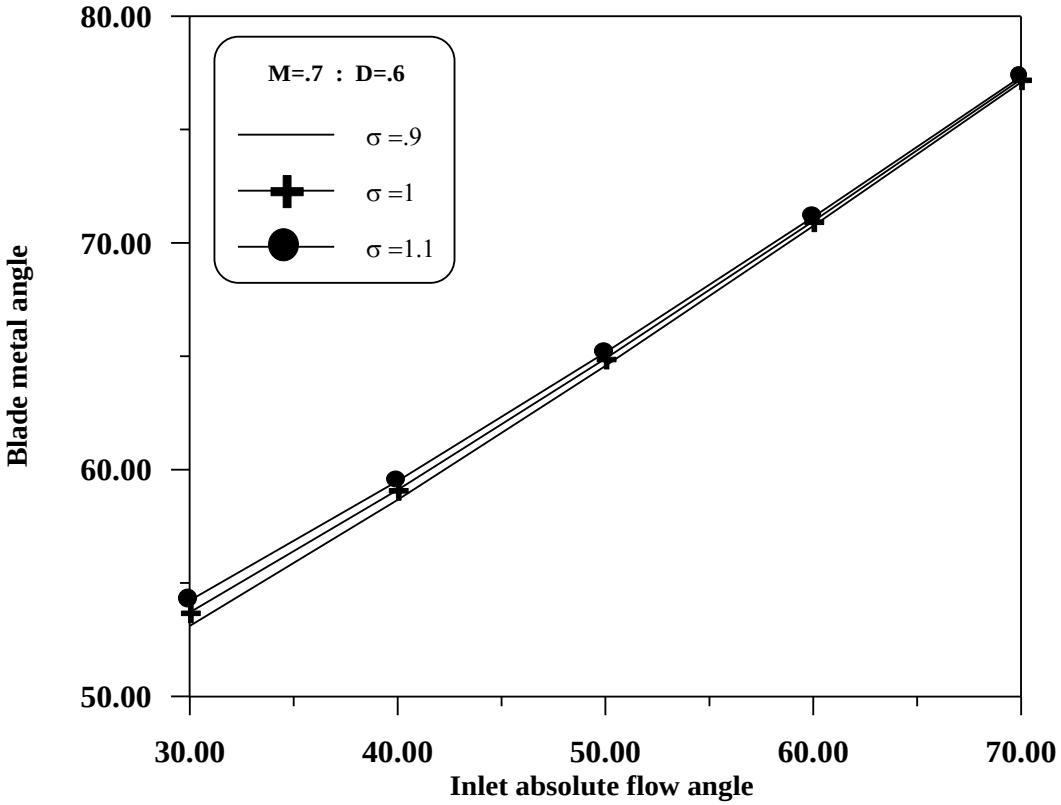

Fig.(٤.١٣) The variation of blade metal angle with inlet absolute flow angle at different solidity factor

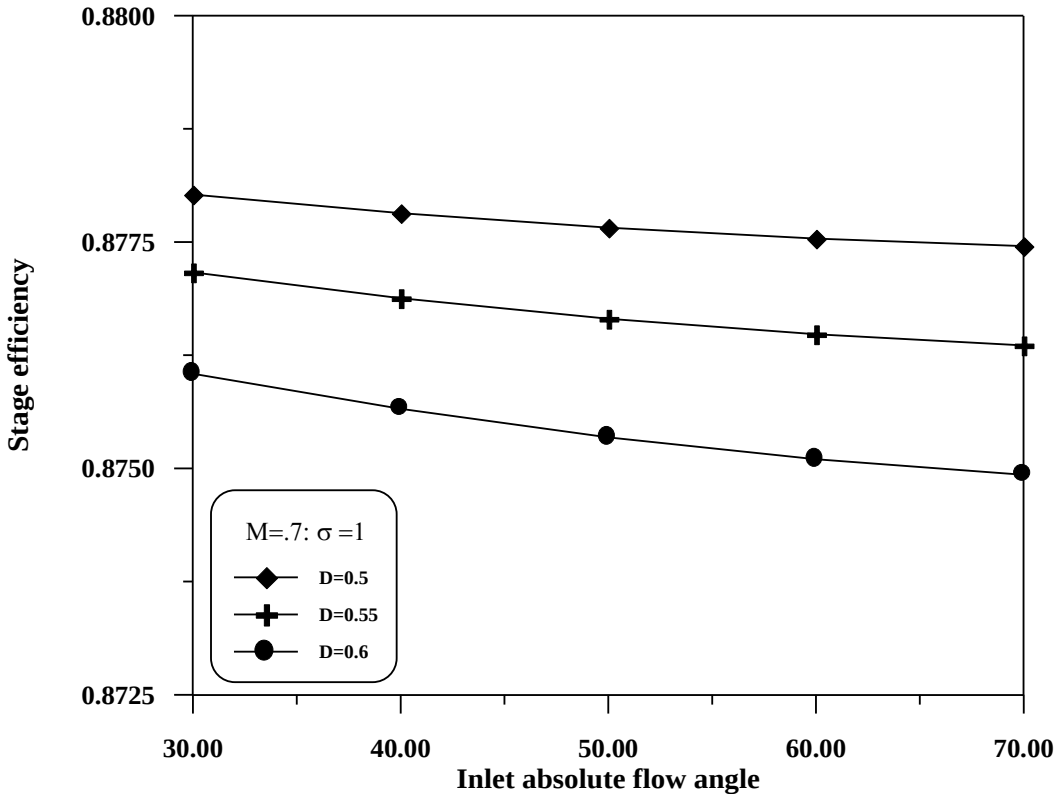

Fig.(٤.١٤)The variation of stage efficiency with inlet absolute flow angle at different diffusion factor

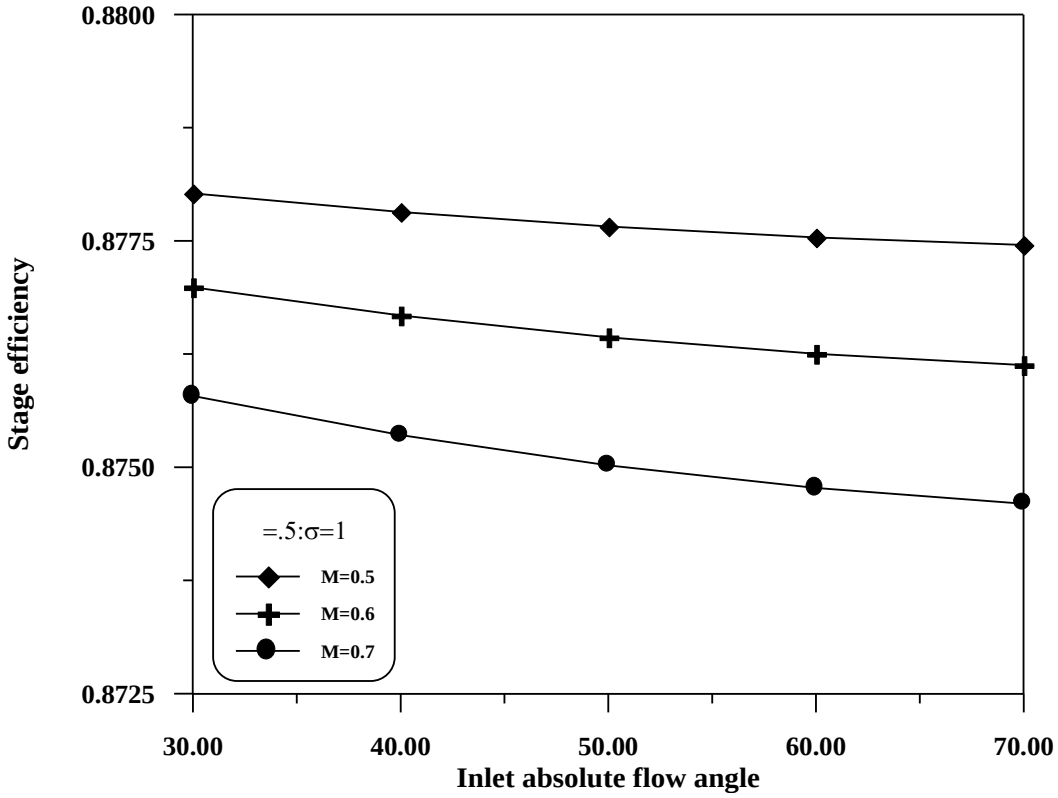

Fig.(٤.١٥) The variation of stage efficiency with inlet absolute flow angle at different Mach number

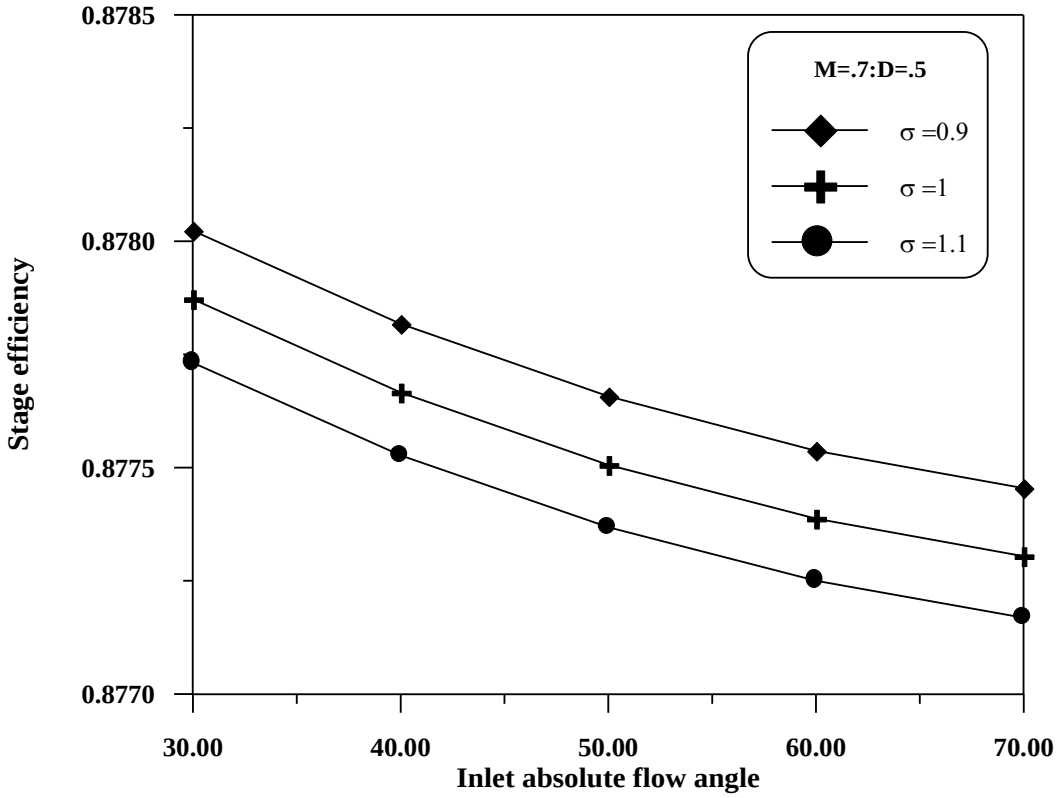

Fig.(٤.١٦) The variation of stage efficiency with inlet absolute flow angle at different solidity factor

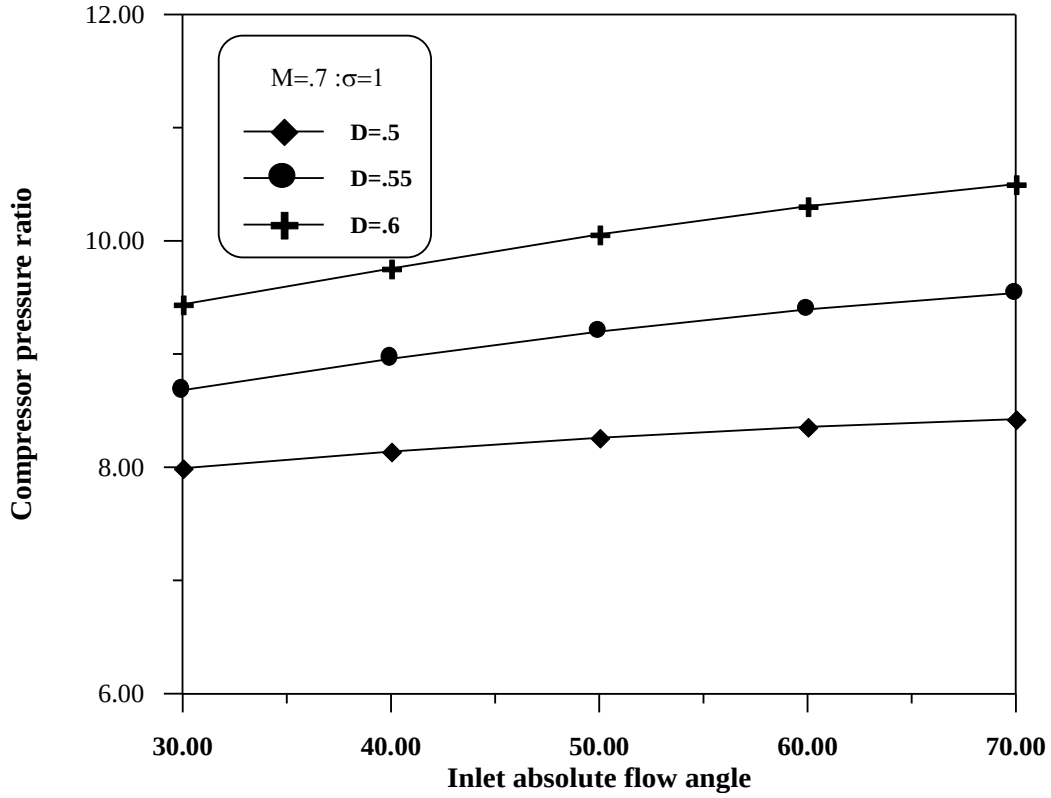

Fig.(٤.١٧) The variation of compressor pressure ratio with inlet absolute flow angle at different diffusion factor

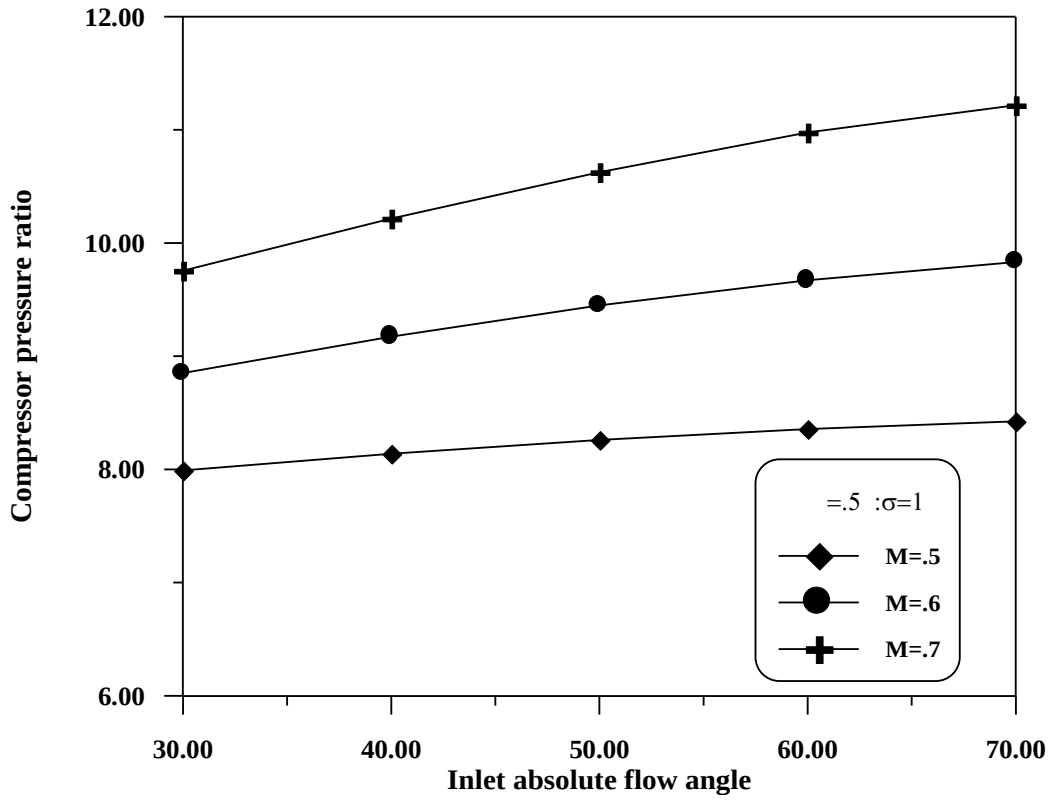

Fig. (٤.١٨) The variation of compressor pressure ratio with inlet absolute flow angle at different Mach number

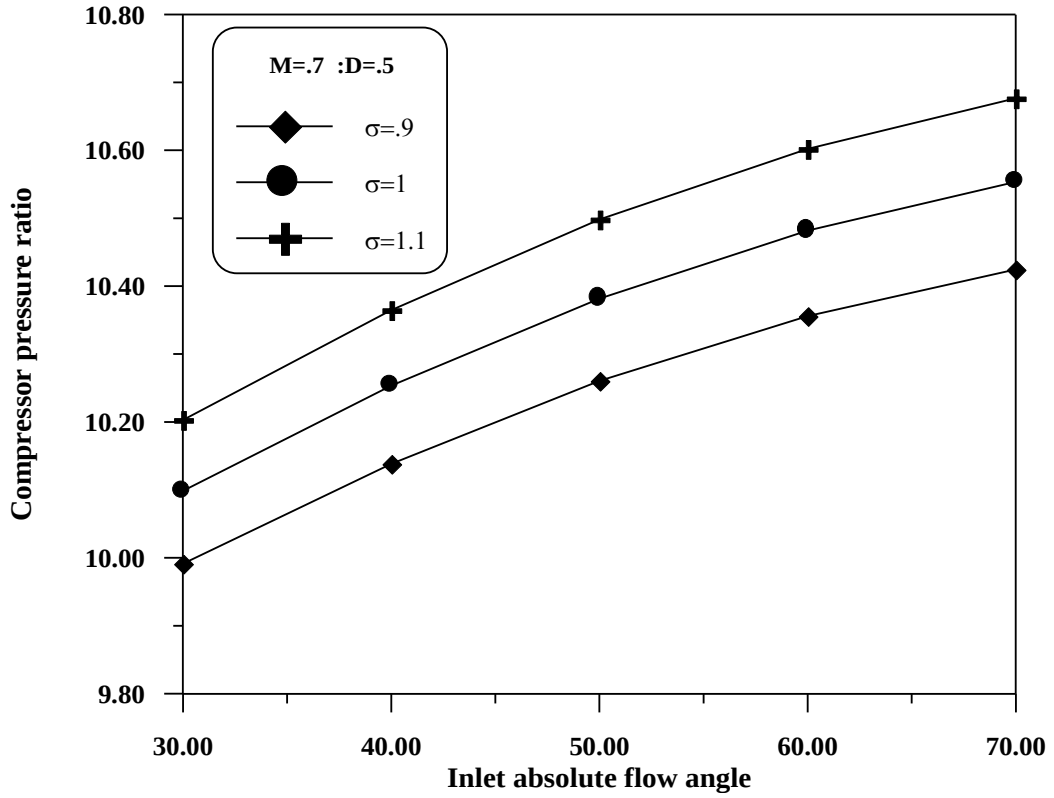

Fig. (٤.١٩) The variation of compressor pressure ratio with inlet absolute flow angle at different solidity factor

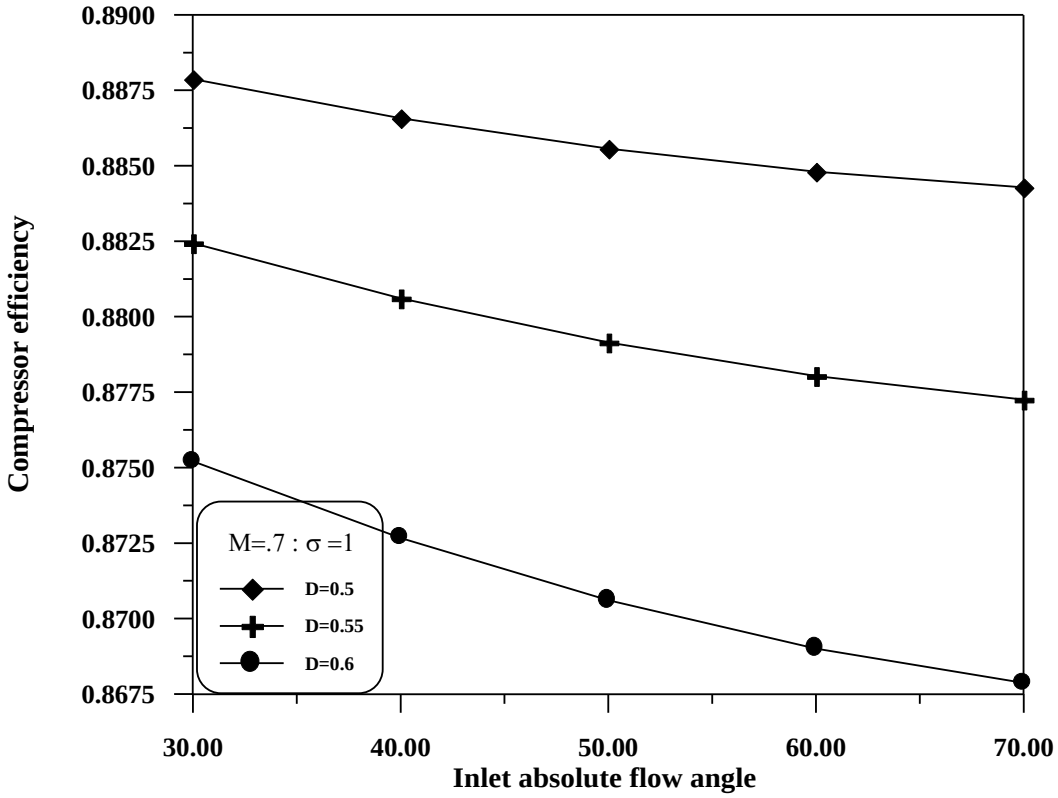

Fig.(٤.٢٠) The variation of compressor efficiency with inlet absolute flow angle at different diffusion factor

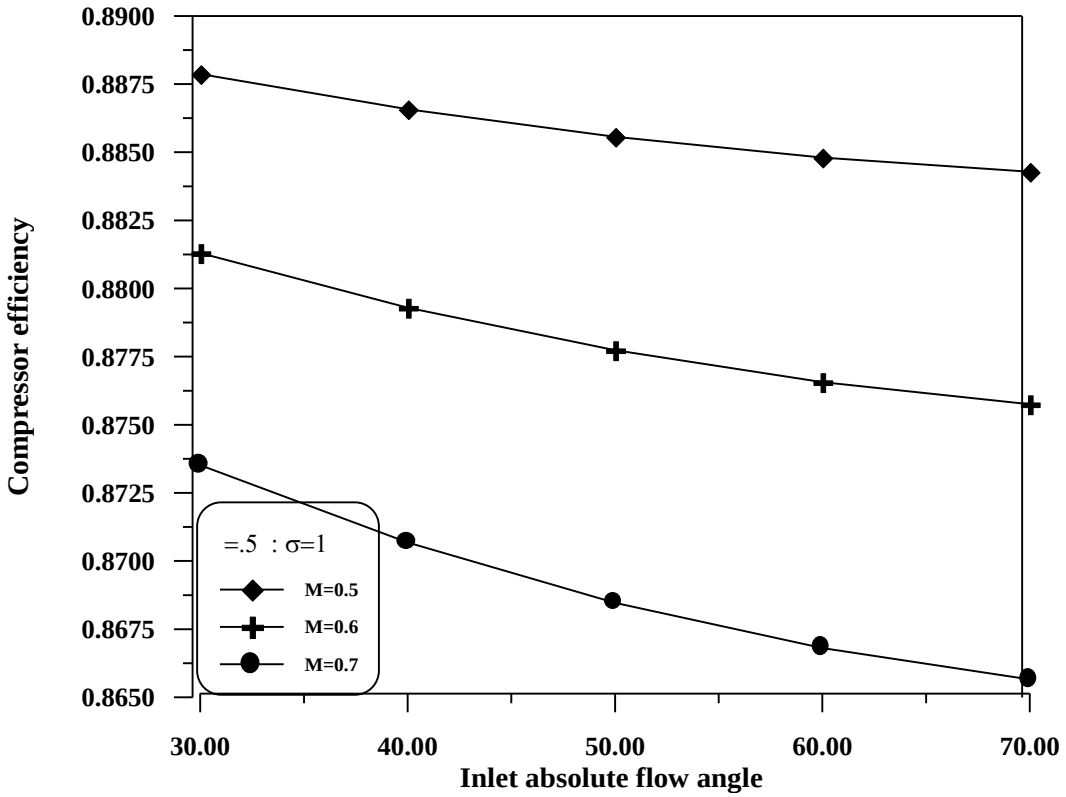

Fig.(٤.٢١) The variation of compressor efficiency with inlet absolute flow angle at different Mach number

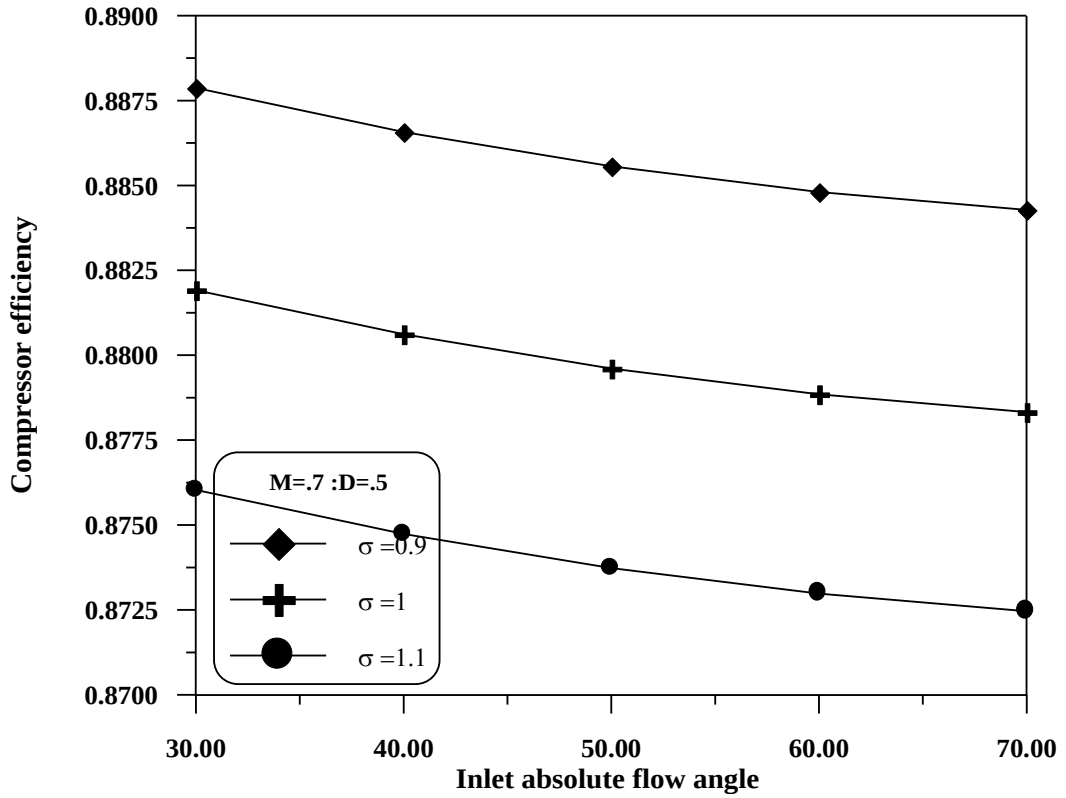

Fig.(٤.٢٢) The variation of compressor efficiency with inlet absolute flow angler at different solidity factor

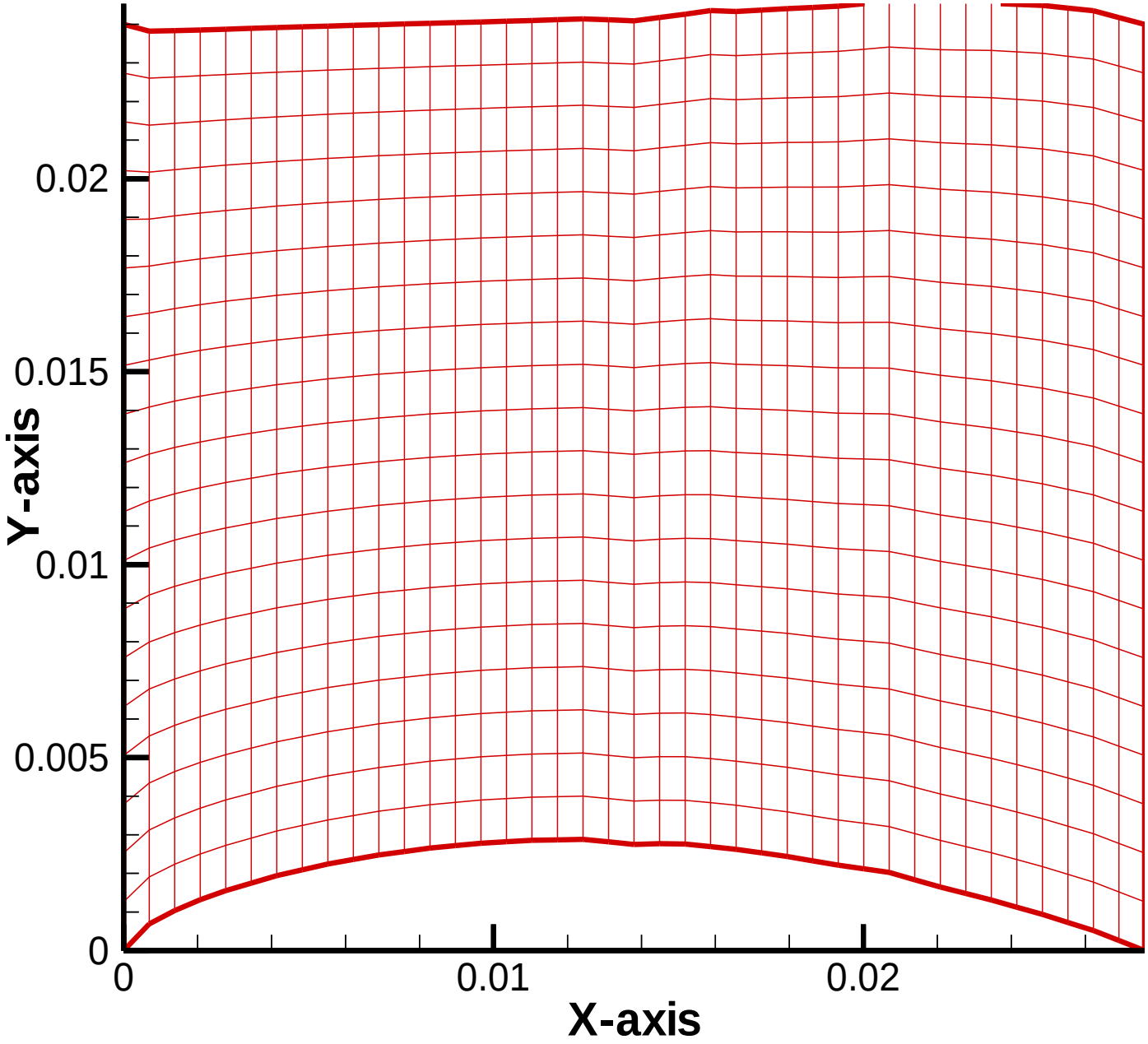

Fig.(٤.٢٣) Mesh of grid generation

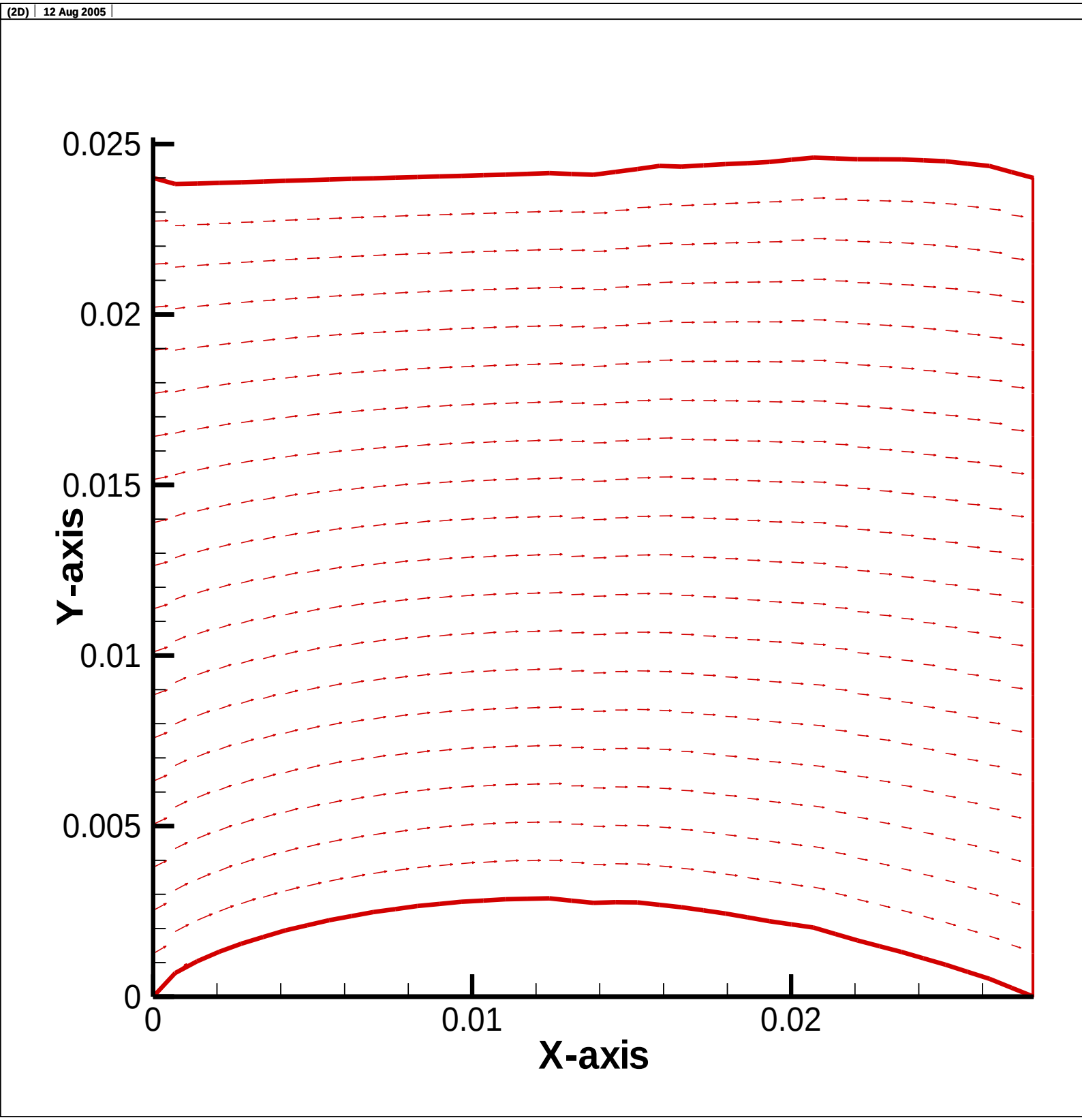

Fig.(٤.٢٤) Velocity vector along the stator blade

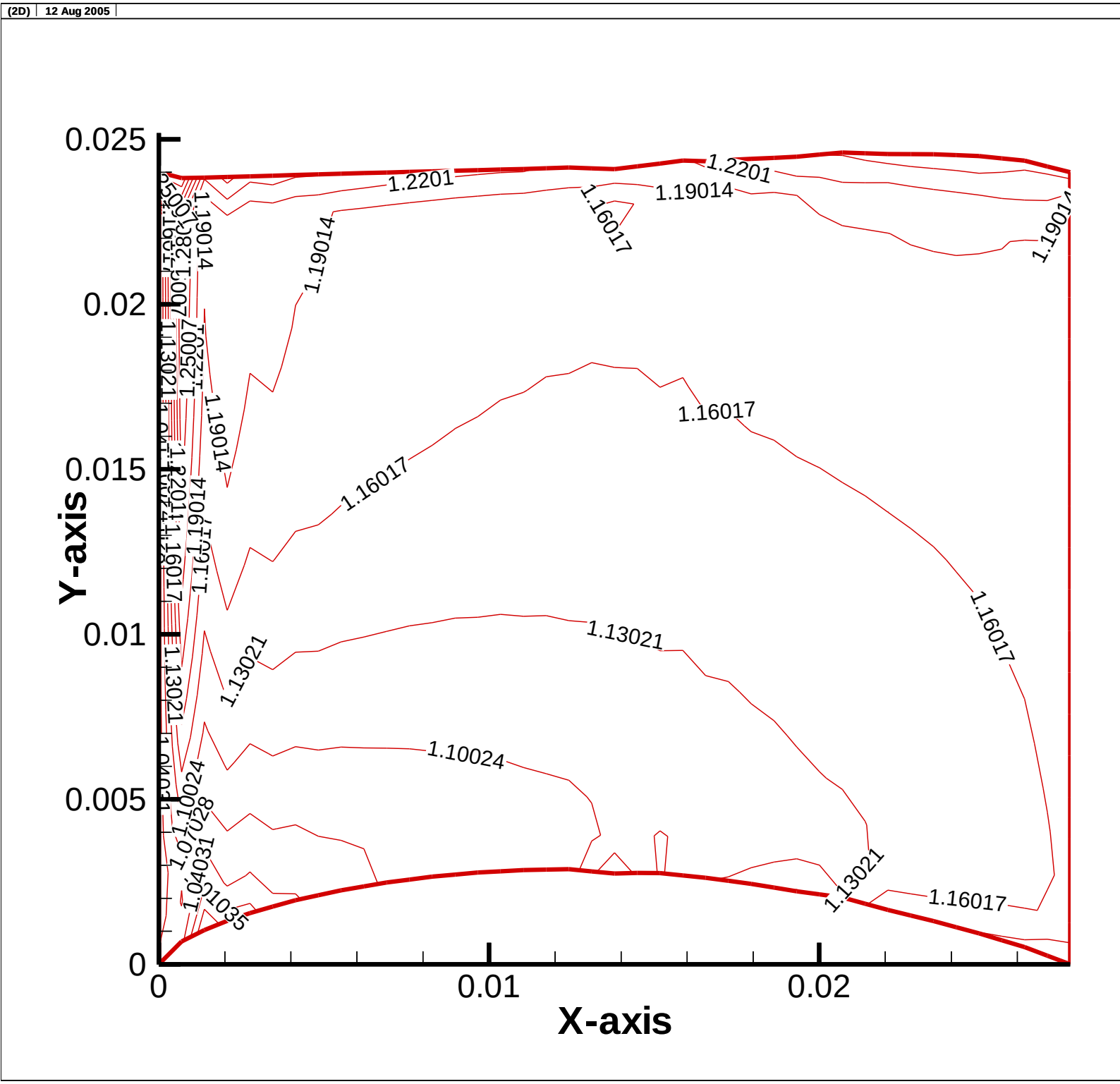

Fig.(٤.٢٥) Contour lines of density along the stator blade

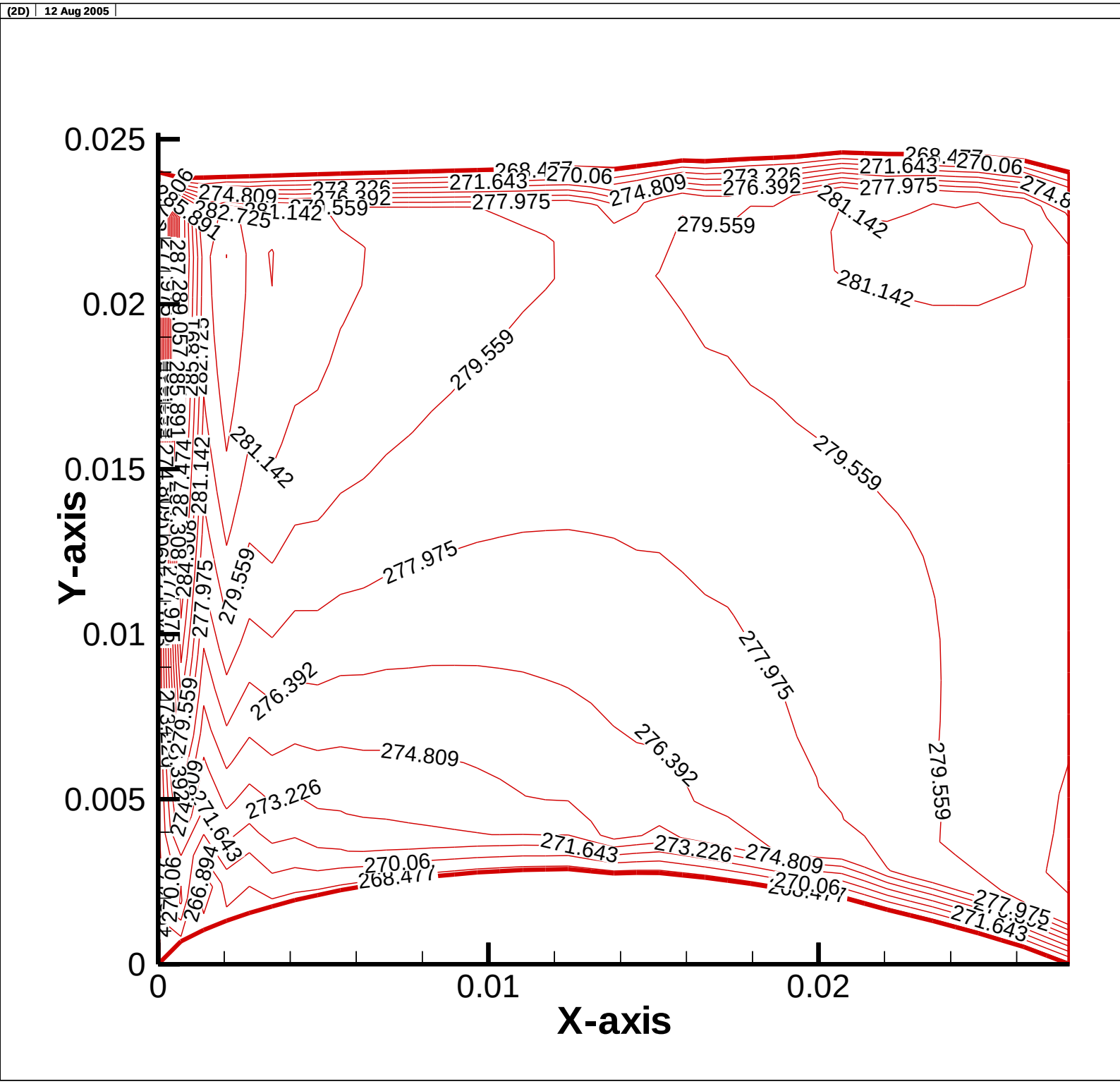

Fig.(٤.٢٦) Contour lines of temperature along the stator blade

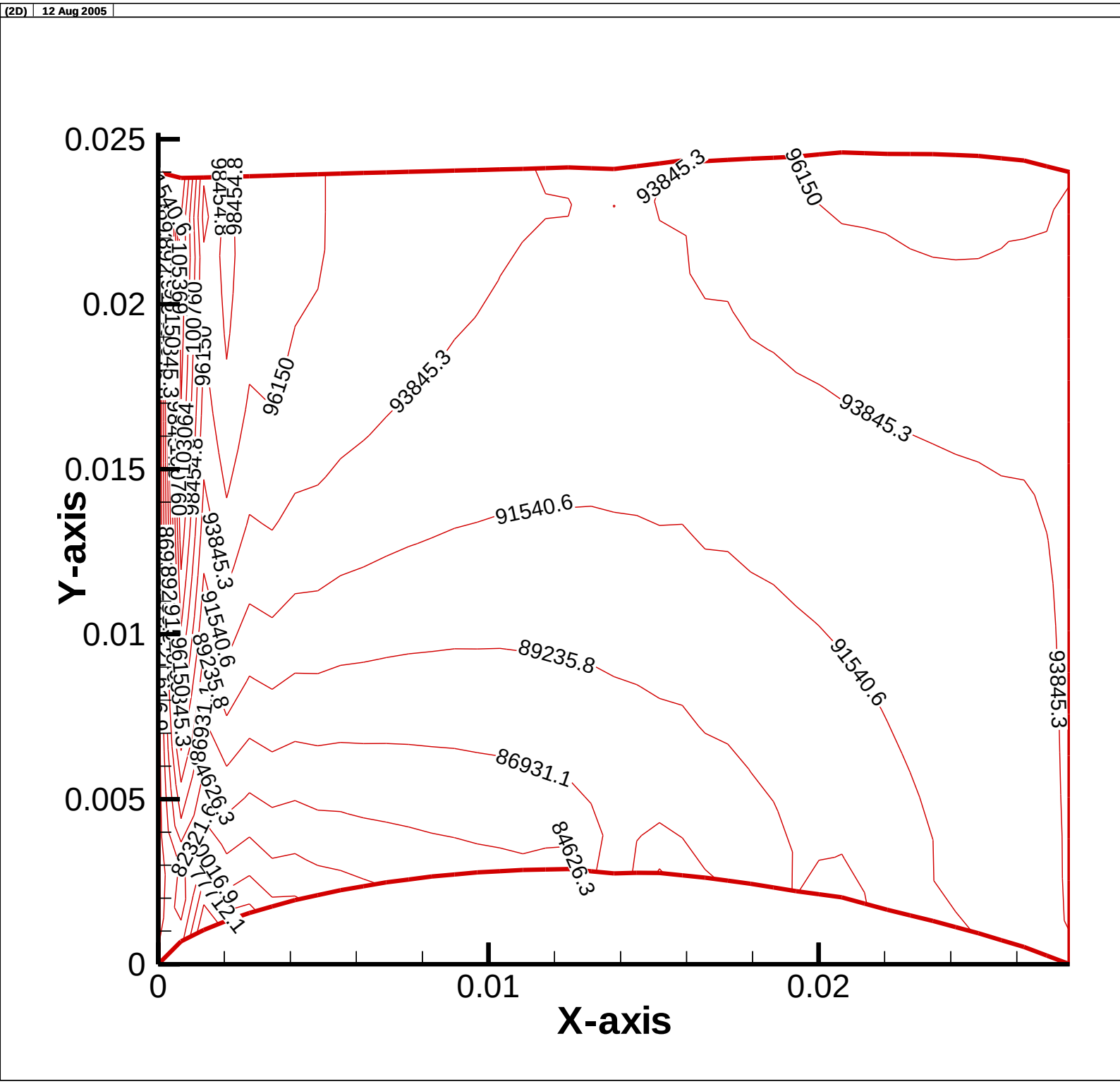

Fig.(٤.٢٧) Contour lines of pressure along the stator blade

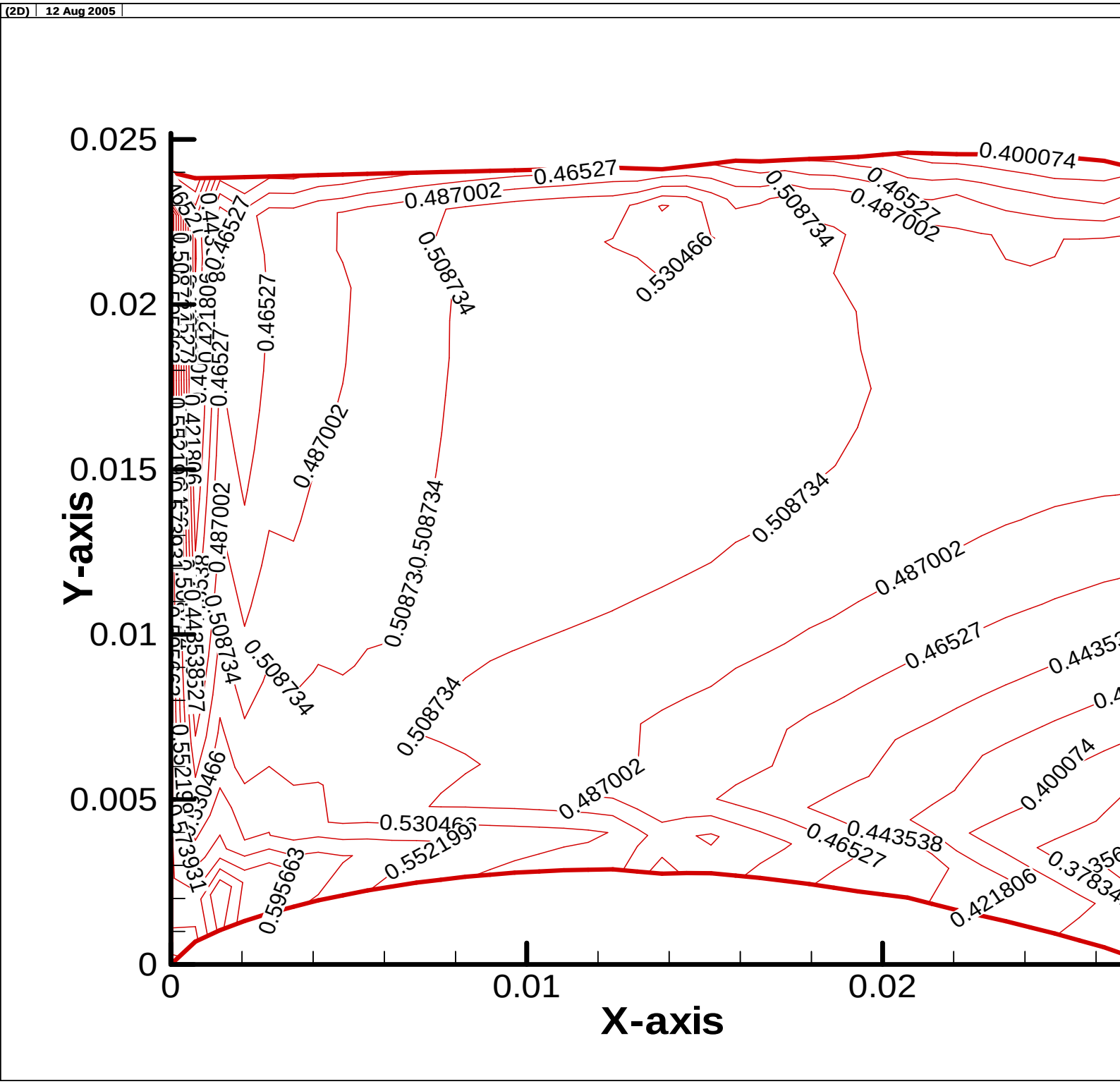

Fig.(٤.٢٨)Contour lines of Mach number along the stator blade

Fig(٤.٣٧)Absolute Mach number distributions along stator blade

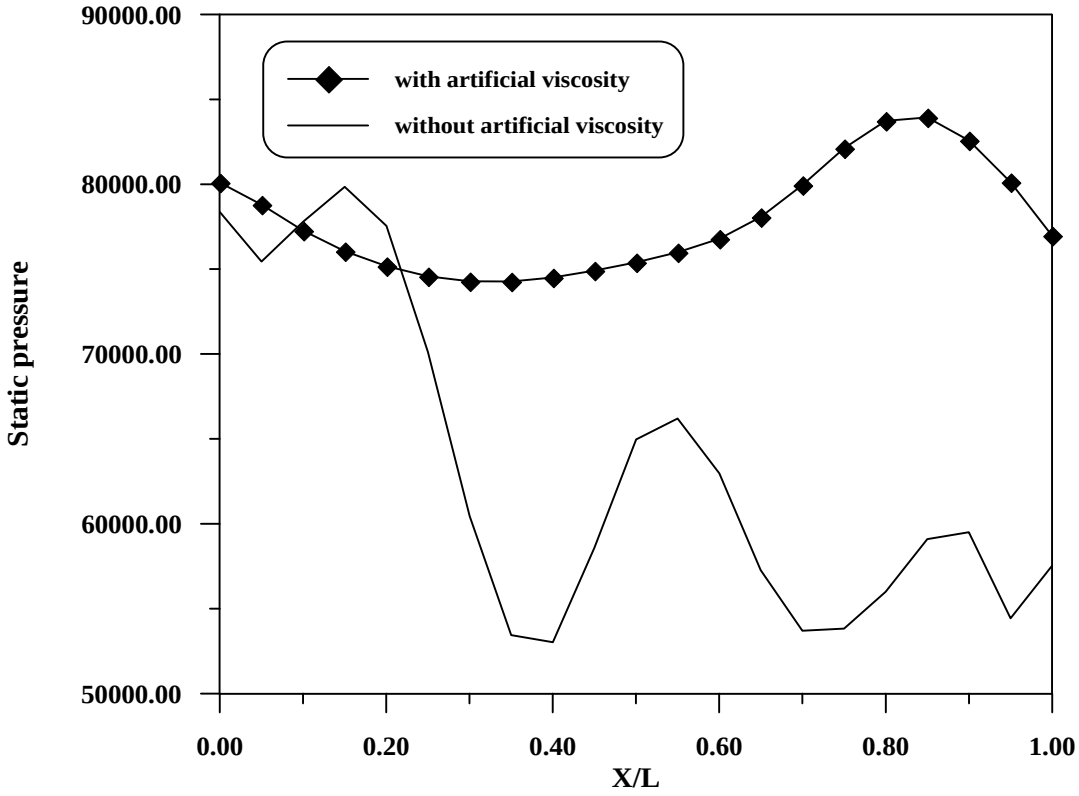

Fig.(٤.٣٨)The variation of static pressure with the fraction of axial chord in the stator passage

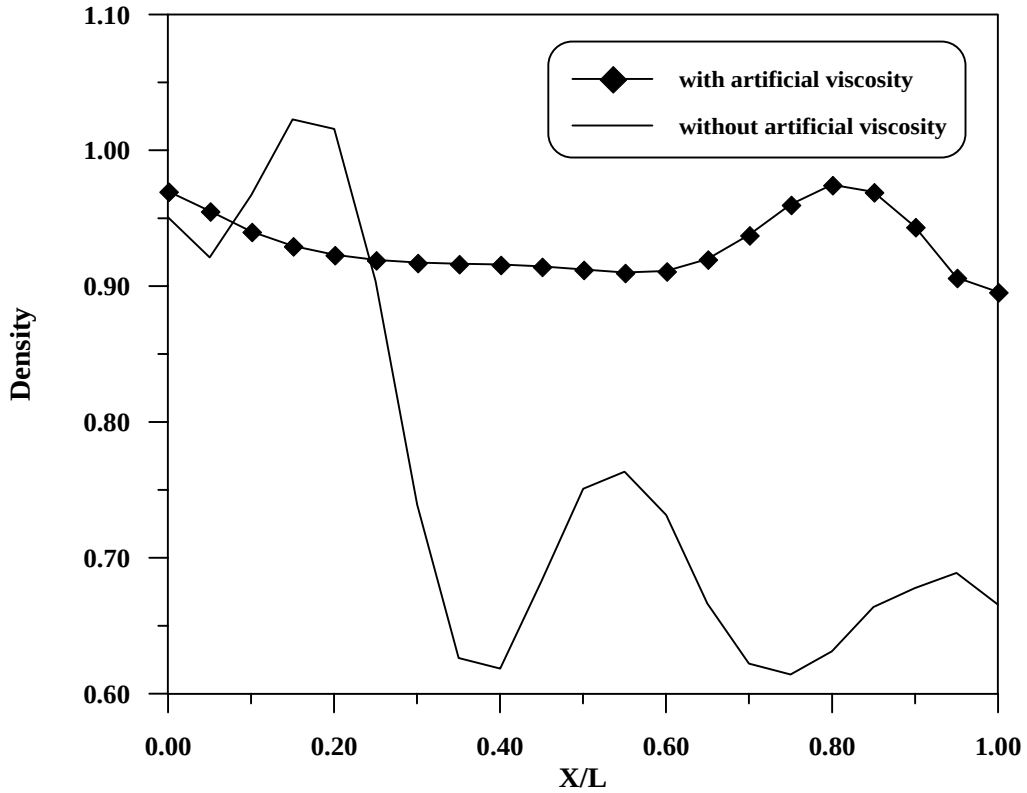

Fig.(٤.٣٩) The variation of density with the fraction of axial chord in the stator passage

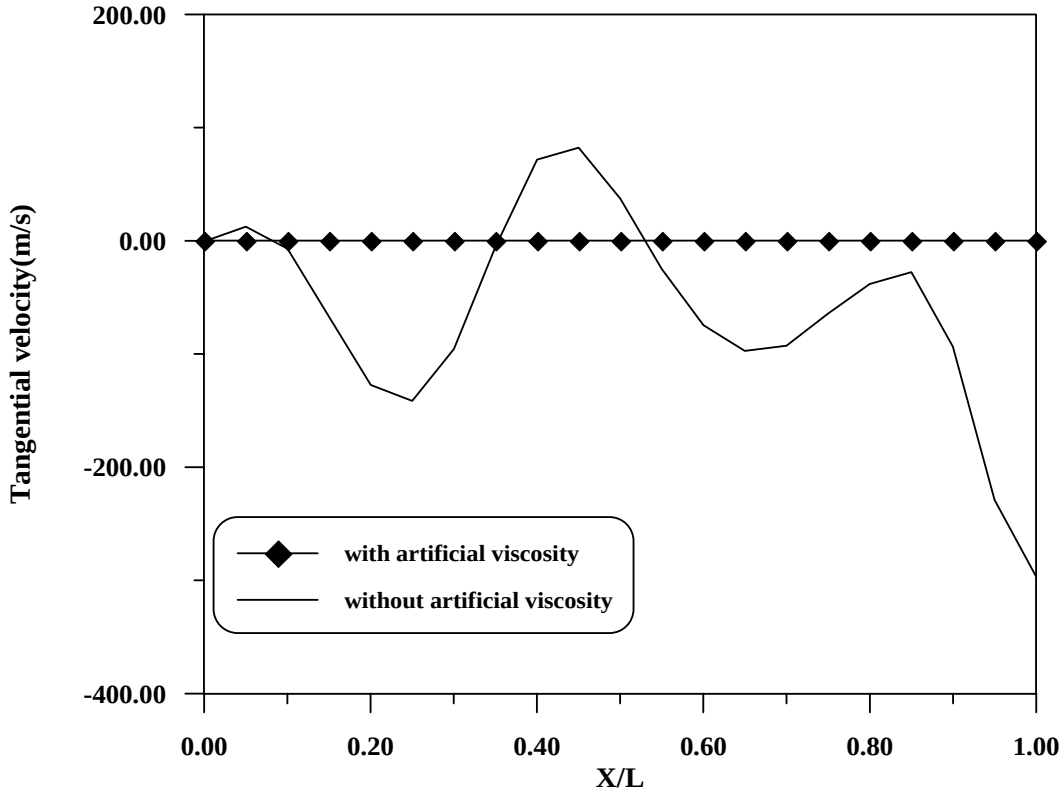

Fig.(٤.٤٠)The variation of radial velocity with the fraction of axial chord in the stator passage

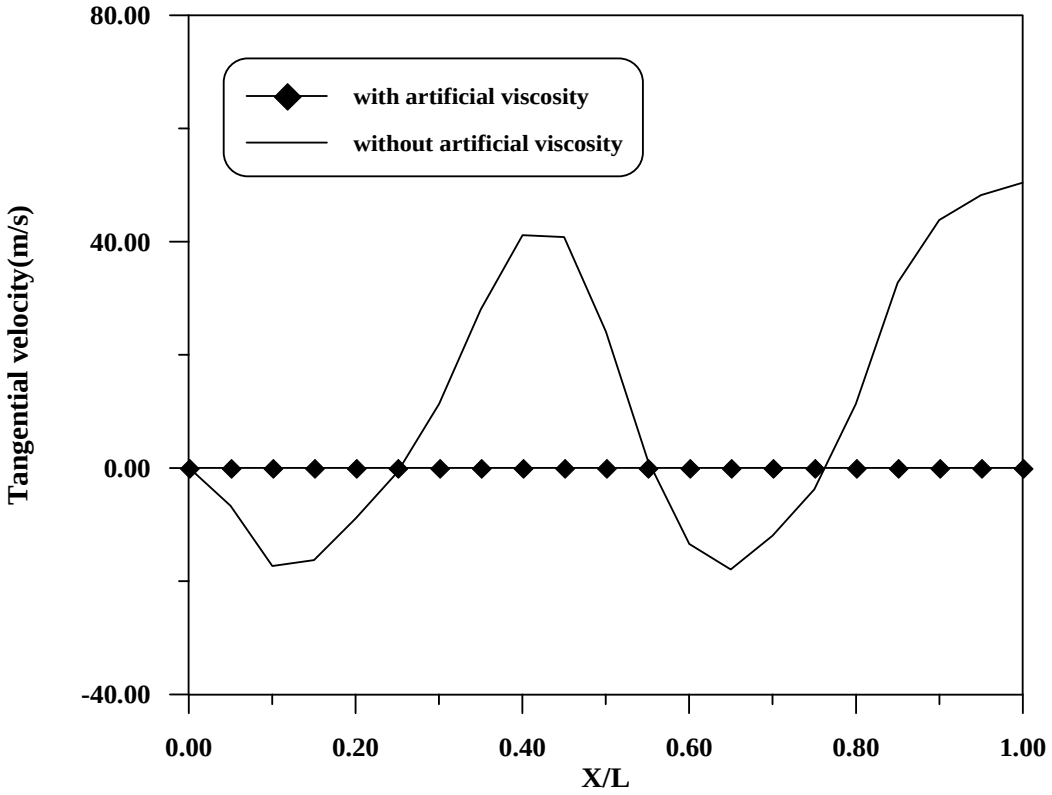

Fig.(٤.٤١) The variation of radial velocity with the fraction of axial chord in the rotor passage

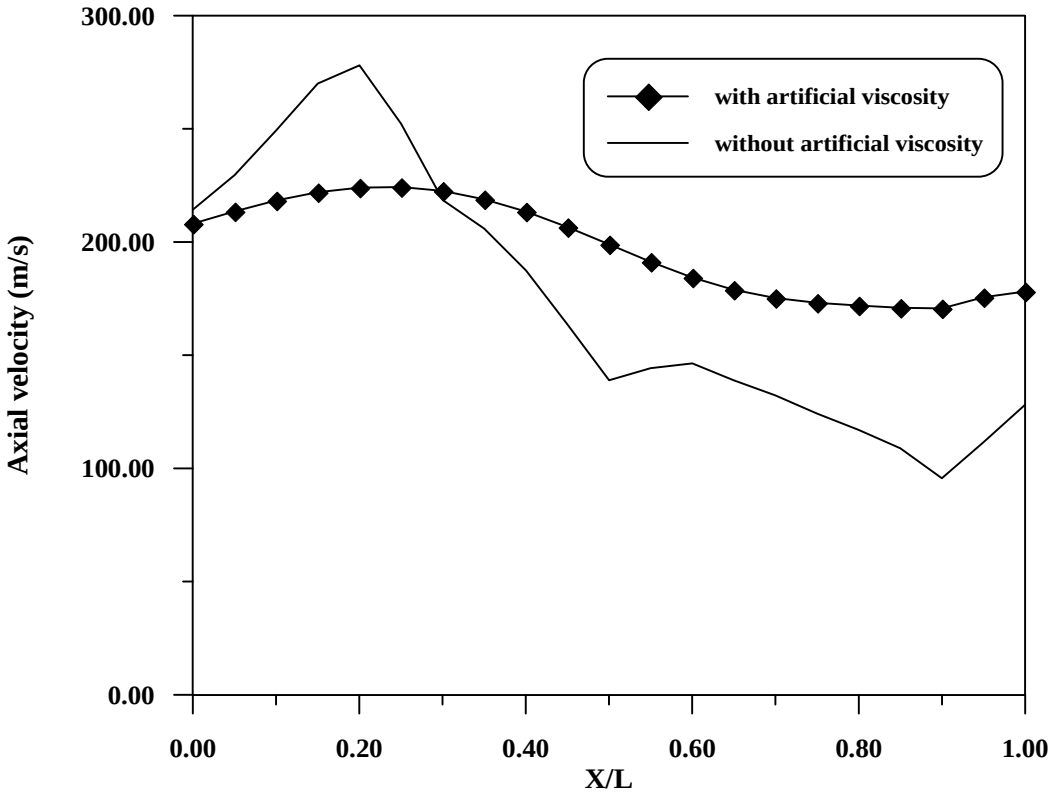

Fig.(٤.٤٢)The variation of axial velocity with the fraction of axial chord in the rotor passage

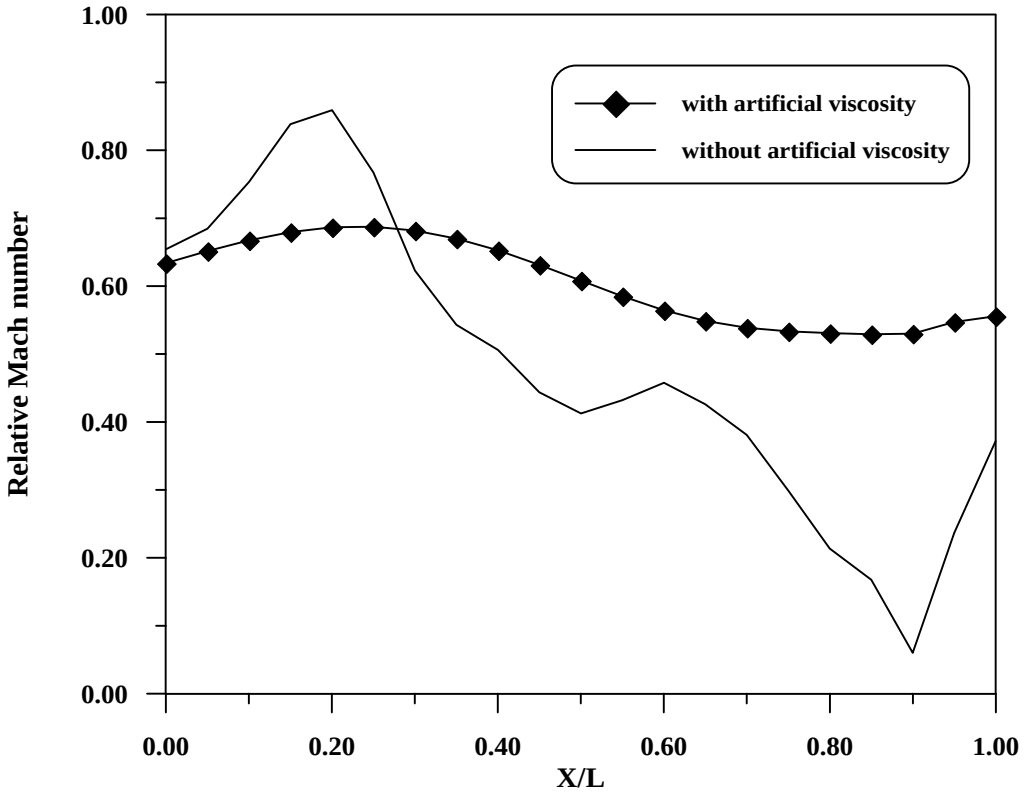

Fig.(٤.٤٣) Relative Mach number distributions along rotor blade

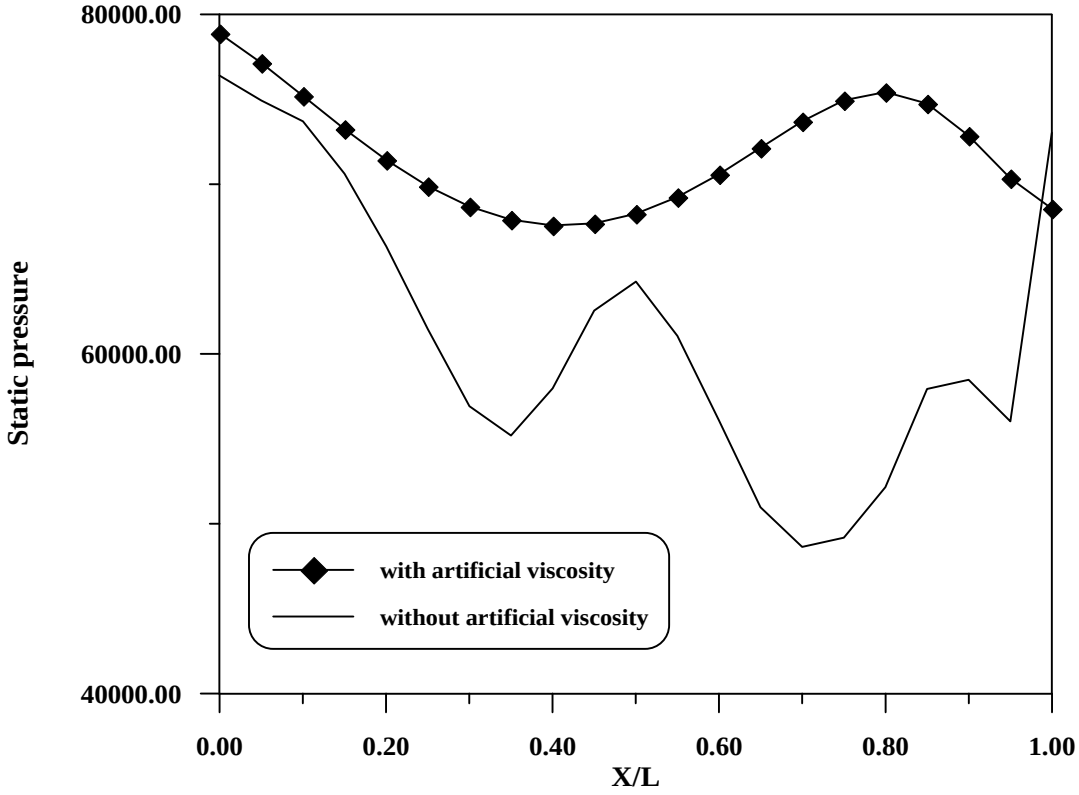

Fig.(٤.٤٤) The variation of static pressure with fraction of axial chord in the rotor passage

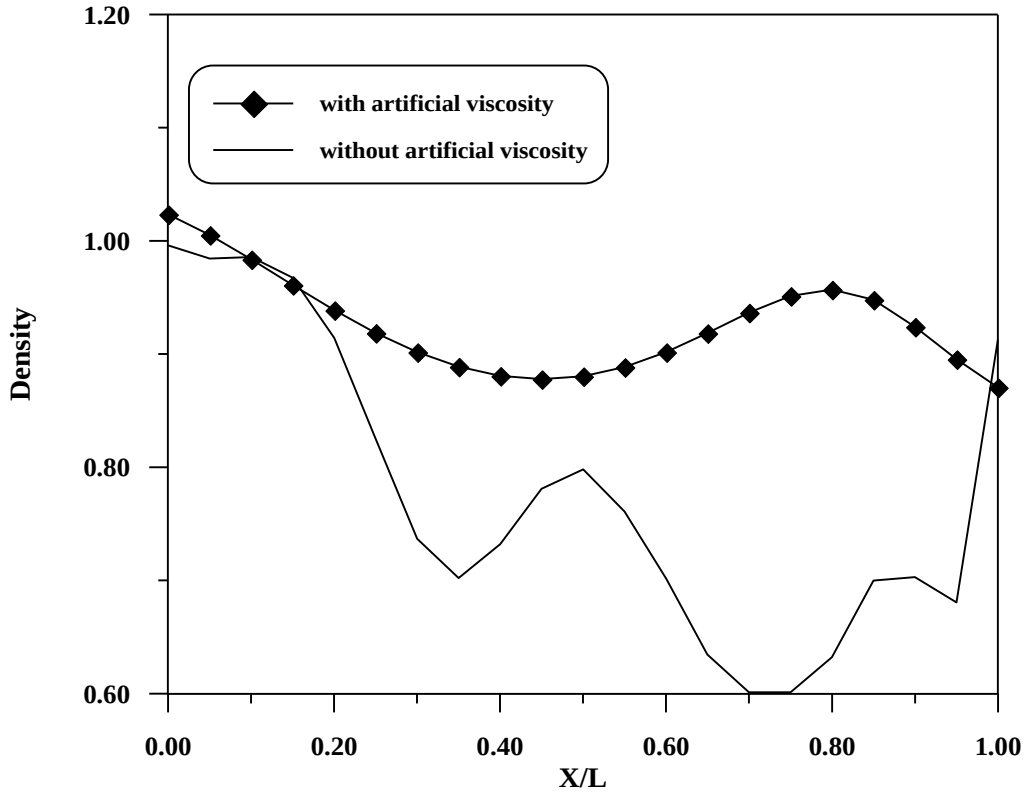

Fig.(٤.٤٥)The variation of density with fraction of axial chord in the rotor passage

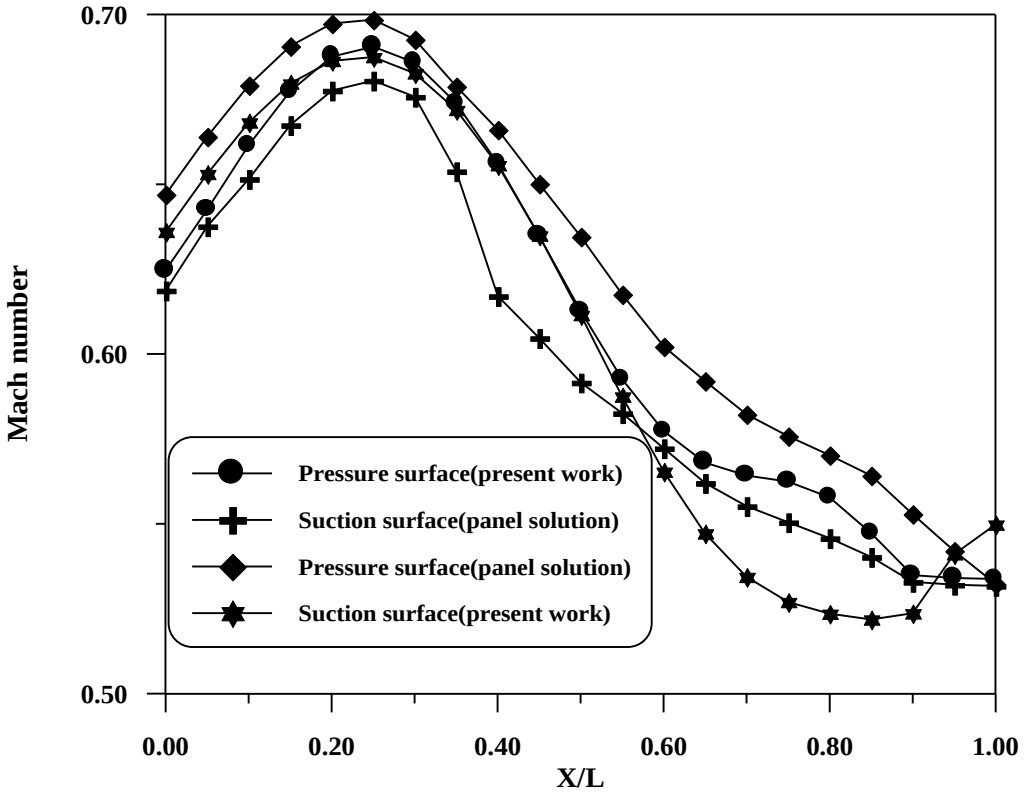

Fig.(٤.٤٦)The comparison between present work and panel solution

List of References

١. Jack D.Mattingly, “Element of Gas Turbine Propulsion” Mechanical Engineering Series, ١٩٩٦.

٢. Budugur Lakshminarayana, “Fluid Dynamics and Heat Transfer Turbomachinery “, John Willey and Sons, Inc., ١٩٩٦.

٣. Ron H.,”A Multiple-Grid Scheme for Solving the Euler Equations “, AIAA Journal, Vol.٢٠, No.١١, November ١٩٨٢.

٤. Denton J.D., “An Improved Time Marching Method for Turbomachinery Flow Calculation”, Journal of Engineering for Power, Vol.١٠٥, July ١٩٨٣.

٥. Young June Moon,”Grid Size Dependence on Convergence for Computation of The Navier-Stokes Equations”AIAA Journal, Vol.٢٤, No.١٠, October ١٩٨٦.

٦. Von Lavante E.” Numerical Solutions of Euler Equations Using Simplified Flux Vector Splitting”AIAA Journal ,Vol.٢٥, No.٨,August.

٧. Gerolymos G. A., “Numerical Integration of the Blade-to-Blade Surface Euler Equations in Viberating Cascades”, AIAA Journal, Vol.٢٦, No.١٢, December ١٩٨٨.

٨. Davis R., Hobbs D. and Weingold H., “Predication of Compressor Cascade Performance Using a Navier-Stokes Technique”, ASME Journal, Vol.١١٠, PP.٥٢٠, ١٩٨٠.

٩. Preaire, Jaime and Ken Morgan, “Finite Element Euler Computations in Three-Dimensional “ Journal for Numerical Methods in Engineering , V.٢٦, PP٢١٣, ١٩٨٨.

List of References

١٠. Sanz W., Gehrer A., “An Implicit TVD Upwind Relaxation Scheme for the Unsteady Two-Dimensional Euler Equations, “ ASME Journal, PP(٩٥-CTP-٧١), ١٩٩٥.

١١. Mohd. Zamri ,” A Two-Dimensional Time Accurate Euler Solver for Turbomachinery Applications “ Birmingham (B١٥٢-TT), England ١٩٩٧.

١٢. Demeulenaere A., “ Three-Dimensional Inverse Method for Turbomachinery Blading Design”, Journal of Turbomachinery, Vol.١٢٠, April ١٩٩٨.

١٣. Amano R., “An Implicit Scheme for Cascade Flow and Heat Transfer Analysis”, Journal of Turbomachinery, Vol.١٢٢, April ٢٠٠٠.

١٤. Thomas H.Pulliam, “Artificial Dissipation Models for the Euler Equations”, AIAA Journal, Vol.٢٤, No.١٢, December ١٩٨٦.

١٥. Arkan Al-Taie and Talib Z. Farje, “Design of an Axial Flow Compressor a Simplified Method”, MCE Conference, ME١٢, ١٩٩٤.

١٦. Oguz M.S.,” Quasi-Three-Dimensional Numerical Design of Turbomachinery Blades”,July ١٩٩٥.

١٧. Matthew D. Montgomery and Joseph M. Verdon,” A Three-Dimensional Linearized Unsteady Euler Analysis for Turbomachinery Blade Rows”, JUNE ١٩٩٦.

١٨. Sabanca and Murat, “Development of a Two-Dimension Euler Solver Using Finite Volume Method for External Flow”, Thesis ١٩٩٧.

١٩. Zang and Camaero R., “Upwind Strategies for the Euler Equations “ Journal of Canadian Aeronautics and Space “Vol.٤٤, No.٣, ١٩٩٨.

List of References

٢٠. Rolf Dornberger and Peter Stoll, “Multidisciplinary Optimization in Turbomachinery Design “ European Congress on Computational Methods in Applied Scinces and Engineering, ٢٠٠٠.

٢١. Ergun, “Sensitivity Analysis in Turbomachinery Cascade Design Optimization” ٢٠٠٠.

٢٢. Helmut Sobieczky٢٠٠٢,”Parameterized Geometry Formulation for Inverse Design Optimization”, ٣rd AIAA Theoretical Fluid Dynamics Conference, June ٢٠٠٢.

٢٣. Zaid Wassil, “Quasi-Three-Dimension Low Speed Viscous Flow Between Two Axial Compressor Cascade Blades “, Thesis ٢٠٠٠.

٢٤. Ali Khader, ”Unsteady Viscous Flow Between Two Axial Compressor Cascade Blades”, Thesis ٢٠٠٠.

٢٥. Anderson Dale A., John G. Tannehill and Richard H. Pletcher, “Computational Fluid Mechanics and Heat Transfer “ ١٩٨٤.

٢٦. Hoffmann Klaus A.,”Computational Fluid Dynamics for Engineering “, ١٩٨٩.

٢٧. Joe F.Thompson, “Grid Generation Techniques in Computational Fluid Dynamics”, AIAA Journal, Vol.٢٢, No.١١, November ١٩٨٤.

٢٨. John D.Anderson,”Computational Fluid Dynamics “, McGraw Hill,Inc., ١٩٩٥.

٢٩. E. R. McFarland, “Solution of Plane Cascade Flow Using Improved Surface Singularity Methods” Journal of Transactions of the ASME, Vol.١٠٤, July ١٩٨٢.

٣٠. Cohen H. Rogers G.F.C. and H. I. H. Saravanamnttoo, “Gas Turbine Theory”, John Wiley and Sons , Inc., New York , ١٩٨٧ .

List of References